

# The physics of dipolar bosonic quantum gases

T Lahaye<sup>1,2,3</sup>, C Menotti<sup>4</sup>, L Santos<sup>5</sup>, M Lewenstein<sup>6,7</sup> and T Pfau<sup>1</sup>

<sup>1</sup> 5. Physikalisches Institut, Universität Stuttgart, Pfaffenwaldring 57, D-70550 Stuttgart, Germany

<sup>2</sup> Université de Toulouse, UPS, Laboratoire Collisions Agrégats Réactivité, IRSAMC, F-31062 Toulouse, France

<sup>3</sup> CNRS, UMR 5589, F-31062 Toulouse, France

<sup>4</sup> CNR-INFM BEC and Dipartimento di Fisica, Università di Trento, I-38050 Povo, Italy

<sup>5</sup> Institut für Theoretische Physik, Leibniz Universität Hannover, Appelstr. 2, D-30167, Hannover, Germany

<sup>6</sup> ICFO-Institut de Ciències Fotòniques, 08860 Castelldefels (Barcelona), Spain

<sup>7</sup> ICREA-Institució Catalana de Recerca i Estudis Avançats, 08010 Barcelona, Spain

E-mail: [t.pfau@physik.uni-stuttgart.de](mailto:t.pfau@physik.uni-stuttgart.de)

Received 14 May 2009

Published 19 November 2009

Online at [stacks.iop.org/RoPP/72/126401](http://stacks.iop.org/RoPP/72/126401)

## Abstract

This paper reviews the recent theoretical and experimental advances in the study of ultra-cold gases made of bosonic particles interacting via the long-range, anisotropic dipole–dipole interaction, in addition to the short-range and isotropic contact interaction usually at work in ultra-cold gases. The specific properties emerging from the dipolar interaction are emphasized, from the mean-field regime valid for dilute Bose–Einstein condensates, to the strongly correlated regimes reached for dipolar bosons in optical lattices.

(Some figures in this article are in colour only in the electronic version)

## Contents

<b>1. Introduction</b>	2	5.5. Trapped gas: excitations	14
1.1. Bose–Einstein condensation and a new quantum era	2	5.6. Trapped gas: roton-maxon spectrum	15
1.2. Interactions	2	<b>6. Dynamics of a dipolar gas</b>	17
<b>2. Dipole–dipole interaction</b>	3	6.1. Self-similar expansion in the Thomas–Fermi regime	17
2.1. Properties of the dipole–dipole interaction	3	6.2. A quantum ferrofluid	18
2.2. Tuning of the dipole–dipole interaction	5	6.3. Collapse dynamics	18
<b>3. Creation of a dipolar gas</b>	5	<b>7. Non-linear atom optics with dipolar gases</b>	20
3.1. Polar molecules	5	7.1. Solitons	20
3.2. Rydberg atoms	6	7.2. Vortices	22
3.3. Light-induced dipoles	6	7.3. Pattern formation	22
3.4. Magnetic dipoles	6	<b>8. Dipolar effects in spinor condensates</b>	23
<b>4. Non-local Gross–Pitaevskii equation</b>	8	8.1. Ground state	23
4.1. Pseudo-potential and Gross–Pitaevskii equation	8	8.2. Dynamics and Einstein–de Haas effect	23
4.2. Validity of non-local Gross–Pitaevskii equation	9	8.3. Experimental results	24
4.3. Variational approach and hydrodynamics	10	<b>9. Dipolar gases in optical lattices</b>	25
<b>5. Ground-state properties and excitations</b>	10	9.1. Bose–Einstein condensates in optical lattices	25
5.1. Homogeneous gas: phonon instability	10	9.2. Bloch oscillation damping due to dipole–dipole interactions	26
5.2. Trapped gas: elongation of the cloud	10	9.3. Strongly correlated lattice gases. Bose–Hubbard Hamiltonian	26
5.3. Trapped gas: geometrical stabilization	11		
5.4. Trapped gas: Thomas–Fermi regime	13		

9.4. Quantum phases of dipolar lattice gases	28	10.2. Dipolar gases and trapped ions	34
9.5. Metastable states of dipolar lattice gases	30	10.3. ‘Dipolar art’	35
9.6. Bilayer and multilayer dipolar lattice gases. Interlayer effects	31	<b>Acknowledgments</b>	35
9.7. Tailoring interactions with polar molecules	32	<b>Appendix A. Fourier transform of the dipolar interaction</b>	36
9.8. Self-assembled structures	33	<b>Appendix B. Stark effect of the rigid rotor</b>	36
<b>10. Outlook</b>	34	<b>References</b>	37
10.1. From chromium to heteronuclear molecules to Rydberg atoms	34		

## 1. Introduction

### 1.1. Bose–Einstein condensation and a new quantum era

The achievement of Bose–Einstein condensation (BEC) of dilute gases in 1995 [1–3] marked the beginning of a new era in atomic, molecular and optical physics and quantum optics. For the AMO community it was immediately clear that the specific experimental techniques of these fields could be used to study problems usually encountered in condensed matter physics: degenerate quantum many-body systems. The condensed matter community at this stage remained much more skeptical and argued that at the very end what was achieved experimentally was the regime of weakly interacting Bose gases, that had been thoroughly investigated by condensed matter theorists in the 1950s and 1960s [4, 5]. For solid-state/condensed matter experts the very fact that the AMO experiments dealt with confined systems of finite size and typically inhomogeneous density was of technical, rather than fundamental importance. Nevertheless, the Nobel foundation decided to give its yearly prize in 2001 to Cornell, Wieman and Ketterle ‘for the achievement of Bose–Einstein condensation in dilute gases of alkali atoms, and for early fundamental studies of the properties of the condensate’ [6, 7]. Today, from the perspective of some years, we see that due to the efforts of the whole community these fundamental studies have enriched amazingly the standard ‘condensed matter’ understanding of static and dynamical properties of weakly interacting Bose gases [8].

At the same time, the AMO community continued the efforts to extend the BEC physics toward new regimes and new challenges. The progress in this direction was indeed spectacular and at the beginning of the third millennium it is clear both for AMO and condensed matter communities that we are entering a truly new quantum era with unprecedented possibilities of control on many-body systems. In particular it became clear that the regime of strongly correlated systems may be reached with ultra-cold atoms and/or molecules. Few years after the first observation of BEC, atomic degenerate Fermi gases [9–12] have been achieved. This has paved the way toward the observations of Fermi superfluidity (described in the weak interaction limit by Bardeen–Cooper–Schrieffer (BCS) theory [5]), and the so-called BEC-BCS crossover in the limit of strong correlations (for recent reviews of an enormous activity in this field see [13, 14]). Even earlier, following the seminal proposal by Jaksch *et al* [15], Greiner *et al* [16] observed the signatures of the quantum phase transition from

the superfluid to the so-called Mott insulator state for bosons confined in an optical lattice.

Nowadays, ultra-cold atomic and molecular systems are at the frontier of modern quantum physics, and are seriously considered to offer more control than solid-state systems. It is generally believed that these systems will find highly non-trivial applications in quantum information (either as quantum simulators, i.e. quantum computers for a special purpose, or as universal ones) or quantum metrology. At the level of theory a fascinating ‘grand unification’ takes place: AMO, condensed matter, nuclear physics and even high energy physics theorists join their efforts to work on ultra-cold gases (for recent reviews see [13, 14, 17]).

### 1.2. Interactions

Although quantum gases are very dilute systems (with densities typically ranging from  $10^{14}$  to  $10^{15}$  cm $^{-3}$ ), most of their properties are governed by the interaction between particles. Usually, in the ultra-cold regime characteristic of quantum gases (temperatures in the nanokelvin range), only s-wave scattering between particles can take place. This allows one to replace the real interatomic potential (which at long distances is the usual van der Waals interaction) by a pseudo-potential, which is short range, isotropic and characterized by a single parameter, the s-wave scattering length  $a$ . This *contact interaction* potential reads as

$$U_{\text{contact}}(\mathbf{r}) = \frac{4\pi\hbar^2 a}{m} \delta(\mathbf{r}) \equiv g\delta(\mathbf{r}), \quad (1.1)$$

where  $m$  is the atomic mass. For a large number of atomic species, the magnitude and even the sign of the scattering length  $a$  can be tuned by means of an external magnetic field. This phenomenon, called Feshbach resonance [18, 19], has found multiple applications since its first experimental observation in cold gases [20, 21].

Despite its simplicity, the interaction potential (1.1) is responsible for an extremely rich variety of physical properties of quantum gases. As we mentioned above, already for weakly interacting Bose gases, well described by mean-field theory, the interactions play a crucial role in the static and dynamic properties of Bose–Einstein condensates [8, 22]; one of the most fascinating properties they are responsible for is the superfluid character of those gases. The interactions between particles obviously play an even more crucial role in the very active field concerning the study of strongly correlated systems realized with ultra-cold atoms [14, 17].

For all those reasons, in the last few years, there has been a quest for realizing quantum gases with different, richer interactions, in order to obtain even more interesting properties. Several researchers, including<sup>8</sup> Rzążewski, Shlyapnikov, Zoller, Kurizki, You, DeMille, Baranov, Meystre, Pu and some of us, have pointed out that the dipole–dipole interaction, acting between particles having a permanent electric or magnetic dipole moment, should lead to a novel kind of degenerate quantum gas already in the weakly interacting limit. Its effects should be even more pronounced in the strongly correlated regime.

The dipole–dipole interaction has attracted huge interest for two reasons:

- Significant experimental progress was made in recent years in the cooling and trapping of polar molecules [23], and of atomic species having a large magnetic moment. For the case of polar molecules, a very promising technique is to associate ultra-cold atoms by means of Feshbach resonances, and then to use photoassociation to bring the weakly bound Feshbach molecules to their ground state [24]. In practice this technique requires a very good phase stability of the involved lasers. A few months ago Jin and Ye groups at JILA have been able to create a gas of motionally ultra-cold rubidium–potassium molecules in their ground rovibrational state [25]; similar work was done in the group of Weidemüller with LiCs molecules [26]. These amazing achievements open the way toward degenerate gases with dominant dipole–dipole interactions. For the case of magnetic dipoles, Bose–Einstein condensation of  $^{52}\text{Cr}$ , a species with a large magnetic moment of  $6\mu_B$ , was achieved in 2004 [27], and has since then allowed for the first experimental investigations of the unique properties of dipolar quantum gases [28]. Although the relative effect of the dipole forces in chromium can be tuned using the Feshbach resonance technique, they are typically smaller, or at most on the same order as the van der Waals forces. Nevertheless their influence on the physics of the chromium BEC is stunning, as we shall see in the following.
- The properties of the dipole–dipole interaction are radically different from the ones of the contact interaction [29]. Indeed, one directly sees from expression (2.2), giving the interaction energy between two dipoles polarized along the same direction, that the dipole–dipole interaction is *long-range* (it decays as  $1/r^3$ , where  $r$  is the distance between the particles) and *anisotropic* (the strength and sign of the interaction depend on the angle  $\theta$  between the polarization direction and the relative position of the particles). Note that if one limits oneself to neutral particles, the dipole–dipole interaction is the only interaction between electric or magnetic multipole moments which is long-range (interactions between higher order multipoles decay fast enough at large distances so that they can be replaced by a short range contact pseudo-potential at low temperatures). Long range and/or anisotropic interactions are known already, in



**Figure 1.** The Rosensweig instability [32] of a ferrofluid (a colloidal dispersion in a carrier liquid of subdomain ferromagnetic particles, with typical dimensions of 10 nm) in a magnetic field perpendicular to its surface is a fascinating example of the novel physical phenomena appearing in classical physics due to long range, anisotropic interactions. Figure reprinted with permission from [34]. Copyright 2007 by the American Physical Society.

classical fluids [30, 31], to lead to completely new physical phenomena (see for example the case of ferrofluids [32] in figure 1). Similarly, anisotropy of interactions lies behind the fascinating physics of liquid crystals [33]. As we will argue in this review, dipole interactions in quantum gases also lead to a variety of novel, fascinating and sometimes completely unexpected effects.

This review is organized as follows. After a brief description of the main properties of the dipole–dipole interaction (section 2) and of the systems in which it can be studied (section 3), the mean-field theory for a weakly interacting, polarized dipolar condensate is presented (section 4). We derive here the non-local Gross–Pitaevskii equation and discuss its applicability. In subsequent sections we describe a number of properties of dipolar BECs, in particular their static and dynamic properties (sections 5 and 6). In section 7 we enter the very rich field of non-linear, non-local atom optics with dipolar gases. Section 8 is devoted to the physics of dipolar spinor condensates. Finally, strongly correlated systems obtained by loading a dipolar BEC into an optical lattice are described in section 9. Because of the lack of space, some very interesting topics are not addressed here; in particular, for a review of the properties of dipolar Fermi gases and of (strongly correlated) rapidly rotating dipolar condensates, the reader is referred to the recent review article [35].

## 2. Dipole–dipole interaction

### 2.1. Properties of the dipole–dipole interaction

For two particles 1 and 2 with dipole moments along the unit vectors  $e_1$  and  $e_2$ , and whose relative position is  $r$  (see figure 1(a)), the energy due to the dipole–dipole interaction reads as

$$U_{dd}(r) = \frac{C_{dd}}{4\pi} \frac{(e_1 \cdot e_2) r^2 - 3(e_1 \cdot r)(e_2 \cdot r)}{r^5}. \quad (2.1)$$

The coupling constant  $C_{dd}$  is  $\mu_0\mu^2$  for particles having a permanent magnetic dipole moment  $\mu$  ( $\mu_0$  is the permeability of vacuum) and  $d^2/\epsilon_0$  for particles having a permanent electric dipole moment  $d$  ( $\epsilon_0$  is the permittivity of vacuum). For a

<sup>8</sup> We apologize in advance if we have forgotten someone.

polarized sample where all dipoles point in the same direction  $z$  (figure 1(b)), this expression simplifies to

$$U_{\text{dd}}(\mathbf{r}) = \frac{C_{\text{dd}}}{4\pi} \frac{1 - 3 \cos^2 \theta}{r^3}, \quad (2.2)$$

where  $\theta$  is the angle between the direction of polarization and the relative position of the particles. Two main properties of the dipole–dipole interaction, namely its long-range ( $\sim 1/r^3$ ) and anisotropic character, are obvious from (2.1) and (2.2), and contrast strongly with the short-range, isotropic contact interaction (1.1) usually at work between particles in ultra-cold atom clouds.

*Long-range character.* In a system of particles interacting via short-range interactions, the energy is extensive in the thermodynamic limit. In contrast, in systems with long-range interactions, the energy per particle does not depend only on the density, but also on the total number of particles. It is easy to see that a necessary condition for obtaining an extensive energy is that the integral of the interaction potential  $U(\mathbf{r})$

$$\int_{r_0}^{\infty} U(\mathbf{r}) d^D r, \quad (2.3)$$

where  $D$  is the dimensionality of the system and  $r_0$  some short-distance cutoff, converges at large distances. For interactions decaying at large distances as  $1/r^n$ , this implies that one needs to have  $D < n$  in order to consider the interaction to be short range. Therefore, the dipole–dipole interaction ( $n = 3$ ) is long range in three dimensions, and short range in one and two dimensions. For a more detailed discussion, including alternative definitions of the long-range character of a potential, the reader is referred to [36].

*Anisotropy.* The dipole–dipole interaction has the angular symmetry of the Legendre polynomial of second order  $P_2(\cos \theta)$ , i.e. d-wave. As  $\theta$  varies between 0 and  $\pi/2$ , the factor  $1 - 3 \cos^2 \theta$  varies between  $-2$  and  $1$ , and thus the dipole–dipole interaction is repulsive for particles sitting side by side, while it is attractive (with twice the strength of the previous case) for dipoles in a ‘head-to-tail’ configuration (see figures 2(c) and (d)). For the special value  $\theta_m = \arccos(1/\sqrt{3}) \simeq 54.7^\circ$ —the so-called ‘magic angle’ used in high resolution solid-state nuclear magnetic resonance [37, 38]—the dipole–dipole interaction vanishes.

*Scattering properties.* Usually, the interaction potential between two atoms separated by a distance  $r$  behaves like  $-C_6/r^6$  at large distances. For such a van der Waals potential, one can show that in the limit of a vanishing collision energy, only the s-wave scattering plays a role. This comes from the general result stating that for a central potential falling off at large distances as  $1/r^n$ , the scattering phase shifts  $\delta_\ell(k)$  scale, for  $k \rightarrow 0$ , as  $k^{2\ell+1}$  if  $\ell < (n-3)/2$ , and as  $k^{n-2}$  otherwise [39]. In the ultra-cold regime, the scattering is thus fully characterized by the scattering length  $a$ . In the study of quantum gases, the true interaction potential between the atoms can then be replaced by a pseudo-potential having the

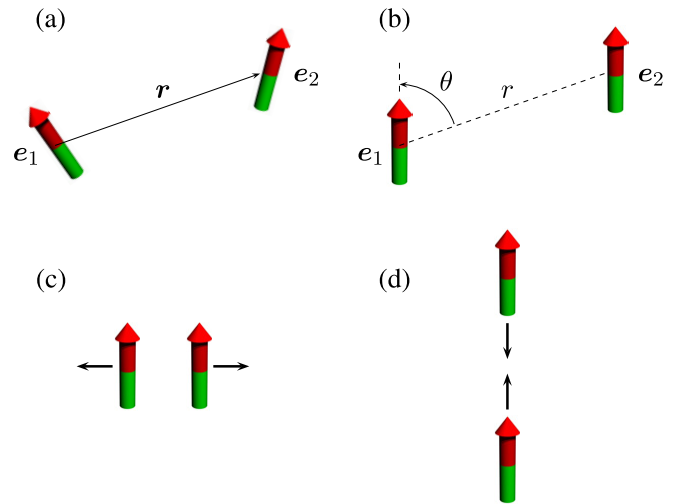


**Figure 2.** Two particles interacting via the dipole–dipole interaction. (a) Non-polarized case; (b) polarized case; (c) two polarized dipoles side by side repel each other (black arrows); (d) two polarized dipoles in a ‘head-to-tail’ configuration attract each other (black arrows).

same scattering length, the so-called contact interaction given by (1.1).

In the case of the dipole–dipole interaction, the slow decay as  $1/r^3$  at large distances implies that for all  $\ell$ ,  $\delta_\ell \sim k$  at low momentum, and all partial waves contribute to the scattering amplitude. Moreover, due to the anisotropy of the dipole–dipole interaction, partial waves with different angular momenta couple with each other. Therefore, one cannot replace the true potential by a short-range, isotropic contact interaction. This specificity of the dipolar interaction has an interesting consequence in the case of a polarized Fermi gas: contrary to the case of a short-range interaction, which freezes out at low temperature, the collision cross section for identical fermions interacting via the dipole–dipole interaction does not vanish even at zero temperature. This could be used to perform evaporative cooling of polarized fermions, without the need for sympathetic cooling via a bosonic species.

Dipolar interactions also play an important role in determining inelastic scattering properties. In particular, because of its anisotropy, the dipole–dipole interaction can induce spin–flips, leading to dipolar relaxation. The cross-section for dipolar relaxation scales with the cube of the dipole moment [40], and therefore plays a crucial role in strongly dipolar systems (see section 3.4.1). Dipolar relaxation is usually a nuisance, but can in fact be used to implement novel cooling schemes inspired by adiabatic demagnetization as described in section 3.4.3.

*Fourier transform.* In view of studying the elementary excitations in a dipolar condensate, as well as for numerical calculations, it is convenient to use the Fourier transform of the dipole–dipole interaction. The Fourier transform

$$\widetilde{U}_{\text{dd}}(\mathbf{k}) = \int U_{\text{dd}}(\mathbf{r}) e^{-i\mathbf{k}\cdot\mathbf{r}} d^3 r \quad (2.4)$$

of (2.2) reads as

$$\widetilde{U}_{\text{dd}}(\mathbf{k}) = C_{\text{dd}}(\cos^2 \alpha - 1/3), \quad (2.5)$$

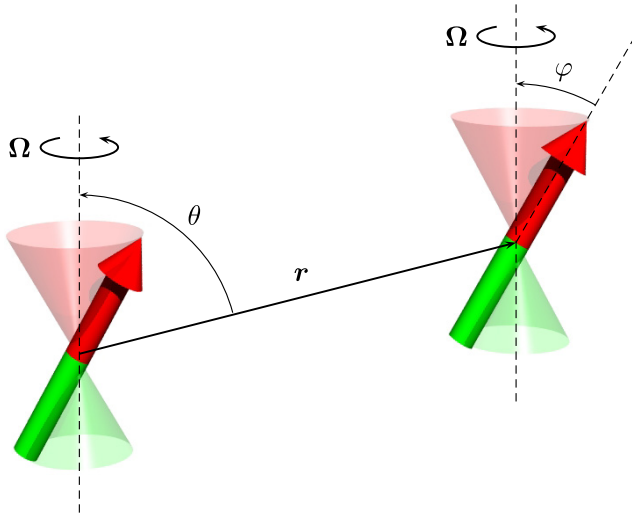


**Figure 3.** Tuning of the dipole–dipole interaction can be obtained by making the dipoles precess around  $z$  using a rotating field.

where  $\alpha$  is the angle between  $\mathbf{k}$  and the polarization direction (see appendix A). Remarkably, in three dimensions, the Fourier transform of the dipole–dipole interaction does not depend on the modulus of the wavevector  $\mathbf{k}$ , a feature which is shared by the contact interaction (1.1), whose Fourier transform is simply  $g$ .

### 2.2. Tuning of the dipole–dipole interaction

By using a rotating polarizing field, it is possible, by time-averaging, to tune the dipole–dipole interaction, namely to reduce its effective strength and even change its sign [41]. For definiteness we consider here the case of magnetic dipoles  $\boldsymbol{\mu}$  in a magnetic field  $\mathbf{B}(t) = B\mathbf{e}(t)$  (see figure 3). The unit vector  $\mathbf{e}(t) = \cos\varphi\mathbf{e}_z + \sin\varphi[\cos(\Omega t)\mathbf{e}_x + \sin(\Omega t)\mathbf{e}_y]$  is rotated about the  $z$ -axis on a cone of aperture  $2\varphi$  at an angular frequency  $\Omega$  which is small compared with the Larmor frequency  $\mu B/\hbar$ , but much larger than the trapping frequencies. Then, only the time average over a period  $2\pi/\Omega$  of the dipole–dipole interaction (2.1) with  $\mathbf{e}_1 = \mathbf{e}_2 = \mathbf{e}(t)$  plays a role in determining the properties of the gas. This time-averaged potential reads as

$$\langle U_{\text{dd}}(t) \rangle = \frac{C_{\text{dd}}}{4\pi} \frac{1 - 3\cos^2\theta}{r^3} \left[ \frac{3\cos^2\varphi - 1}{2} \right]. \quad (2.6)$$

The last factor between brackets decreases from 1 to  $-1/2$  when the tilt angle  $\varphi$  varies from 0 to  $\pi/2$ , and vanishes when  $\varphi$  is equal to the magic angle  $\theta_m$ . The ‘inverted’ configuration ( $\varphi > \theta_m$ ) in which the averaged dipole–dipole interaction is attractive for particles sitting side by side, allows exploration of otherwise inaccessible physics (see section 7 for some examples of applications).

## 3. Creation of a dipolar gas

In order to realize a quantum gas with significant dipole–dipole interactions, one can use particles having either an electric dipole moment  $d$  or a magnetic dipole moment  $\mu$ . Usually, the dipolar coupling is much higher in the electric case. Indeed,

**Table 1.** Dipolar constants for various atomic and molecular species. For the molecular species, the (yet unknown) scattering length is assumed to be  $100a_0$  (as the  $C_6$  coefficient of the dimer is comparable to that of a single atom, the order of magnitude of the scattering length is similar, but obviously the actual value highly depends on the details of the potential).

Species	Dipole moment	$a_{\text{dd}}$	$\varepsilon_{\text{dd}}$
$^{87}\text{Rb}$	$1.0 \mu_{\text{B}}$	$0.7 a_0$	0.007
$^{52}\text{Cr}$	$6.0 \mu_{\text{B}}$	$16 a_0$	0.16
KRb	0.6 D	$2.0 \times 10^3 a_0$	20
$\text{ND}_3$	1.5 D	$3.6 \times 10^3 a_0$	36
HCN	3.0 D	$2.4 \times 10^4 a_0$	240

the typical order of magnitude of  $d$  for an atomic or molecular system is  $d \sim q_e a_0$ , where  $q_e$  is the electron charge and  $a_0$  the Bohr radius, while the magnetic moments are on the order of the Bohr magneton  $\mu_{\text{B}}$ . Using the definitions of  $a_0$  and  $\mu_{\text{B}}$  in terms of fundamental constants, one sees that the ratio of magnetic to electric dipolar coupling constants is

$$\frac{\mu_0 \mu^2}{d^2 / \varepsilon_0} \sim \alpha^2 \sim 10^{-4}, \quad (3.1)$$

where  $\alpha \simeq 1/137$  is the fine structure constant.

For a given species, it is convenient to define various quantities to quantify the strength of the dipolar interaction. From the dipole moment (i.e. the dipolar coupling constant  $C_{\text{dd}}$ ) and the mass  $m$  of the particle, one can define the following length:

$$a_{\text{dd}} \equiv \frac{C_{\text{dd}} m}{12\pi\hbar^2}. \quad (3.2)$$

This ‘dipolar length’ is a measure of the absolute strength of the dipole–dipole interaction. However, in some circumstances, it is the ratio

$$\varepsilon_{\text{dd}} \equiv \frac{a_{\text{dd}}}{a} = \frac{C_{\text{dd}}}{3g} \quad (3.3)$$

of the dipolar length to the  $s$ -wave scattering length, comparing the relative strength of the dipolar and contact interactions, which determines the physical properties of the system. This dipolar parameter needs to be non-negligible if one wants to observe dipolar effects. The numerical factors in (3.2) are chosen in such a way that for  $\varepsilon_{\text{dd}} \geq 1$  a homogeneous condensate is unstable against 3D collapse (see section 5.1). Table 1 summarizes some typical numerical values of the dipolar constants for various atomic and molecular species.

In this section, we review the different systems that can be used in principle to study experimentally the effect of the dipole–dipole interaction in degenerate quantum gases. We first address the various candidates having an *electric* dipole moment, either static or induced by a laser. The case of *magnetic* dipoles (the only system to date in which strong dipolar effects in a quantum gas have been observed) is then described, with an emphasis on the experimental techniques used to achieve Bose–Einstein condensation of chromium.

### 3.1. Polar molecules

Due to their strong electric dipole moment, polar molecules are ideal candidates to show dipolar effects. Three requirements

need to be fulfilled in order for a molecule to have a significant dipole moment:

- (i) a *heteronuclear* molecule, having a permanent dipole moment, is needed<sup>9</sup>;
- (ii) the molecule must be in a low rovibrational state in order to have a dipole moment whose magnitude is not vanishingly small (as would be the case for a highly excited vibrational state, especially for Feshbach molecules; indeed, the dipole moment scales asymptotically as  $R^{-7}$  with the internuclear separation  $R$  [44]) and to be stable against collisional relaxation;
- (iii) an external electric field (with a typical value on the order of  $10^4$  V cm<sup>-1</sup>) must be applied to *orient* the molecule in the laboratory frame and approach the asymptotic value of the permanent electric dipole moment along the internuclear axis (indeed, the ground state  $J = 0$  is rotationally symmetric and therefore the dipole moment averages to zero; only via a mixing with higher rotational levels, induced by the electric field, does the average dipole become non-zero, see [appendix B](#)). Note that this effect can be used to tune the strength of the dipole–dipole interaction (but not its sign, unlike the rotating field method described in [section 2.2](#)). Using additional microwave fields allows for advanced tailoring of the interactions between molecules [45].

If these requirements are met, the dipole moment is on the order of one Debye ( $1 \text{ D} \simeq 3.335 \times 10^{-30} \text{ C m}$ ). Assuming that the order of magnitude for the scattering length is similar to that of atoms commonly used in BEC experiments (typically around  $100 a_0$ ), the corresponding value of  $\varepsilon_{\text{dd}}$  is on the order of 100 (see [table 1](#)), meaning that the properties of such a quantum gas would be dominated by the dipole–dipole interaction.

Quantum degenerate gases of polar molecules are a ‘Holy Grail’ of experimental molecular physics. Progress has been made recently in cooling of molecules, with techniques such as Stark deceleration (see, e.g. [46] for a review) or buffer-gas cooling [47–49], but the densities and temperatures achieved so far are still orders of magnitude away from the quantum degenerate regime. A very promising approach to degeneracy, actively explored by several groups [24–26], is to start from already ultra-cold atomic mixtures and then use a Feshbach resonance to create heteronuclear molecules [18]. Created in a highly excited vibrational state, they must then be brought to the vibrational ground state, e.g. by photoassociation using STIRAP processes, as demonstrated recently [25, 26]. A recent review on cold and ultracold molecules is given in [50].

### 3.2. Rydberg atoms

Extraordinarily large electric dipole moments can be obtained for highly excited Rydberg atoms. As the Kepler radius—and thus the dipole moment—scales with  $n^2$ , where  $n$  is the main quantum number, the dipolar interaction energy can in principle scale as  $n^4$ . Individual Rydberg atoms experience

<sup>9</sup> Note, however, that exotic *homonuclear* molecules, such as the ultra-long-range Rydberg molecules predicted in [42] and recently observed in [43], can have a permanent dipole moment.

lifetimes which scale with  $n^{-3}$ . However, due to the weak binding of the valence electrons and the strong and partially attractive forces between Rydberg atoms, the lifetime of a dense gas is limited to time scales much shorter than the lifetime of a free Rydberg atom [51]. Therefore, Rydberg atoms in a BEC [52] are currently investigated as a frozen gas. Collective behavior in the excitation dynamics has been observed, as well as the excitation blockade due to dipolar interactions [53]. However, hydrodynamic collective phenomena due to moving dipoles have not been observed to date. Besides the static dipolar interaction also van der Waals interactions ( $\propto n^{11}$ ) and ac dipolar interactions can occur if neighboring energy levels allow for resonant energy transfer via a so-called Förster resonance.

### 3.3. Light-induced dipoles

Atoms in their ground state, which is a parity eigenstate, do not possess an electric dipole moment. Their electric polarizability is usually very small, such that extreme electric field strengths would be necessary to induce a sizable dipolar interaction [54–56]. Following Kurizki and co-workers, one might consider using resonant excitation of a dipole optical allowed transition to induce an ac dipole moment on the order of one atomic unit  $ea_0$ . However, as this dipole moment also couples to the vacuum modes of the radiation field, the spontaneous light forces scale just as the light-induced dipolar interactions which makes their observation very difficult. Nevertheless, the anisotropic nature of the interaction might be used for a proof of principle experiment, which would allow discrimination of the spontaneous light forces from the dipolar forces [57]. Such interactions have the same form as retarded interactions between two dipoles [58]: they contain  $1/r^3$ ,  $1/r^2$  and radiative  $1/r$  terms multiplied by the appropriate factors oscillating with the spatial period of the laser wavelength. Using an arrangement of several laser fields it has been proposed to cancel all anisotropic  $1/r^3$  terms, leaving an effective isotropic, gravity-like  $1/r$  potential [59–62]. In some situations this may lead to self-trapping of the BEC. Even before the discovery of the roton instability [63] discussed in [section 5.6](#), a similar effect was predicted in a gas with laser-induced dipole–dipole interactions [60]. Such interactions lead naturally to density modulations of the BEC as in supersolid [62], and other effects, such as one-dimensional compression of the condensate [61] or squeezing [64]. Laser-induced interactions lead in particular to interesting density modulations in the condensate, somewhat analogous to self-assembled ‘supersolids’ (see [section 9.4](#)). Due to the above mentioned limitations caused by spontaneous emission, these proposals have not been realized yet. The situation in this respect might be more promising if one uses CO<sub>2</sub> lasers [65]. Molecules polarized by microwave fields also offer interesting perspectives<sup>10</sup>.

### 3.4. Magnetic dipoles

In alkali atoms, the maximum magnetic moment in the ground state is of one Bohr magneton ( $\mu_B$ ), and thus the magnetic dipolar effects are very weak. However, very recently, dipolar

<sup>10</sup> O’Dell D, private communication.

effects have been observed in spinor  $^{87}\text{Rb}$  condensates (see section 8) and in condensates with a very small scattering length (obtained using a Feshbach resonance), either by studying the size of the condensate (case of  $^7\text{Li}$ , see section 5.2) or by using atom interferometry (case of  $^{39}\text{K}$ , see section 9.2).

Some other atoms, such as chromium, erbium, europium, dysprosium and others, have a large magnetic moment of several Bohr magnetons in their ground state, and thus experience significant magnetic dipole–dipole interaction. Among them, only  $^{52}\text{Cr}$  has been Bose-condensed to date [27, 66]. Chromium has a magnetic dipole moment of  $6\mu_B$ , and a scattering length of about  $100a_0$  [67]. This gives  $\varepsilon_{\text{dd}} \simeq 0.16$  [68], which allows one to observe a perturbative effect of the dipolar interaction on the expansion dynamics of the cloud [69]. Here we briefly describe the main steps leading to the creation of a  $^{52}\text{Cr}$  BEC, with a special emphasis on the specificities arising from the dipole–dipole interaction.

**3.4.1. Creation of a BEC of  $^{52}\text{Cr}$ .** Chromium can be laser cooled using the  $^7\text{S}_3 \leftrightarrow ^7\text{P}_4$  transition at 425.6 nm (see figure 4). However, strong excited state collisions limit the density in a magneto-optical trap (MOT) to relatively low values [70]. Therefore, in a typical MOT configuration, the steady state atom number in a Cr MOT is limited to a few  $10^6$ . In addition the cooling transition is not closed, as there is a decay channel from the  $^7\text{P}_4$  state to the metastable state  $^5\text{D}_4$  (via an intercombination transition) with a branching ratio of approximately 1 : 250 000. These facts seem to rule out any hope of achieving Bose condensation of chromium by standard methods. However, the atoms in the metastable state have a magnetic dipole moment of  $6\mu_B$  which is strong enough so that they remain magnetically trapped in the inhomogeneous magnetic field configuration of the MOT. One can thus accumulate large atom numbers in the metastable state  $^5\text{D}_4$  (where they are decoupled from the MOT light and thus do not suffer from excited state collisions), and then, at the end of the MOT phase, repump them using light at 663.2 nm. In this way, one ends up with more than  $10^8$  ground state atoms magnetically trapped. In [71], the magnetic field configuration of the MOT was modified to that of an Ioffe–Pritchard trap, allowing a continuous loading of a magnetic trap, in which rf evaporative cooling could be performed.

However, when the density in the magnetic trap becomes too high, one cannot gain anymore in phase-space density due to increasing *dipolar relaxation*. This two-body loss mechanism, in which the spin of one of the colliding atoms is flipped (this is allowed as the dipole–dipole interaction does not conserve the spin, but only the *total* angular momentum), is especially important for chromium, compared with the case of alkalis, as its cross section scales as the cube of the magnetic dipole moment. Typical relaxation rates of  $\beta \sim 10^{-12} \text{ cm}^{-3} \text{ s}^{-1}$  were measured in  $^{52}\text{Cr}$  at magnetic fields of about 1 G [40], thus preventing the achievement of BEC in the (magnetically trapped) low-field seeking state  $m_S = +3$ .

The way to circumvent dipolar relaxation is to optically pump the atoms into the absolute ground state  $m_S = -3$  (via the  $^7\text{S}_3 \leftrightarrow ^7\text{P}_3$  transition at 427.6 nm, see figure 4) and hold them in an optical dipole trap. Then, in the presence of a

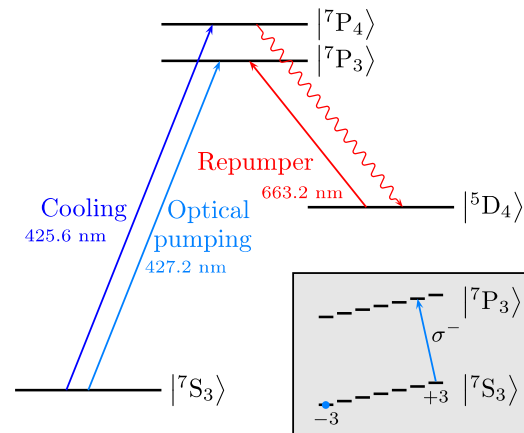


**Figure 4.** Scheme of the energy levels of  $^{52}\text{Cr}$  relevant for the realization of a  $^{52}\text{Cr}$  BEC. The inset (in gray) gives details of the optical pumping.

magnetic field such that the Zeeman splitting between adjacent spin states is much higher than the thermal energy, dipolar relaxation is energetically forbidden. One can then perform evaporative cooling in the dipole trap and obtain a chromium condensate [27]. Recently, an alternative method has been used to obtain  $^{52}\text{Cr}$  condensates, using direct loading of the optical dipole trap [66].

**3.4.2. Feshbach resonances in  $^{52}\text{Cr}$ .** A very appealing feature of  $^{52}\text{Cr}$  is the existence of several Feshbach resonances. These allow tuning of the scattering length  $a$ , which, close to resonance, varies with the applied external magnetic field  $B$  as

$$a = a_{\text{bg}} \left( 1 - \frac{\Delta}{B - B_0} \right), \quad (3.4)$$

where  $a_{\text{bg}}$  is the background scattering length,  $B_0$  is the resonance position (where  $a$  diverges) and  $\Delta$  the resonance width. In order to study the effect of the dipole–dipole interaction in a BEC, it is of course interesting to use the Feshbach resonance to *reduce* the scattering length toward zero by approaching  $B_0 + \Delta$  from above, thus enhancing  $\varepsilon_{\text{dd}}$ .

In  $^{52}\text{Cr}$ , for magnetic fields  $B$  below 600 G, a total of 14 resonances were found by monitoring inelastic losses in a thermal cloud of atoms in the  $|^7\text{S}_3, m_S = -3\rangle$  state [72]. An accurate assignment of the resonances was possible by considering the selection rules and the shifts of the resonances imposed by the dipole–dipole interaction only. In contrast to other atomic species, the dipolar contribution is therefore dominant as compared with other coupling mechanisms, such as second order spin-orbit coupling, which have the same symmetry. The inclusion of dipole–dipole interaction in multichannel calculations [72] gave a theoretical understanding of the width  $\Delta$  of the various resonances, which turns out to be relatively small (the broadest one, located at  $B_0 = 589 \text{ G}$ , having a predicted width of  $\Delta = 1.7 \text{ G}$  only).

In [73], this resonance was used to enhance dipolar effects in a BEC. An active control of the magnetic field at the level of  $3 \times 10^{-5}$  in relative value was implemented, allowing for a control of  $a$  at the level of  $\sim a_0$ . Figure 5 shows the measured variation of  $a$ , inferred from the released energy during expansion (see section 6.2).

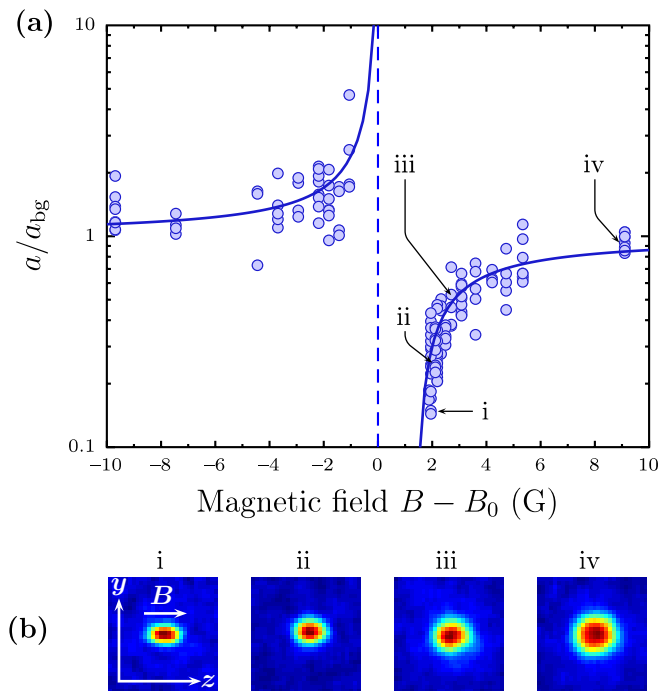


**Figure 5.** (a) Measured variation of the scattering length across the 589 G Feshbach resonance in  $^{52}\text{Cr}$  [73]. (b) Absorption images of the condensate after expansion for different values of the magnetic field. One clearly observes a decrease in size and an increase in ellipticity when  $a$  decreases.

**3.4.3. Demagnetization cooling.** The large magnetic dipole moment of  $^{52}\text{Cr}$  is responsible for strong spin-flip collisions, which, as we have seen above, prevent condensation of Cr in a magnetic trap. However, these inelastic collisions can be used to implement a novel cooling scheme, proposed in [74] and demonstrated experimentally in [75]. This technique is inspired by the well-known *adiabatic demagnetization* used in solid-state physics to cool paramagnetic salts [76]. In the context of cold atoms this scheme was proposed for the first time in [77], and termed ‘elevator cooling’. Particularly important was the analysis of the limitations of the scheme due to reabsorption effects in the Raman repumping process.

The principle of this novel cooling mechanism is represented schematically in figure 6. Dipolar relaxation introduces a coupling between spin and external degrees of freedom. It can thus be used to cool an atomic cloud by letting a sample, initially polarized in the lowest energy state (in a field  $B_0 \gg k_B T_0/\mu$ , where  $T_0$  is the cloud temperature), relax toward full thermal equilibrium at a field  $B_1 \sim k_B T_0/\mu$ : energy is then absorbed by the spin reservoir at the expense of the kinetic energy (see figure 6). The temperature of the sample thus decreases, by an amount which can be up to a few tens of per cent. By optical pumping, the sample can be polarized again, and a new cycle can begin. One can also use a continuous cooling scheme, with the optical pumping light always on, and a ramp in magnetic field. This scheme can be seen as an evaporation process (where one selects the most energetic particles in the cloud) in which the evaporated particles have their energy decreased and are then ‘recycled’ by injecting them back into the trap; it is therefore lossless.

Note that this scheme is applicable for all dipolar species with a large enough dipolar relaxation rate. This rate scales as the third power of the electronic spin. There could even be a variant of this cooling technique for electric dipole moments in heteronuclear molecules. As under optimized conditions any scattered photon in the cooling cycle takes more energy than the mean motional energy, the number of required photons for a certain cooling rate is much lower than in regular laser cooling techniques. Therefore the requirements for the closedness of an optical transition used here are much less stringent as compared with regular laser cooling techniques.

This scheme has been successfully applied to Cr, allowing for a reduction of the cloud temperature by a factor of two (from 20 to 11  $\mu\text{K}$ ), with almost no atom loss [75]. This cooling technique is therefore much more efficient than evaporative cooling, where the decrease in atom number is large. An important figure of merit for cooling schemes in view of obtaining quantum degeneracy is the gain  $\chi$  in phase-space density  $\rho$  per atom loss:

$$\chi \equiv -\frac{d \ln \rho}{d \ln N}. \quad (3.5)$$

For evaporative cooling,  $\chi$  is limited in practice<sup>11</sup> to values of about 4. In [75], the measured efficiency of demagnetization cooling reached  $\chi \simeq 11$ .

The practical limitations in view of achieving lower temperatures lie essentially in the control of the polarization of the optical pumping light, as any residual  $\sigma^+$  component yields a heating of the cloud, and in the control of stray magnetic fields at the milligauss level. However, the recoil temperature should be attainable in principle with this technique [77], which could be used, in the future, to realize dipolar condensates with large atom numbers. Note that the dipolar coupling mechanism between spin and motional degrees of freedom demonstrated in this cooling experiment is the same as the one employed in the proposals to observe the quantum version of the Einstein–de Haas effect, as explained in section 8.

## 4. Non-local Gross–Pitaevskii equation

Dipolar interactions are expected to change many of the properties of the gas, even in the non-degenerate case, where thermodynamical quantities can be affected. For example, dipolar interactions lead to a shift in the critical temperature for condensation [78, 79], which, although negligible for Cr condensates, could be significant for strongly dipolar systems made out of polar molecules. However, the most dramatic effects of the dipolar interactions arise for pure condensates. In the sections below, unless otherwise stated, we thus consider the case of a gas at zero temperature.

### 4.1. Pseudo-potential and Gross–Pitaevskii equation

To describe dilute (and therefore weakly interacting) BECs at zero temperature, the mean-field approach gives extremely

<sup>11</sup> Using a higher evaporation threshold increases  $\chi$ , but the evaporation time then increases prohibitively.

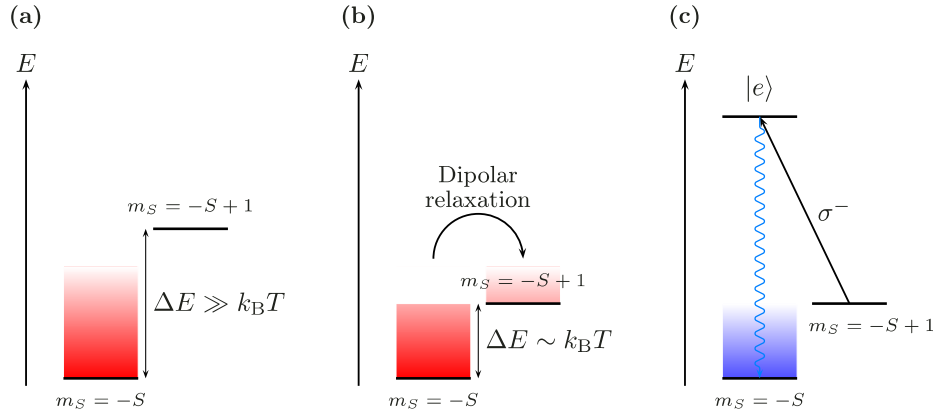


**Figure 6.** Principle of demagnetization cooling. (a) If the magnetic field is large enough so that the Zeeman splitting  $\Delta E$  between adjacent Zeeman sublevels is much higher than the thermal energy  $k_B T$ , dipolar relaxation is energetically suppressed, and the system, fully polarized in  $m_S = -S$ , is stable. (b) If one reduces the magnetic field so that  $\Delta E \sim k_B T$ , dipolar relaxation occurs, and some kinetic energy is converted into Zeeman energy. (c) By applying an optical pumping pulse of  $\sigma^-$  polarized light, one can polarize the cloud again, but with a decrease in the temperature since the optical pumping process deposits an energy which is only on the order of the recoil energy. The excess Zeeman energy is taken away by the spontaneously emitted photons.

good results [8, 22]. In the case of short-range van der Waals interactions and low energy scattering further simplification can be made, namely the van der Waals interaction potential  $V_{\text{vdW}}(\mathbf{r} - \mathbf{r}')$  may be replaced by the pseudo-potential

$$\frac{4\pi\hbar^2 a}{m} \delta(\mathbf{r} - \mathbf{r}') \frac{\partial}{\partial |\mathbf{r} - \mathbf{r}'|} |\mathbf{r} - \mathbf{r}'|. \quad (4.1)$$

This result has been obtained for the first time in the seminal paper by Huang and Yang [80] for the case of a gas of hard spheres. It has however more general meaning and holds for arbitrary short-range potentials. In the language of many-body theory it is the result of the  $T$ -matrix, or ladder approximation applied to many-body systems [4]. It amounts to the resummation of diagrams corresponding to multiple two-body scattering. Note that when acting on a non-singular function, the pseudo-potential is not different from the simple contact (Fermi) potential  $4\pi\hbar^2 a \delta(\mathbf{r} - \mathbf{r}')/m$ . This is however not true when we deal with singular, yet square integrable functions. In fact, strictly speaking, the contact potential  $4\pi\hbar^2 a \delta(\mathbf{r} - \mathbf{r}')/m$  is mathematically ill-defined [81].

In the mean-field theory, where the use of contact interactions is legitimate, the order parameter  $\psi(\mathbf{r}, t)$  of the condensate is the solution of the Gross–Pitaevskii equation (GPE) [8]:

$$i\hbar \frac{\partial \psi}{\partial t} = -\frac{\hbar^2}{2m} \Delta \psi + (V_{\text{ext}} + g|\psi|^2)\psi. \quad (4.2)$$

The non-linear term proportional to  $g$  accounts for the effect of interactions within the mean-field approximation, and  $V_{\text{ext}}$  denotes the external potential. The normalization of  $\psi$  chosen here is  $\int |\psi|^2 = N$ , where  $N$  is the total atom number.

#### 4.2. Validity of non-local Gross–Pitaevskii equation

In the simple man’s approach, to include dipolar effects, one just needs to add an extra term to the mean-field potential  $g|\psi|^2$  to account for the effect of the dipole–dipole interaction, and

one gets

$$i\hbar \frac{\partial \psi}{\partial t} = -\frac{\hbar^2}{2m} \Delta \psi + (V_{\text{ext}} + g|\psi|^2 + \Phi_{\text{dd}})\psi, \quad (4.3)$$

where  $\Phi_{\text{dd}}$  is the dipolar contribution to the mean-field interaction:

$$\Phi_{\text{dd}}(\mathbf{r}, t) = \int |\psi(\mathbf{r}', t)|^2 U_{\text{dd}}(\mathbf{r} - \mathbf{r}') d^3 r'. \quad (4.4)$$

This term is *non-local* (due to the long-range character of the dipolar interaction) and makes it much more complicated to solve the GPE, even numerically, as one now faces an integro-differential equation. In the time-independent case, the left-hand side of the above equation has to be replaced by  $\mu\psi$ , with  $\mu$  the chemical potential, and the GPE becomes

$$-\frac{\hbar^2}{2m} \Delta \psi + (V_{\text{ext}} + g|\psi|^2 + \Phi_{\text{dd}})\psi = \mu\psi. \quad (4.5)$$

It should be stressed that, due to the long-range and anisotropic character of the dipole–dipole interactions, it is by no means obvious that one can put the pseudo-potential and the real potential into one single equation—obviously this implies that the long- and short-range physics can somehow be treated separately.

Questions concerning the validity of (4.4) were a subject of intensive studies in recent years. In their pioneering papers, You and Yi [55, 56] have constructed, in the spirit of the ladder approximation, a pseudo-potential for the general case of anisotropic potentials. Their results were rigorous, but perturbative, in the sense that the Born scattering amplitude from the pseudo-potential reproduced the exact one. The conclusion was that, away from shape resonances, the generalized GPE (4.4) is valid, and the effective pseudo-potential has the form (assuming for instance that we deal with electric dipoles)

$$V_{\text{eff}}(\mathbf{r} - \mathbf{r}') = \frac{4\pi\hbar^2 a(d)}{m} \delta(\mathbf{r} - \mathbf{r}') \frac{\partial}{\partial |\mathbf{r} - \mathbf{r}'|} |\mathbf{r} - \mathbf{r}'| + \frac{1}{4\pi\epsilon_0} \frac{d^2 - 3(\mathbf{n} \cdot \mathbf{d})^2}{|\mathbf{r} - \mathbf{r}'|^3}, \quad (4.6)$$

where  $\mathbf{n} = (\mathbf{r} - \mathbf{r}')/|\mathbf{r} - \mathbf{r}'|$ , whereas  $a(d)$  depends effectively on the strength of the dipole moment  $d = |d|$  (see also [83]).

Derevianko succeeded in deriving a more rigorous version of the pseudo-potential with a velocity dependence [82], which was then used in [84] to calibrate the dipole interactions. The author predicted that the effects of dipole interactions should be significantly enhanced due to the velocity dependent part of the pseudo-potential. Unfortunately, these conclusions were too optimistic due to some incorrect factors in the expressions of [82, 85, 86].

Further important contributions to these questions came from Bohn and Blume [87, 88]. These authors studied the instability and collapse of the trapped dipolar gas and compared the mean-field (MF) results with diffusive Monte Carlo (DMC) calculations. The DMC results agreed quite accurately with the MF ones, provided the variation of the s-wave scattering length with the dipole moment was properly taken into account. In fact, this dependence had been already noted in [55, 56], and can be traced back to the fact that the rigorous form of dipole–dipole interactions contains already a contact  $\delta(\mathbf{r})$  term [58]. Very careful discussion of the differences between the GPE approach, and more exact numerical results of diffusive quantum Monte Carlo methods, were presented recently by Astrakharchik *et al* [89]. These authors point out several differences between DMC and GPE results in a wide range of parameters, especially reflected in the frequency of the low energy excitation ‘breathing’ mode. Very recently, Wang [90] has managed to derive a general effective many-body theory for polar molecules in the strongly interacting regime. Wang’s approach allows one to go beyond the Born approximation approach of Yi and You. One of the surprising results is that close to shape resonances, anisotropic effects of dipole–dipole interactions are strongly reduced. Phonon dispersion relations scale as  $\sqrt{|p|}$  as in the case of a Coulomb gas.

#### 4.3. Variational approach and hydrodynamics

The time-independent GPE can be obtained from the minimization of the energy functional:

$$E[\psi] = \int \left[ \frac{\hbar^2}{2m} |\nabla\psi|^2 + V_{\text{trap}}|\psi|^2 + \frac{g}{2}|\psi|^4 + \frac{1}{2}|\psi|^2 \int U_{\text{dd}}(\mathbf{r} - \mathbf{r}') |\psi(\mathbf{r}')|^2 d^3r' \right] d^3r. \quad (4.7)$$

In this context the chemical potential appears simply as a Lagrange multiplier arising from the constraint on the normalization of the macroscopic wavefunction  $\psi$ . Minimizing the energy functional (4.7) within a space of trial wavefunctions depending on a small number of variational parameters is a convenient way to approach in a simple manner a variety of problems; a typical example being the trap geometry dependence of the stability of a dipolar BEC (see section 5.3). Variational approaches can be extended to the time-dependent case by replacing the energy functional (4.7) by an appropriate Lagrange action [91, 92].

A useful reformulation of the Gross–Pitaevskii equation is obtained by writing  $\psi = \sqrt{n} \exp(iS)$ , with  $n$  the atomic

density and  $S$  the phase of the order parameter, related to the superfluid velocity field by  $\mathbf{v} = (\hbar/m)\nabla S$ . Substituting this expression in (4.3) and separating real and imaginary parts, one gets the following set of hydrodynamic equations:

$$\frac{\partial n}{\partial t} + \nabla \cdot (n\mathbf{v}) = 0, \quad (4.8)$$

which is nothing more than the equation of continuity expressing the conservation of mass, and an Euler-like equation:

$$m \frac{\partial \mathbf{v}}{\partial t} = -\nabla \left( \frac{m\mathbf{v}^2}{2} + gn + V_{\text{ext}} + \Phi_{\text{dd}} - \frac{\hbar^2}{2m} \frac{\Delta\sqrt{n}}{\sqrt{n}} \right). \quad (4.9)$$

The last term in (4.9), proportional to the Laplacian of  $\sqrt{n}$  is the *quantum pressure* term arising from inhomogeneities in the density and vanishes in the limit of BECs containing a large number of atoms (Thomas–Fermi limit, see section 5.4).

## 5. Ground-state properties and excitations

### 5.1. Homogeneous gas: phonon instability

Because of the partially attractive character of the dipole–dipole interaction, the stability of a dipolar BEC is a problem that needs to be addressed. Indeed it is well known [8] that a homogeneous condensate with attractive contact interactions ( $a < 0$ ) is unstable, as the Bogoliubov excitations have imaginary frequencies at low momentum.

We consider here a homogeneous dipolar condensate, having an equilibrium density  $n_0$ . By considering small density and velocity perturbations with frequency  $\omega$  and wavevector  $\mathbf{k}$ , and linearizing the hydrodynamic equations (4.8) and (4.9) around equilibrium, one can show that the excitation spectrum is given by

$$\omega = k \sqrt{\frac{n_0}{m} \left[ g + \frac{C_{\text{dd}}}{3} (3 \cos^2 \alpha - 1) \right] + \frac{\hbar^2 k^2}{4m^2}}, \quad (5.1)$$

which corresponds to the usual Bogoliubov spectrum  $\omega = k\sqrt{gn_0/m + \hbar^2 k^2/(4m^2)}$  [8] with the Fourier transform  $g$  of the contact interaction (1.1) complemented by that (2.5) of the dipole–dipole interaction. With the definition (3.3) for  $\varepsilon_{\text{dd}}$ , (5.1) implies that a dipolar uniform condensate is unstable for  $\varepsilon_{\text{dd}} > 1$ , as phonons ( $k \rightarrow 0$ ) acquire imaginary frequencies, the most unstable situation being in the case of a direction of the wavevector perpendicular to the orientation of the dipoles ( $\alpha = \pi/2$ ). At first sight, this might seem counterintuitive: as dipoles side by side repel each other, one could conclude (wrongly) that the most unstable phonons correspond to those for which  $\mathbf{k}$  is parallel to the dipoles. Figure 7 shows how one can understand intuitively this behavior.

### 5.2. Trapped gas: elongation of the cloud

As in the case of a BEC with contact interactions, in the presence of an external trap (usually harmonic in experiments) new properties arise for a dipolar condensate. A prominent effect of the dipole–dipole interaction is to elongate the

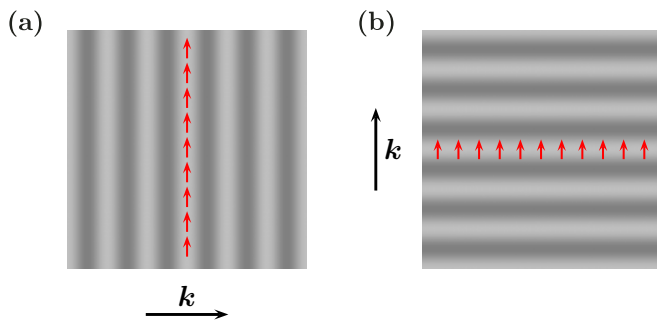


**Figure 7.** (a) A phonon with  $k$  perpendicular to the direction of dipoles ( $\alpha = \pi/2$ ) creates planes of higher density (light gray), in which the dipoles are *in* the plane, corresponding to an instability (see section 5.3 for a discussion of the geometry dependence of the stability of a trapped dipolar gas). (b) For  $k$  parallel to the direction of dipoles ( $\alpha = 0$ ) the dipoles point *out* of the planes of high density; such a perturbation is thus stable.

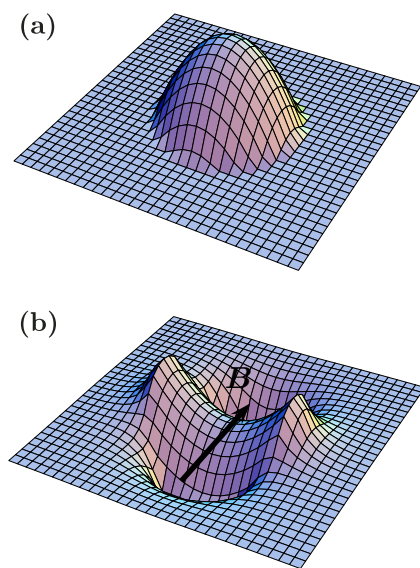


**Figure 8.** (a) Inverted parabola density distribution  $n(r)$  in the Thomas-Fermi regime in the absence of dipole-dipole interaction. (b) Saddle-like mean-field dipolar potential (5.2) induced by the density distribution displayed in (a).

condensate along the direction  $z$  along which the dipoles are oriented [56, 93, 94]. This *magnetostriction* effect (a change of the shape and volume of the atomic cloud due to internal magnetic forces) can be understood in a very simple way for a spherically symmetric trap (of angular frequency  $\omega$ ) in the perturbative regime  $\varepsilon_{\text{dd}} \ll 1$ . To zeroth order, the density distribution is given, in the Thomas-Fermi limit, by  $n(r) = n_0(1 - r^2/R^2)$ , where  $R$  is the Thomas-Fermi radius of the condensate (see figure 8(a)). One can then calculate to first order in  $\varepsilon_{\text{dd}}$  the mean-field dipolar potential (4.4) created by this distribution; one finds [41]

$$\Phi_{\text{dd}}(\mathbf{r}) = \varepsilon_{\text{dd}} \frac{m\omega^2}{5} (1 - 3\cos^2\theta) \begin{cases} r^2 & \text{if } r < R, \\ \frac{R^5}{r^3} & \text{if } r > R, \end{cases} \quad (5.2)$$

i.e. the dipolar mean-field potential has the shape of a saddle, with minima located on the  $z$ -axis (see figure 8(b)). It is therefore energetically favorable for the cloud to become

elongated along  $z$ . One can actually show that this conclusion remains valid even if the cloud is anisotropic, and for larger values of  $\varepsilon_{\text{dd}}$  [95–97].

Very recently, the spatial extent of a  $^7\text{Li}$  BEC was studied as a function of the scattering length close to a Feshbach resonance [98]. For very small scattering lengths, the elongation effect due to the dipole-dipole interaction could be seen unambiguously, in spite of the small value of the magnetic dipole moment.

### 5.3. Trapped gas: geometrical stabilization

A BEC with pure contact *attractive* interactions ( $a < 0$ ) is unstable in the homogeneous case, but, in a trap, stabilization by the quantum pressure can occur for small atom numbers, namely if

$$\frac{N|a|}{a_{\text{ho}}} \leq 0.58, \quad (5.3)$$

where  $N$  is the atom number and  $a_{\text{ho}} = \sqrt{\hbar/(m\omega)}$  is the harmonic oscillator length corresponding to the trap frequency  $\omega$  [99]. Here the trap has been supposed isotropic, but, for anisotropic traps, the dependence on the trap geometry is weak [100].

The situation is radically different in the case of a BEC with dipolar interactions. Due to the anisotropy of the dipole-dipole interaction, the partially attractive character of the interaction can be ‘hidden’ by confining the atoms more strongly in the direction along which the dipoles are aligned. Let us consider for simplicity a cylindrically symmetric trap, with a symmetry axis  $z$  coinciding with the orientation of the dipoles. The axial (resp. radial) trapping frequency is denoted as  $\omega_z$  (respectively  $\omega_\rho$ ). It is then intuitively clear that for a prolate trap (aspect ratio  $\lambda = \omega_z/\omega_\rho < 1$ ), the dipole-dipole interaction is essentially attractive, and in such a trap a dipolar BEC should be unstable, even in the presence of a (weak) repulsive contact interaction (see figure 9(a)). In contrast, in a very oblate trap, the dipole-dipole interaction is essentially repulsive, leading to a stable BEC even in the presence of weak attractive contact interactions (see figure 9(b)). One therefore expects that, for a given value of  $\lambda$ , there exists a critical value  $a_{\text{crit}}$  of the scattering length below which a dipolar BEC is unstable; from the discussion above,  $a_{\text{crit}}$  should intuitively be a decreasing function of  $\lambda$ , and the asymptotic value of  $a_{\text{crit}}$  for  $\lambda \rightarrow 0$  (respectively  $\lambda \rightarrow \infty$ ) should be positive (respectively negative).

A simple way to go beyond this qualitative picture and obtain an estimate for  $a_{\text{crit}}(\lambda)$  is to use a variational method. For this purpose, we assume that the condensate wavefunction  $\psi$  is Gaussian, with an axial size  $\sigma_z$  and a radial size  $\sigma_\rho$  that we take as variational parameters:

$$\psi(r, z) = \sqrt{\frac{N}{\pi^{3/2}\sigma_\rho^2\sigma_z a_{\text{ho}}^3}} \exp\left[-\frac{1}{2a_{\text{ho}}^2}\left(\frac{r^2}{\sigma_\rho^2} + \frac{z^2}{\sigma_z^2}\right)\right]. \quad (5.4)$$

Here,  $a_{\text{ho}} = \sqrt{\hbar/(m\bar{\omega})}$  is the harmonic oscillator length corresponding to the average trap frequency  $\bar{\omega} = (\omega_\rho^2\omega_z)^{1/3}$ . Inserting ansatz (5.4) into the energy functional (4.7) leads to the following expression for the energy:

$$E(\sigma_\rho, \sigma_z) = E_{\text{kin}} + E_{\text{trap}} + E_{\text{int}}, \quad (5.5)$$

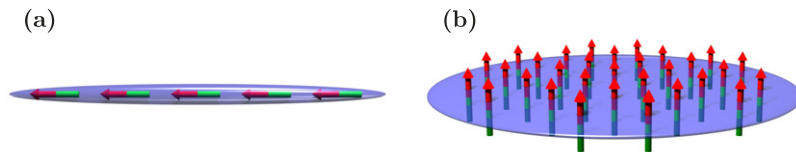


**Figure 9.** Intuitive picture for the geometry-dependent stability of a trapped dipolar BEC. (a) In a prolate (cigar-shaped) trap with the dipoles oriented along the weak confinement axis of the trap, the main effect of the dipole–dipole interaction is attractive, which leads to an instability of the condensate. (b) In an oblate (pancake-shaped) trap with the dipoles oriented along the strong confinement axis, the dipole–dipole interaction is essentially repulsive, and the BEC is stable.

with the kinetic energy

$$E_{\text{kin}} = \frac{N\hbar\bar{\omega}}{4} \left( \frac{2}{\sigma_\rho^2} + \frac{1}{\sigma_z^2} \right), \quad (5.6)$$

the potential energy due to the trap

$$E_{\text{trap}} = \frac{N\hbar\bar{\omega}}{4\lambda^{2/3}} (2\sigma_\rho^2 + \lambda^2\sigma_z^2) \quad (5.7)$$

and the interaction (contact and dipolar) energy

$$E_{\text{int}} = \frac{N^2\hbar\bar{\omega}a_{\text{dd}}}{\sqrt{2\pi}a_{\text{ho}}}\frac{1}{\sigma_\rho^2\sigma_z} \left( \frac{a}{a_{\text{dd}}} - f(\kappa) \right). \quad (5.8)$$

The dipolar contribution in the last part is most easily calculated in momentum space as

$$\begin{aligned} E_{\text{dd}} &= \frac{1}{2} \int n(\mathbf{r})n(\mathbf{r}')U_{\text{dd}}(\mathbf{r}-\mathbf{r}')d^3r d^3r' \\ &= \frac{1}{2(2\pi)^3} \int \widetilde{U}_{\text{dd}}(\mathbf{k})\tilde{n}^2(\mathbf{k})d^3k, \end{aligned} \quad (5.9)$$

where  $\tilde{n}(\mathbf{k})$  is the Fourier transform of the density distribution (and therefore, in this case, still a Gaussian). In (5.8),  $\kappa = \sigma_\rho/\sigma_z$  is the aspect ratio of the cloud (which differs from that of the trap due to the elongation induced by the dipole–dipole interaction as discussed above), and  $f$  is given by

$$f(\kappa) = \frac{1+2\kappa^2}{1-\kappa^2} - \frac{3\kappa^2 \text{artanh}\sqrt{1-\kappa^2}}{(1-\kappa^2)^{3/2}}. \quad (5.10)$$

The function  $f(\kappa)$ , displayed in figure 10, is monotonically decreasing, has asymptotic values  $f(0) = 1$  and  $f(\infty) = -2$  and vanishes for  $\kappa = 1$  (implying that for an isotropic density distribution the dipole–dipole mean-field potential averages to zero).

To determine the stability threshold  $a_{\text{crit}}(\lambda)$ , one needs to minimize (5.5) with respect to  $\sigma_\rho$  and  $\sigma_z$  for fixed values of  $N$ ,  $\lambda$  and  $\bar{\omega}$ . For  $a > a_{\text{crit}}$ , one has a (at least local) minimum of energy for finite values of  $\sigma_{\rho,z}$ , while as soon as  $a < a_{\text{crit}}$ , no such minimum exists. Figure 11 shows contour plots of  $E(\sigma_\rho, \sigma_z)$  for  $N = 20\,000$ ,  $\lambda = 10$  and different values of  $a$ , clearly showing that  $a_{\text{crit}}(10) \simeq -8.5a_0$  for the chosen parameters. In figure 13, the critical scattering length  $a_{\text{crit}}(\lambda)$  obtained in this way is shown as a thick line for  $\bar{\omega} = 2\pi \times 800$  Hz and  $N = 20\,000$  atoms. In the limit  $N \rightarrow \infty$ , the asymptotic behavior of this curve ( $a_{\text{crit}}^\infty(0) = a_{\text{dd}}$  and  $a_{\text{crit}}^\infty(\infty) = -2a_{\text{dd}}$ ) can be easily understood, as only the sign of the interaction term (5.8) (which scales as  $N^2$  and

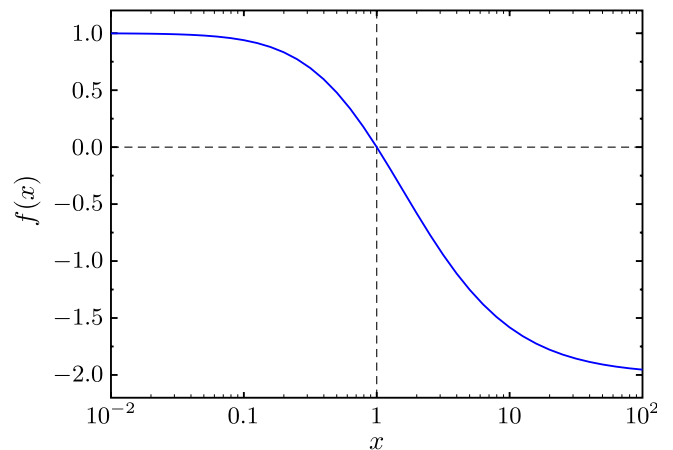


**Figure 10.** The function  $f(x)$  entering the calculation of the dipolar mean-field energy.

not as  $N$  like the kinetic and potential energy) determines the stability. For an extremely pancake-shaped trap  $\lambda \rightarrow \infty$ , the cloud has an aspect ratio  $\kappa \rightarrow \infty$ , and, as  $\lim_{x \rightarrow \infty} f(x) = -2$ , the condensate is (meta-)stable only if  $a > -2a_{\text{dd}}$ . In the same way, one readily understands that for  $\lambda \rightarrow 0$ , the critical scattering length is  $a_{\text{dd}}$ . The minimal value of  $\lambda$  for which a purely dipolar condensate ( $a = 0$ ) is stable is the one for which  $\kappa = 1$  and is found numerically to be close to  $\lambda \simeq 5.2$  [56, 93, 96, 101, 102].

In [102], the influence of the trapping geometry on the stability of a  $^{52}\text{Cr}$  BEC was investigated experimentally. A combination of an optical dipole trap and one site of a long period (7  $\mu\text{m}$ ) optical lattice provided an harmonic trap cylindrically symmetric along the  $z$ -direction (along which the dipoles are aligned), with an aspect ratio  $\lambda$  that could be varied over two orders of magnitude (from  $\lambda \simeq 0.1$ —prolate trap—to  $\lambda \simeq 10$ —oblate trap—), while keeping the average trap frequency  $\bar{\omega} = (\omega_\rho^2\omega_z)^{1/3}$  almost constant (with a value of  $2\pi \times 800$  Hz). Using the Feshbach resonance at 589 G, the scattering length was ramped adiabatically to a final value  $a$  and the atom number in the BEC was measured. A typical measurement is shown in figure 12. When  $a$  is reduced, the atom number decreases, first slowly, and then very abruptly when  $a$  approaches a critical value  $a_{\text{crit}}$ , below which no condensate can be observed. Figure 13 shows the measured value of  $a_{\text{crit}}$  as a function of  $\lambda$ . One clearly observes that for prolate traps,  $a_{\text{crit}}$  is close to  $a_{\text{dd}}$ , as expected from the discussion above, while for the most pancake-shaped trap  $\lambda = 10$  the critical scattering length is close to zero: for such a geometry, a purely dipolar condensate is stable. The solid

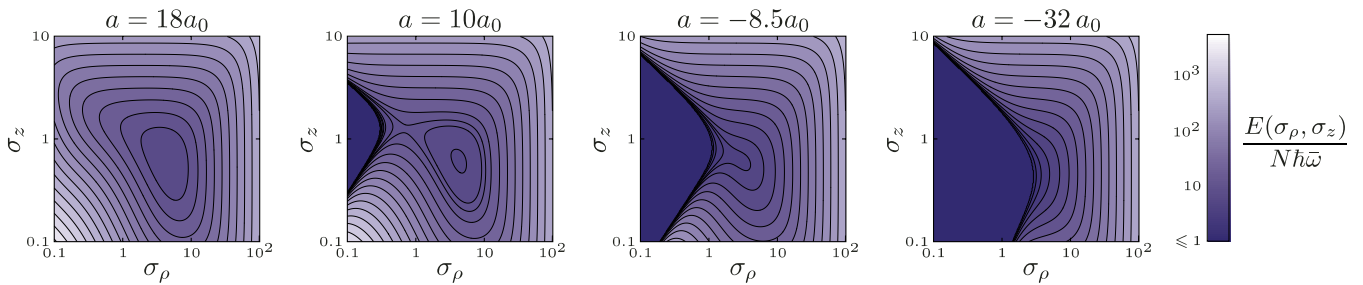


**Figure 11.** The energy landscape  $E(\sigma_\rho, \sigma_z)$  as a function of the variational parameters  $\sigma_\rho$  and  $\sigma_z$  of the Gaussian ansatz, for a trap of aspect ratio  $\lambda = 10$ , and various values of the scattering length  $a$ . When  $a$  decreases, one goes from a *global* minimum (at  $a = 18a_0$ ) to a *local* minimum corresponding to a metastable condensate (at  $a = 10a_0$ ). This local minimum vanishes at  $a = a_{\text{crit}}$  (here  $-8.5a_0$ ). Below  $a_{\text{crit}}$ , the energy can be lowered without bound by forming an infinitely thin cigar-shaped cloud.

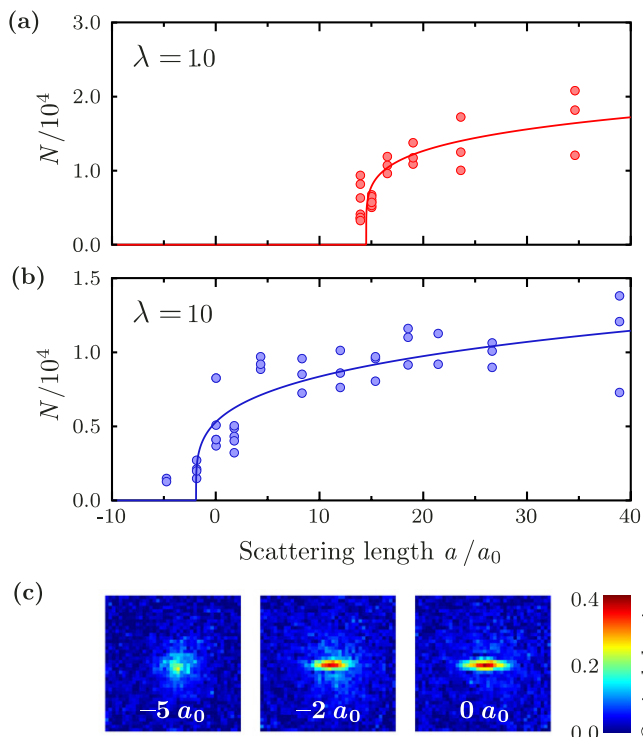


**Figure 12.** Experimental observation of the geometry-dependent stability of a dipolar BEC. (a) BEC atom number  $N$  as a function of  $a$  for a spherical trap;  $N$  vanishes for  $a$  smaller than  $a_{\text{crit}} \simeq 15a_0$ . (b) For an oblate trap ( $\lambda = 10$ ), one has  $a_{\text{crit}} \simeq -2a_0$ ; such a trap can thus stabilize a purely dipolar BEC. In (a) and (b) the solid lines are fits to the empirical threshold law  $(a - a_{\text{crit}})^\beta$ . (c) Sample images of the atomic cloud as a function of  $a$  for  $\lambda = 10$ .

line is the stability threshold  $a_{\text{crit}}(\lambda)$  obtained by the Gaussian ansatz for a number of atoms  $N = 2 \times 10^4$ , which shows good agreement with the measurements. Note that for the parameters used in the experiment, the critical scattering length for pure contact interaction, given by (5.3) would be  $-0.3a_0$  for  $\lambda = 1$ , which clearly shows that the instability is driven here by the dipole–dipole interaction.

To calculate the exact stability threshold, one needs to resort to a numerical solution of the GPE (4.3); the result of such a calculation [103] is displayed as a thin line in figure 13 and shows very good agreement with the data. The numerical solution reveals, for some values of the parameters  $(\lambda, a)$  close to the instability region, the appearance of ‘biconcave’

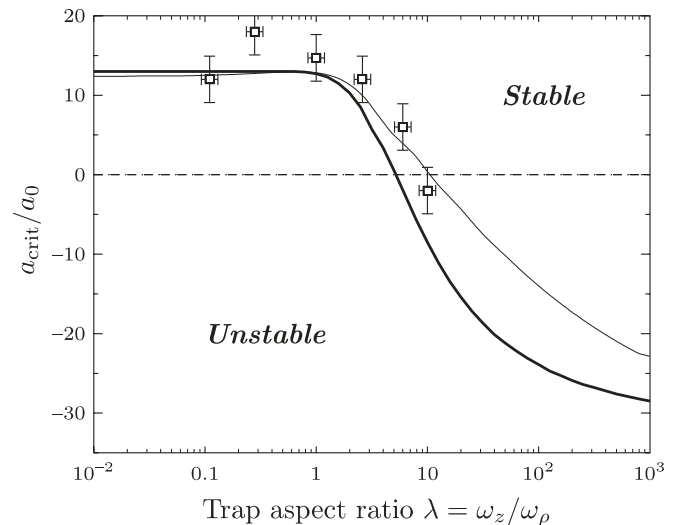


**Figure 13.** Stability diagram of a dipolar condensate in the plane  $(\lambda, a)$ . The dots with error bars correspond to the experimental data [102]; the thick solid line to the threshold  $a_{\text{crit}}(\lambda)$  obtained using the Gaussian ansatz (5.4) with  $N = 20\,000$ ; the thin solid line to the numerical solution of the GPE (4.3) [103].

condensates, where the density has a local minimum at the center of the trap [104]<sup>12</sup>.

#### 5.4. Trapped gas: Thomas–Fermi regime

As we shall see in the following sections, a very important approximation in the case of dipolar gases is the so-called Thomas–Fermi (TF) limit, in which quantum pressure effects are neglected. Amazingly, the TF solutions for the ground state of the trapped BEC have the same inverted parabola shape as in the case of contact interactions. This has been pointed out for the first time in [63], where, however, the trapping was restricted to the  $z$ -direction, while in the other directions

<sup>12</sup> The experimental observation of such biconcave condensate (which shows in a striking manner the long-range character of the dipole–dipole interaction) is difficult for several reasons: (i) the density dip does not survive in time of flight (which implies that *in situ* imaging would be needed to detect it), (ii) it has a small contrast of only a few per cent and (iii) the regions in the plane  $(\lambda, a)$  where the biconcave condensate exists have a very small area. However, the use of potentials flatter than harmonic traps, such as a quartic or a box-like potential, should relax considerably the constraints (ii) and (iii) (Ronen, 2008, private communication).

the systems were assumed to be homogeneous. The Thomas–Fermi approach was also used to study fermionic dipolar gases (see [105] and references therein).

The exact solutions of the dipolar BEC hydrodynamics in 3D were presented in a series of beautiful papers by O’Dell *et al* [95] and Eberlein *et al* [96]. These authors have used spheroidal coordinates and solved the TF equations for the ground state in cylindrically symmetric traps. They have also considered the stability of the three most relevant perturbations: local density perturbations, ‘scaling’ perturbations and ‘Saturn-ring’ perturbations. The subtle question of the applicability of the TF approximation in dipolar BECs was recently addressed in [106].

In particular, the ground state density in the cylindrically symmetric case has the form

$$n(\mathbf{r}) = n_0 \left( 1 - \frac{\rho^2}{R_x^2} - \frac{z^2}{R_z^2} \right), \quad (5.11)$$

for  $n(\mathbf{r}) \geq 0$ , where  $n_0 = 15N/(8\pi R_x^2 R_z)$ . These expressions are exactly the same as in the case of contact interactions. The difference is, of course, in the explicit expressions for the radii:

$$R_x = R_y = \left[ \frac{15gN\kappa}{4\pi m\omega_x^2} \left\{ 1 + \varepsilon_{\text{dd}} \left( \frac{3\kappa^2 f(\kappa)}{2(1-\kappa^2)} - 1 \right) \right\} \right]^{1/5}, \quad (5.12)$$

and  $R_z = R_x/\kappa$ . The condensate aspect ratio  $\kappa$  is determined by the transcendental equation

$$3\kappa\varepsilon_{\text{dd}} \left[ \left( \frac{\omega_z^2}{2\omega_x^2} + 1 \right) \frac{f(\kappa)}{1-\kappa^2} - 1 \right] + (\varepsilon_{\text{dd}} - 1)(\kappa^2 - \omega_z^2/\omega_x^2) = 0, \quad (5.13)$$

where  $f(\kappa)$  is defined in (5.10). A plot of the condensate aspect ratio as a function of  $\varepsilon_{\text{dd}}$  is shown in figure 14. The TF approach is also extremely useful to study the dynamics of dipolar condensates, for instance their free expansion (see section 6.1).

### 5.5. Trapped gas: excitations

The unusual properties of the ground state of dipolar condensates have their counterpart in the excitations of the system. They are expected to exhibit novel character and symmetries, as well as new types of instabilities. Indeed, as we shall see in the next subsection, even in the pancake traps with dipole moments polarized orthogonally to the pancake plane, the excitation spectrum reveals an instability, at the so-called roton–maxon minimum. Before discussing the pancake case, let us first consider in this section the case of a moderate aspect ratio of the trap.

The study of the excitations of a dipolar BEC should in principle be realized using the non-local Bogoliubov–de Gennes (BdG) equations. Such an approach is however technically very difficult, and for this reason approximate methods are useful. We discuss here the results of pioneering papers (see [55, 56, 101] and references therein). Góral and Santos [101] apply the dynamical variational principle, developed for the contact GPE in [91, 92]. The idea consists

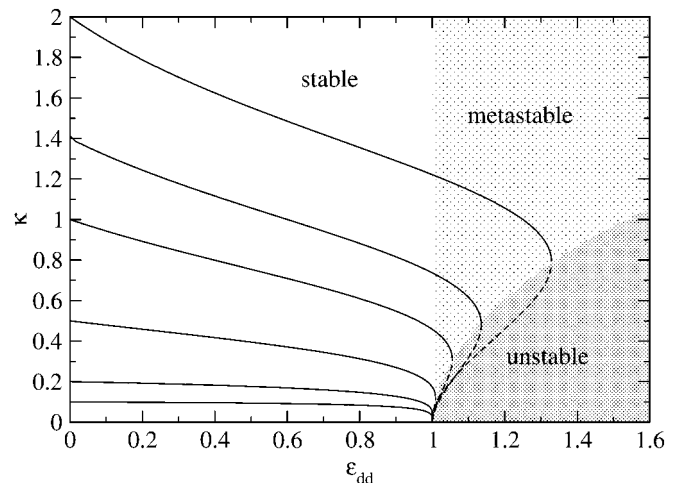


**Figure 14.** Aspect ratio  $\kappa$  of the condensate as a function of the dipole–dipole to s-wave coupling ratio  $\varepsilon_{\text{dd}}$ . Each line is for a different trap aspect ratio  $\gamma = \omega_z/\omega_x$ , which can be read off by noting that  $\kappa(\varepsilon_{\text{dd}} = 0) = \gamma$ . When  $0 < \kappa < 1$  the condensate is prolate; for  $\kappa > 1$  it is oblate. Likewise, for  $0 < \gamma < 1$  the trap is prolate, and when  $\gamma > 1$  the trap is oblate (figure courtesy of Eberlein).

of writing the time-dependent condensate wavefunction in the Gaussian form:

$$\psi(x, y, z, t) = A(t) \prod_{\eta=x,y,z} \exp[-\eta^2/2w_\eta(t)^2 - i\eta^2\beta_\eta(t)], \quad (5.14)$$

with time-dependent variational parameters describing the Gaussian widths  $w_\eta(t)$  and phases  $\beta_\eta(t)$ , while  $A(t)$  takes care of the normalization. The dynamical variational principle implies equations of motions for the widths and phases. Stationary solutions of these equations describe the ground state BEC, small deviations from the ground state describe the lowest energy excitations. Góral and Santos consider the case of a polarized dipolar gas and discuss the influence of dipole–dipole forces on the stability of the condensate and the excitation spectrum. The authors extend their discussion of the ground state and excitation properties to the case of a gas composed of the two anti-parallel dipolar components.

One of the most interesting results of this paper is the study of the nature of the collapse instability. In the standard case of contact interactions three modes are relevant at low energies (see figure 15): two ‘quadrupole’-like modes (1 and 3) and one ‘monopole’ mode (2). It is the latter one which becomes unstable at the collapse (when the scattering length changes sign). The frequency of the breathing monopole mode 2 goes to zero in a certain manner, namely, if  $\gamma$  denotes the ratio of the non-linear energy to the trap energy, and  $\gamma_c$  is correspondingly its critical value, the frequency of the breathing monopole mode 2 goes to zero as  $|\gamma - \gamma_c|^{1/4}$  [107, 108] when  $\gamma$  approaches criticality from below.

In the case of dipolar gases with dominant dipole interaction the situation is similar only for aspect ratios  $\lambda \ll 1$  far from criticality, where the lowest frequency mode is the breathing mode, and its frequency tends to zero as  $|\gamma_{\text{dd}} - \gamma_c|^\beta$ , with  $\beta \simeq 1/4$ , when the energy of the dipolar interactions

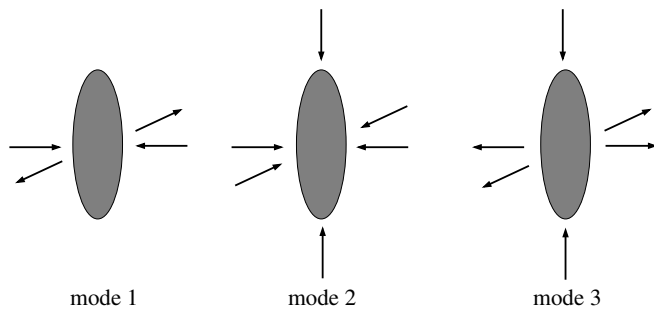


**Figure 15.** Graphical representation of the oscillation modes of the condensate; modes 1 and 3 are ‘quadrupole’-like, mode 2 is the breathing ‘monopole’ mode.

approaches the criticality. Numerical analysis indicates that as one approaches the criticality the exponent  $\beta$  remains close to  $1/4$ , but the geometry of the zero frequency mode is completely different: it attains the quadrupole character and becomes a superposition of modes 1 and 3. Very close to the criticality the exponent  $\beta$  grows up to the value  $\simeq 2$ . These results imply already that one should expect for the dipolar gas a completely different character of the collapse dynamics than for a gas with contact interactions and negative scattering length. We will discuss it in detail in the next section.

The variational method employing the Gaussian ansatz is evidently the simplest approach to study the excitations and dynamics of the dipolar BECs, and for this reason it was used by many authors. After the seminal experiments of the JILA group with  $^{85}\text{Rb}$ , in which efficient, i.e. practically loss-free control of the scattering length was achieved [109], Yi and You used this method to investigate the possibility of observing dipolar effects in the shape oscillations and expansion of a dipolar condensate [110, 111].

Direct solution of the Bogoliubov–de Gennes equations is, as we said, difficult, but not impossible. First of all, they become easier to solve in the Thomas–Fermi (TF) limit. The first step toward it was made in the ‘roton–maxon’ paper of Santos *et al* [63]. These authors considered an infinite pancake trap (i.e. a slab) with dipoles oriented along the  $z$ -direction and in the TF limit. It turns out that the density profile in the TF limit is given by an inverted parabola, just as in the case of the standard BEC [8]. The BdG equations for excitations close to the critical parameter region, where the ‘rotonization’ of the spectrum appears, can be solved analytically in terms of series of Gegenbauer polynomials, as we discuss in the next subsection.

Very recently, in a beautiful paper, Ronen *et al* [112] developed an efficient method for solving BdG equations for the dipolar BEC with cylindrical symmetry. The algorithm is very fast and accurate, and is based on an efficient use of the Hankel transform. The authors study excitations in different geometries (from cigar to pancake; for typical results of BdG spectra, see figure 16) and in particular they calculate for the first time the dipolar condensate depletion for various regimes of parameters.

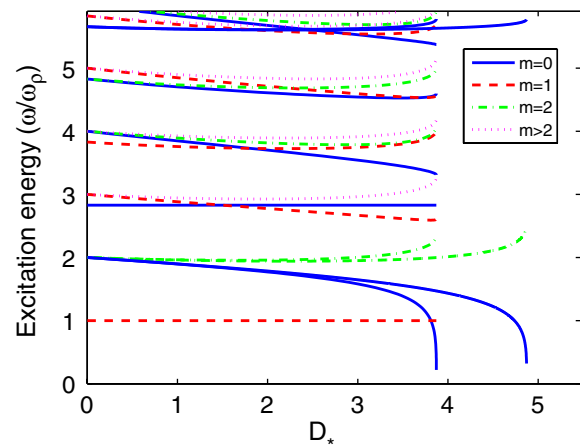


**Figure 16.** Excitation frequencies as a function of the dipolar parameter  $D_* = (N - 1)mC_{\text{dd}}/(4\pi\hbar^2 a_{\text{ho},\rho})$  for a dipolar BEC in the JILA pancake trap [113] ( $\omega_z/\omega_\rho = \sqrt{8}$ ), with a zero scattering length. Plotted are modes with  $m = 0 - 4$ . The three lines that extend to higher  $D_*$  are the variational results of [101] (figure courtesy of Ronen).

### 5.6. Trapped gas: roton–maxon spectrum

As we have mentioned, a dipolar gas exhibits two kinds of instabilities. In cigar-like traps, when the dipole is oriented along the trap axis, the dipolar interactions have an attractive character and the gas collapses. The collapse is similar to the case of the contact interactions with negative scattering length, but has a different geometrical nature, and different critical scaling behavior. There is, however, another instability mechanism that occurs even in quasi-2D pancake traps for dipoles polarized perpendicularly to the trap plane (along the  $z$ -axis). In this case, when the dipolar interactions are sufficiently strong, the gas, despite the quasi-2D trap geometry, feels the 3D nature of the dipolar interactions, i.e. their partially attractive character. This so-called ‘roton–maxon’ instability has been discovered in [63], and discussed by many authors since then.

In the original paper [63] the authors considered an infinite pancake trap (slab geometry) with dipoles oriented along the  $z$ -direction perpendicular to the trap plane. The roton–maxon physics occurs in the TF limit in the  $z$ -direction. The condensate was hence assumed to have a TF shape along the  $z$ -axis and constant amplitude with respect to  $x$  and  $y$  coordinates. The 3D Bogoliubov–de Gennes equations were then solved. Here, we follow a somewhat simplified effective 2D approach of [114], which nevertheless captures the main physics. The bosons are also polarized along the  $z$ -direction, so that the dipolar interaction in momentum space reads  $V_{\text{dd}} = C_{\text{dd}}(k_z^2/k^2 - 1/3)$ . We also introduce the ratio  $\beta = 3\varepsilon_{\text{dd}}/(4\pi)$ . As we shall see below, the cases of repulsive (attractive) contact interactions with  $g \geq 0$  ( $g < 0$ ) lead to qualitatively different physics. We first consider the case of positive  $g$ .

In the standard quasi-2D approach, one assumes that the condensate has a Gaussian shape along the  $z$ -direction, with the width determined by the harmonic potential. The problem is then projected onto 2D by integrating over the condensate profile. Such an approach is valid when the chemical potential

$\mu \ll \hbar\omega$ . However, the roton–maxon instability occurs outside this regime and hence the standard quasi-2D approach cannot be employed to understand it.

However we can still use an effective quasi-2D approach, where we assume that the bosonic wavefunction in the  $z$ -direction is given by the TF profile. In this way we may obtain an effectively 2D model with the dipole interactions ‘averaged’ along the  $z$ -direction. This approach corresponds approximately to the approach of [63], with the only difference being that for the lowest energy branch of excitations we neglect their ‘kinetic’ energy, i.e. terms in the Bogoliubov–de Gennes equation involving derivatives with respect to  $z$ . The quantitative differences between the exact results of [63], and the present effective quasi-2D approach amount typically to 10–20% in the entire regime of  $\beta \leq 2$  (which is the relevant regime for rotonization [63]). Qualitatively, both approaches describe the same physics and the same mechanism of appearance of the instability, namely the momentum dependence of the dipole–dipole interactions.

For the purpose of this review we apply yet another approximation, and use for simplicity a Gaussian profile in the  $z$ -direction with a variationally determined width  $\ell$ , which turns out to be of the order of the TF radius  $\ell \simeq \ell_{\text{TF}}/\sqrt{5}$ . The dipolar interaction in 2D, after integrating out the  $z$ -direction, takes the form

$$V_{\text{eff}} = \frac{C_{\text{dd}}}{4\pi\ell} \mathcal{V}(k_{\perp}),$$

where

$$\mathcal{V}(k_{\perp}) = 1 - \frac{3}{2} \sqrt{\frac{\pi}{2}} k_{\perp} \ell \operatorname{erfc}[k_{\perp} \ell / \sqrt{2}] \exp[k_{\perp}^2 \ell^2 / 2], \quad (5.15)$$

and  $k_{\perp}^2 = k_x^2 + k_y^2$ ,  $\tilde{k}_{\perp} = k_{\perp} \ell$ . The Hamiltonian that generated the Bogoliubov–de Gennes equations reduces then in the absence of the contact interactions, i.e. for  $g = 0$ , to  $H = \sum_{\mathbf{k}_{\perp}} \Omega(\mathbf{k}_{\perp}) b_{\mathbf{k}_{\perp}}^{\dagger} b_{\mathbf{k}_{\perp}}$ , where  $b_{\mathbf{k}_{\perp}}^{\dagger}$  and  $b_{\mathbf{k}_{\perp}}$  are Bogoliubov quasi-particle operators. The excitation spectrum is given, in units of the trap frequency, by

$$\Omega^2(\tilde{k}_{\perp}) = \frac{\tilde{k}_{\perp}^4}{4} + g_{3\text{d}} \mathcal{V}(\tilde{k}_{\perp}) \tilde{k}_{\perp}^2, \quad (5.16)$$

where the dimensionless interaction strength is defined as  $g_{3\text{d}} = mC_{\text{dd}}n\ell/(4\pi\hbar^2)$ . The interaction in (5.15) is repulsive for small momenta and attractive in the high momentum limit (with a zero-crossing at  $k_{\perp} \ell \simeq 1$ ). Due to this fact the properties of the excitation spectrum in (5.16) are very different from those of bosons with contact interactions. For any bosonic density,  $\Omega(\mathbf{k}_{\perp})$  exhibits two regimes: (i) phonon spectrum for small momenta and (ii) free particle spectrum for higher momenta. For  $g_{3\text{d}}$  greater than a certain critical value,  $\Omega(\mathbf{k}_{\perp})$  has a minimum (see figure 17) at the intermediate momentum regime. Following Landau, the excitations around the minimum are called ‘rotons’ and  $\Omega(\tilde{k}_0)$  is known as the ‘roton gap’ [63]. With increasing  $g_{3\text{d}}$  the ‘roton’ gap decreases and eventually vanishes for a critical particle density. When the critical density is exceeded,  $\Omega(\tilde{k}_0)$  becomes imaginary and the condensate becomes unstable.

Once more we stress that in the presence of repulsive contact interactions, the roton instability occurs in pancake

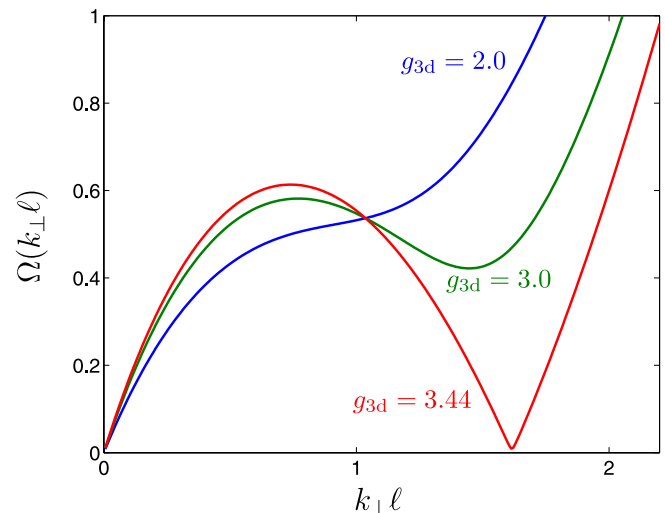


**Figure 17.** The excitation spectrum  $\Omega(k_{\perp})$  as a function of  $k_{\perp}$  for different values of  $g_{3\text{d}}$  (figure courtesy of Dutta).

traps in the regime in which the standard quasi-2D approximation does not hold. The condensate attains the TF profile in the  $z$ -direction and the systems start to experience the 3D (partially attractive) nature of the dipolar forces [115]. The situation is however different if the contact interactions are attractive ( $g < 0$ ). In that case the roton instability already appears in the standard quasi-2D regime, when the chemical potential  $\mu \ll \hbar\omega$ , when the condensate profile is Gaussian with the bare harmonic oscillator width. While in the previous case it was the attractive part of the dipolar interactions that led to the roton instability, in this quasi-2D situation with  $g < 0$  the situation is different. The dipolar interactions (which are on average repulsive in this case) stabilize for  $\mu = (g + 8\pi g_{\text{dd}}/3)n > 0$  the phonon instability (which in the absence of dipole–dipole interaction leads to the well-known collapse for gases with  $a < 0$ ) [116]. Note that  $\mu > 0$  but may be kept well below  $\hbar\omega_z$ . However, due to the momentum dependence of the dipole–dipole interaction (which acquires the form (5.15)), one encounters the roton instability for  $-3/8\pi < \beta < \beta_{\text{cr}}$  (where  $\beta_{\text{cr}}$  depends on the value of  $g$ ), whereas for  $\beta > \beta_{\text{cr}}$  the system is stable (as long as it remains 2D [117]). Note that in this case, a larger dipole strength stabilizes (sic!) the gas. The reason is that the roton in the quasi-2D scenario is not actually induced by the attractive nature of the dipolar interactions at large momenta, but by the fact that  $g < 0$ . As a consequence, quasi-2D roton may occur for much lower momenta than  $1/l_z$ .

The roton spectrum was also studied in quasi-1D geometries [118], a situation in which some analytical results can be obtained.

The presence of a roton minimum in the spectrum of elementary excitations may be revealed in various ways. On the one hand, and using Landau superfluidity criterion [119], it is clear that the superfluid critical velocity is reduced in the presence of a roton minimum [63]. Another alternative experimental signature of the roton could be provided at finite temperatures, where the thermal activation of rotons may induce a ‘halo’ effect in time-of-flight images [120]. Finally,

we would also like to point out that (as discussed in section 7.3) the presence of even a shallow roton minimum may alter dramatically the response of the system against a periodic driving [121].

The question of whether ‘there is a life after the roton instability’ was studied by many researchers, in the hope of finding novel types of stable Bose superfluids that would have supersolid character, i.e. self-assembled density modulations. This is suggested by the fact that the instability occurs at a specific value of the momentum, indicating instability toward a non-uniform ground state [122, 123]. The ultimate answer to the question is negative: the condensate undergoes a sequence of local collapses, as shown for the first time in [116, 124, 125]. In [116] it is shown numerically that in the mean-field theory supersolid states of dipolar BEC are unstable. The authors of [126] use a variational ansatz with density wave modulations along the  $z$ -direction in a cylindrically symmetric trap, and show that it is not stable for a dipolar gas due to the roton instability. It can, however, be stabilized, by allowing for admixture of a single component polarized Fermi gas. This idea was followed further in [127], where the stability of dipolar boson-fermion mixtures in pancake cylindrically symmetric traps was investigated at  $T = 0$  using a variational approach. Fermion-induced interactions stabilize the system in such traps and allow for quantum phase transition from the Gaussian shape BEC to a supersolid state, characterized by a hexagonal density wave.

Interestingly, while fermions stabilize dipolar bosons leading to a novel type of state, the opposite is also true: boson mediated interactions between polarized fermions may lead to the appearance of the ‘exotic’ Fermi superfluids with p-wave, f-wave or even h-wave pairing [114]. All of these states exhibit topological order, and admit non-Abelian anionic excitations [128] that can be used for topologically protected quantum information processing [129].

The discovery of the roton instability in dipolar gases stimulated the search for supersolid structures and density modulations. Ronen *et al* studied angular and radial roton instabilities in purely dipolar BECs in oblate traps [104], and have shown that in some situations the condensate attains a biconcave density profile (see the end of section 5.3). These results have been generalized to the case of finite temperature using the Hartree–Fock–Bogoliubov approach [130]. Such structures are very sensitive to changes in the trapping potential; their relation to the roton instabilities for the case of a trapped dipolar BEC without and with a vortex has been studied in [131]. Dutta and Meystre [124] predicted similar effects in anisotropic traps.

Very recently, the stability, excitations and roton instabilities have been discussed for the case of a dipolar BEC with a vortex [132]. Recent observation of the dipolar effects in Bloch oscillations with  $^{39}\text{K}$  [133, 134] with s-wave scattering tuned to zero stimulated studies of collective excitations and roton instabilities in multilayer stacks of dipolar condensates. In [117, 120], an enhancement of the roton instability was predicted. Note also that, interestingly, a gas of light-induced dipoles (see section 3.3) was predicted by Kurizki and co-workers to display roton instabilities [60].

Finally, let us stress that excitations in a 2D system of dipoles perpendicular to the 2D plane are well described by the Bogoliubov spectrum in the dilute regime. As the density is increased, the roton minimum appears. However, in this strictly 2D case, the roton gap never vanishes in the gas phase, because the interaction potential is purely repulsive. No instability is found as the density is increased; instead the dipolar system crystallizes, as shown in [135].

## 6. Dynamics of a dipolar gas

### 6.1. Self-similar expansion in the Thomas–Fermi regime

In most experiments on BECs, all the information is obtained from an absorption image of the cloud taken after a period of free expansion (‘time of flight’), which acts as a ‘magnifier’ allowing one to resolve optically the BEC (in a trap, the typical size of the BEC is on the order of a few micrometers, making it difficult to image it *in situ* with a good resolution). It is therefore of great practical importance to describe the expansion of a condensate released from a trap.

In the case of a BEC with contact interactions in a harmonic trap of frequencies  $\omega_i$  ( $i = x, y, z$ ) in the Thomas–Fermi limit (see section 5.4), a remarkable property allows for a very simple description of the free expansion [136, 137]: the in-trap density profile of the condensate (which is, in the Thomas–Fermi limit, an inverted parabola) is merely *rescaled* upon time of flight. The Thomas–Fermi radii  $R_i(t)$  at time  $t$  are given by

$$R_i(t) = R_i(0)b_i(t), \quad (6.1)$$

where the scaling parameters  $b_i$  are solution of the following set of coupled differential equations:

$$\ddot{b}_i = \frac{\omega_i^2(0)}{b_i b_x b_y b_z} \quad (i = x, y, z), \quad (6.2)$$

where  $\omega_i(0)$  stands for the trap frequency along the direction  $i$  before the trap is turned off.

The underlying reason for the existence of such a scaling solution is the fact that, for a parabolic density distribution  $n$ , the mean-field term  $gn$  is also quadratic in the coordinates, yielding only quadratic terms in the hydrodynamic equations (4.8) and (4.9). One can show that this property remains valid in the case of dipolar condensate in the Thomas–Fermi limit, as the following non-trivial property holds: if the density distribution  $n$  is parabolic  $n = n_0 \max(0, 1 - \sum_i x_i^2/R_i^2)$ , then the mean-field potential (4.4) due to the dipole–dipole interaction is a quadratic form in the coordinates<sup>13</sup>.

This property can be understood in the following way [96]. Starting from the identity

$$\frac{1 - 3z^2/r^2}{r^3} = -\frac{\partial^2}{\partial z^2} \frac{1}{r} - \frac{4\pi}{3} \delta(\mathbf{r}), \quad (6.3)$$

<sup>13</sup> As shown, in the much more restrictive case of a spherical trap and for  $\epsilon_{\text{dd}} \ll 1$ , in section 5.2 (see (5.2) and figure 8).

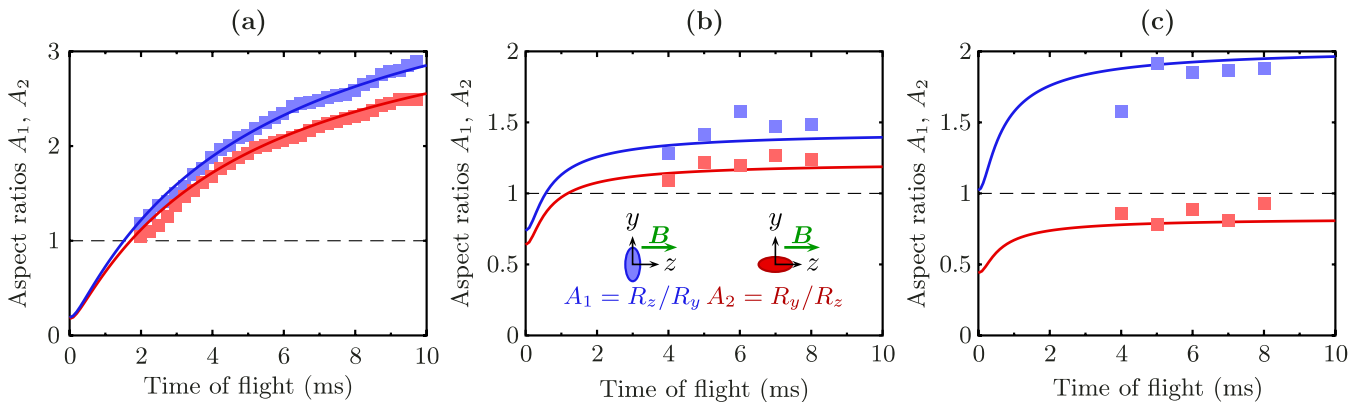


**Figure 18.** Free expansion of a dipolar condensate for two different orientations of the dipoles with respect to the trap axes. The squares are the experimental results; the solid lines are the prediction of the scaling equations (6.6) without any adjustable parameter. (a) Perturbative regime  $\varepsilon_{\text{dd}} = 0.16$ , the dipole–dipole interaction only gives a small departure from the contact interaction prediction (data taken from [97]). (b) Perturbative regime (for a different trap geometry)  $\varepsilon_{\text{dd}} \simeq 0.16$  far above the Feshbach resonance, the effect of the dipole–dipole interaction is similar to case (a). (c) Closer to the resonance, with  $\varepsilon_{\text{dd}} = 0.75$ ; in that case, the dipole–dipole interaction is strong enough to inhibit the usual inversion of ellipticity in time of flight. Data in (b) and (c) are taken from [73].

one can prove that

$$\Phi_{\text{dd}}(\mathbf{r}) = -C_{\text{dd}} \left( \frac{\partial^2}{\partial z^2} \phi(\mathbf{r}) + \frac{1}{3} n(\mathbf{r}) \right), \quad (6.4)$$

where

$$\phi(\mathbf{r}) = \int \frac{n(\mathbf{r}')}{4\pi|\mathbf{r} - \mathbf{r}'|} d^3 r'. \quad (6.5)$$

The last equality shows that the ‘potential’  $\phi$  fulfills Poisson’s equation  $\Delta\phi = -n$ . From this, one deduces that the most general form of  $\phi$ , when one has a parabolic density distribution  $n$ , is a polynomial of order two in the variables  $(x^2, y^2, z^2)$ , and thus, from (6.4), one deduces that  $\Phi_{\text{dd}}$  is also quadratic in  $(x, y, z)$ . The actual analytical calculation of the coefficients of this quadratic form, carried out for the cylindrically symmetric case in [95, 96] and for the general anisotropic case in [97], is far from trivial, especially in the latter case, which involves a generalization of (5.10) to two cloud aspect ratios.

One can then generalize Thomas–Fermi scaling equations (6.2) to the case of a condensate with both contact and dipolar interactions. The corresponding set of differential equations now reads as

$$\ddot{b}_i = \frac{\omega_i^2(0)}{b_i b_x b_y b_z} [1 + \varepsilon_{\text{dd}} F(b_x, b_y, b_z)] \quad (i = x, y, z), \quad (6.6)$$

where the function  $F$  includes the effect of the dipole–dipole interaction [97]. Solving these equations, one can for example study the time evolution, during free expansion, of the cloud aspect ratio to reveal the effects of the dipolar interaction (see section below).

### 6.2. A quantum ferrofluid

The superfluid hydrodynamic equations describing, e.g., the expansion of a condensate are modified by the long-range, anisotropic dipole–dipole interaction. In classical fluids, such magnetic interactions modifying the hydrodynamic properties

can be observed in *ferrofluids*, which are colloidal suspensions of nanometric ferromagnetic particles [32]. In that sense, a dipolar condensate can be called a *quantum ferrofluid*. As seen in the preceding section, a clear and simple way to demonstrate the effect of the dipole–dipole interaction is to study the expansion of the condensate when it is released from the trap.

By measuring the aspect ratio of the condensate as a function of the expansion time for two different orientations of the dipoles with respect to the trap axes, the elongation of the cloud along the magnetization direction could be clearly observed in [69, 97]. However, since  $\varepsilon_{\text{dd}} \simeq 0.16$  for  $^{52}\text{Cr}$  away from Feshbach resonances, the effect, shown in figure 18(a), is small. By using the 589 G Feshbach resonance in order to decrease the scattering length  $a$  and thus enhance  $\varepsilon_{\text{dd}}$ , a much larger effect of the dipole–dipole interaction on the expansion dynamics was observed in [73]. For example, by increasing  $\varepsilon_{\text{dd}}$  to values close to one, the usual inversion of ellipticity of the condensate during the time of flight is inhibited by the strong dipolar forces which keep the condensate elongated even during the expansion, as shown, for example, by the red curve in figure 18(c).

### 6.3. Collapse dynamics

The dynamics of a condensate with pure contact interactions when the scattering length is ramped to a negative value, thus making the condensate unstable, is extremely rich: one observes a fast implosion (‘collapse’) of the condensate, followed by inelastic losses and a subsequent ‘explosion’ of the remnant condensate accompanied by energetic bursts of atoms. The behavior of those ‘Bose–Novae’ has been extensively studied with  $^{85}\text{Rb}$  and  $^7\text{Li}$  condensates [109, 138–140]. More recently, the formation of soliton trains during collapse has been reported [141, 142]. It is then natural to ask whether the collapse of a dipolar condensate displays some specific features arising from the long-range and anisotropic character of the dipole–dipole interaction [143].

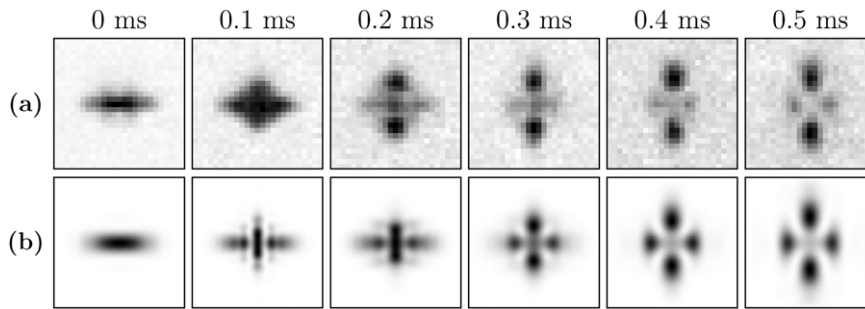


**Figure 19.** (a) Experimental images of a dipolar condensate after collapse and explosion as a function of the time  $t_{\text{hold}}$  between the crossing of the critical scattering length for instability and the release from the trap. The time of flight is 8 ms. (b) Results of a numerical simulation of the collapse dynamics without any adjustable parameter. The field of view is  $130 \mu\text{m} \times 130 \mu\text{m}$ .

In [144], the collapse dynamics of a dipolar  $^{52}\text{Cr}$  BEC when the scattering length  $a$  is decreased (by means of a Feshbach resonance) below the critical value for stability  $a_{\text{crit}}$  was investigated experimentally. A BEC of typically 20 000 atoms was created in a trap with frequencies  $(\nu_x, \nu_y, \nu_z) \simeq (660, 400, 530)$  Hz at a magnetic field of  $\sim 10$  G above the 589 G Feshbach resonance, where the scattering length is  $a \simeq 0.9 a_{\text{bg}}$ . The scattering length  $a$  was then ramped down rapidly to a value  $a_f = 5a_0$ , which is below the collapse threshold  $a_{\text{crit}} \simeq 13a_0$ . After the ramp, the system evolved for an adjustable time  $t_{\text{hold}}$  and then the trap was switched off. The cloud was then imaged after time of flight. The atomic cloud had a clear bimodal structure, with a broad isotropic thermal cloud, well fitted by a Gaussian, and a much narrower, highly anisotropic central feature, interpreted as the remnant BEC. Figure 19(a) shows the time evolution of the condensate when  $t_{\text{hold}}$  is varied. From an initial shape elongated along the magnetization direction  $z$ , the condensate rapidly develops a complicated structure with an expanding, torus-shaped part close to the  $z = 0$  plane. Interestingly, the angular symmetry of the condensate at some specific times (e.g. at  $t_{\text{hold}} = 0.5$  ms) is reminiscent of the d-wave angular symmetry  $1 - 3 \cos^2 \theta$  of the dipole–dipole interaction. Figure 19(b) displays the column density  $\int |\psi(\mathbf{r})|^2 dx$  obtained from a numerical simulation of the three-dimensional GPE

$$i\hbar \frac{\partial \psi}{\partial t} = \left[ \frac{-\hbar^2}{2m} \Delta + V_{\text{trap}} + \int U(\mathbf{r} - \mathbf{r}', t) |\psi(\mathbf{r}', t)|^2 d^3 r' - \frac{i\hbar L_3}{2} |\psi|^4 \right] \psi, \quad (6.7)$$

where

$$U(\mathbf{r}, t) = \frac{4\pi\hbar^2 a(t)}{m} \delta(\mathbf{r}) + \frac{\mu_0 \mu^2}{4\pi} \frac{1 - 3 \cos^2 \theta}{r^3} \quad (6.8)$$

stands for both contact and dipolar interactions. The non-unitary term proportional to  $L_3 \sim 2 \times 10^{-40} \text{ m}^6 \text{ s}^{-1}$  describes three-body losses that occur close to the Feshbach resonance. The agreement between the experimental data and the simulation, performed without any adjustable parameter, is excellent.

The observed cloverleaf patterns are caused by the anisotropic collapse and the subsequent dynamics of the

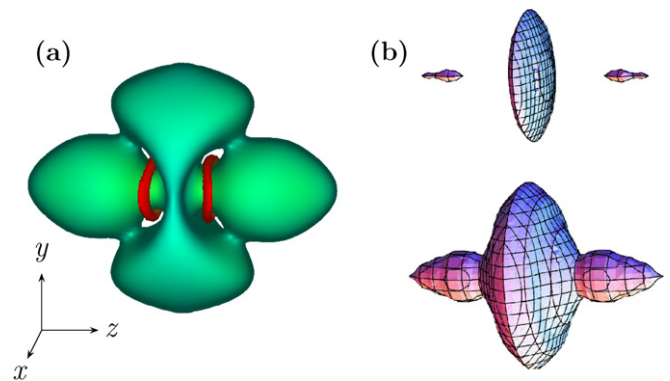


**Figure 20.** Iso-density surfaces of a dipolar BEC after collapse and explosion. (a) Simulation result, showing the location of vortex rings (in red/gray), for the conditions of [144]. (b) Experimentally reconstructed iso-density surfaces (using the inverse Abel transform) for high and low density (top and bottom, respectively) in the case of a cylindrically symmetric situation [145].

system: when the atomic density grows due to the attractive interaction, three-body losses predominantly occur in the high-density region. The centripetal force is then decreased, and the atoms that gathered in this narrow central region are ejected due to the quantum pressure arising from the uncertainty principle. The kinetic energy is supplied by the loss of the negative interaction energy. The collapse occurs mainly in the  $x$ – $y$  direction due to anisotropy of the dipole–dipole interaction (in the absence of inelastic losses, the condensate would indeed become an infinitely thin cigar-shaped cloud along  $z$ , see section 5.3), and therefore the condensate ‘explodes’ essentially radially producing the anisotropic shape of the cloud.

During the collapse, the BEC atom number, which was initially  $N_{\text{BEC}}(0) \simeq 16\,000$ , dropped to a value  $\sim 6000$ . The missing atoms very likely escaped from the trap as energetic molecules and atoms produced in three-body collisions. The simulated atom number as a function of  $t_{\text{hold}}$  matched very well the experimental data.

The numerical simulation gives access not only to the density  $|\psi(\mathbf{r})|^2$ , but also to the phase  $S(\mathbf{r})$  of the order parameter  $\psi$  (i.e. to the velocity field  $\mathbf{v} = \hbar \nabla S / m$ ) and reveals the generation of vortex rings. Figure 20(a) shows the simulated in-trap iso-density surface of a condensate at  $t_{\text{hold}} = 0.8$  ms and the location of the vortex rings (shown as

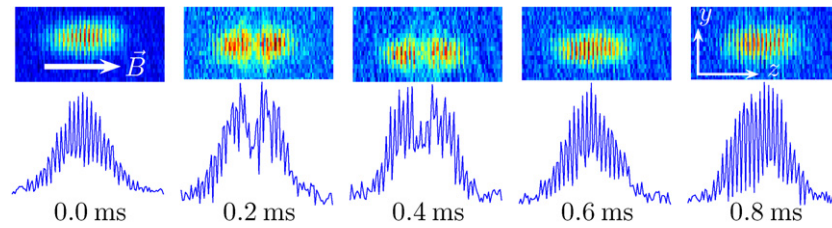


**Figure 21.** Interference pattern of independent condensates for different holding times  $t_{\text{hold}}$  [145].

red curves). The mechanism responsible for the formation of vortex rings can be understood intuitively as follows. During the collapse, due to the strong anisotropy of the dipole–dipole interaction, the atoms ejected in the  $x$ – $y$  plane flow outward, while the atoms near the  $z$ -axis still flow inward, giving rise to the circulation. Thus, the vortex-ring formation is specific to the d-wave collapse induced by the dipole–dipole interaction. Although the vortex rings are not observed directly in the experiment (even when reconstructing the 3D density distribution by means of the inverse Abel transform), the excellent agreement between the experiment and the simulations strongly suggests the creation of vortex rings during the collapse.

In [145], the collapse dynamics of a dipolar BEC was studied for different trap geometries, from prolate to oblate traps. The latter being created by superimposing a large period optical lattice onto the optical trap, it was possible to prepare independent condensates, let them collapse by changing the scattering length and then release the confinement. The observation of high contrast interference fringes after the clouds overlapped (see figure 21) proved for the first time that the post-collapse remnant clouds are truly coherent matter-wave fields.

The collapse observed here has the same physical origin as the phonon instability discussed in section 5.1, and should be distinguished from other possible collapse mechanisms, in particular the roton instability discussed in section 5.6. Note also that the phonon instability in two-dimensional geometries [146] does not necessarily lead to collapse, as we discuss in section 7.3. Recent studies [147, 148] address the collapse dynamics with an emphasis on the fact that *local* collapses can be used as a signature of the roton instability.

## 7. Non-linear atom optics with dipolar gases

As mentioned in section 4, BEC physics is inherently non-linear due to the interparticle interactions. Non-dipolar BECs obey the non-linear Schrödinger equation (NLSE) (4.2), which is identical to that appearing in non-linear optics of Kerr media. Striking resemblances between both fields have been observed, including non-linear atom optics phenomena as four-wave mixing [149], BEC collapse [109] and the creation of bright [141, 150], dark [151–153] and gap [154] solitons. Dipolar BECs obey the NLSE (4.3), where the non-linearity is intrinsically non-local, due to the long-range character of the dipole–dipole interaction. Non-locality appears in many different physical systems, including plasmas [155], where the non-local response is induced by

heating and ionization, nematic liquid crystals, where it is the result of long-range molecular interactions [156], and also photorefractive media [157]. Most interestingly, non-locality plays a crucial role in the physics of solitons and modulational instability [158, 159]. In this section, we review some recent results concerning the non-linear atom optics with dipolar BECs, including qualitatively new phenomena in bright and dark solitons (for recent works on vector and discrete solitons see [160] and [161]), vortices and pattern formation.

### 7.1. Solitons

Since the seminal works of Zakharov [162] it is known that the 1D NLSE with focusing local cubic non-linearity supports the existence of localized waves that travel with neither attenuation nor change of shape due to the compensation between dispersion and non-linearity. These so-called bright solitons occur in diverse fields, most prominently in non-linear optics [163]. Matter-wave bright solitons have been observed in quasi-1D condensates with  $a < 0$  [141, 150]. The quasi-1D condition requires a tight transversal harmonic trap of frequency  $\omega_{\perp}$  such that  $\hbar\omega_{\perp}$  exceeds the mean-field interaction energy. This in turn demands the transversal BEC size to be smaller than the soliton width. When this condition is violated the soliton becomes unstable against transversal modulations, and hence multi-dimensional solitons are not stable in non-dipolar BECs.

Remarkably the latter is not necessarily true in the presence of non-local non-linearity. In particular, any symmetric non-local non-linear response with positive definite Fourier spectrum has been mathematically shown to arrest collapse in arbitrary dimensions [159]. Multidimensional solitons have been experimentally observed in nematic liquid crystals [164] and in photorefractive screening media [165], as well as in classical ferrofluids [166]. Multidimensional solitons have also been discussed in BECs with short-range interactions, by considering the collapse inhibition induced by the first non-local correction to the local pseudo-potential [158, 167]. However, this occurs for an extremely small BEC size [167], which, except for the case of a very small particle number, leads to extremely large densities, at which three-body losses destroy the BEC.

Dipolar BECs in contrast introduce a non-locality at a much larger length scale. As a consequence, and in spite of the fact that, due to the anisotropy of the dipole–dipole interaction, the non-local non-linear response is not positive definite, 2D bright solitons may become stable under appropriate conditions [168]. This may be understood from

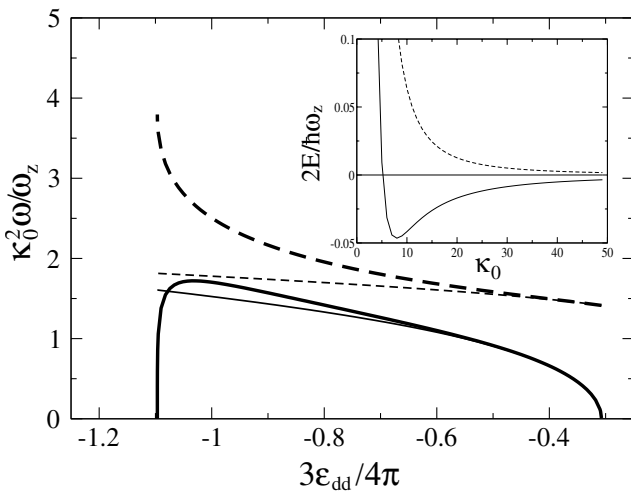


**Figure 22.** Breathing (bold solid) and  $m = \pm 2$  quadrupole (bold dashed) mode of a 2D bright soliton for  $\tilde{g} = 20$ , with  $\kappa_0 = l_\rho/l_z$  the ratio between the condensate widths perpendicular to and along the dipole orientation. Results from a reduced 2D NLSE [168] are shown in thin lines. Inset:  $E(\kappa_0)$  for  $\tilde{g} = 500$  and  $\varepsilon_{dd} = -0.42$  (dashed) and  $\varepsilon_{dd} = -0.84$  (solid).

a simplified discussion where we consider no trapping in the  $xy$ -plane and a strong harmonic confinement with frequency  $\omega_z$  in the  $z$ -direction, along which the dipoles are oriented. A good insight into the stability of 2D solitons may be obtained from a Gaussian ansatz  $\Psi(\mathbf{r}) \propto \exp(-\rho^2/2l_\rho^2 - z^2/2l_z^2)$ , where  $l_z = \sqrt{\hbar/m\omega_z}$  and  $l_\rho = \kappa_0 l_z$  is the  $xy$ -width. Introducing this ansatz into the non-local NLSE (4.3) we obtain the system energy, which up to a constant is

$$E = \frac{\pi \hbar \omega_z}{\kappa_0^2} \{2\pi + \tilde{g}[1 - \varepsilon_{dd} f(\kappa_0)]\}, \quad (7.1)$$

where  $\tilde{g} = g/\sqrt{2\pi\hbar\omega_z}l_z^3$  and  $f(\kappa)$  is defined in (5.10). As mentioned above, in the absence of dipole–dipole interaction ( $\varepsilon_{dd} = 0$ ), 2D localized solutions are unstable, since  $E(\kappa_0) \propto \kappa_0^{-2}$  either grows with  $L_\rho$  (collapse instability) or decreases with  $L_\rho$  (expansion instability). Dipolar BECs are remarkably different due to the additional dependence  $f(\kappa_0)$ , which may allow for a minimum in  $E(\kappa_0)$  (inset in figure 22), i.e. for a stable localized wavepacket. From the asymptotic values  $f(0) = -1$  and  $f(\infty) = 2$  localization is just possible if  $\varepsilon_{dd}\tilde{g} < 2\pi + \tilde{g} < -2\varepsilon_{dd}\tilde{g}$ . A simple inspection shows that this condition is fulfilled only if  $\varepsilon_{dd} < 0$ , i.e. for the dipole–dipole interaction tuned with rotating fields (see section 2.2). Note also that if  $Na/l_z \gg 1$ , the stability condition reduces to  $|\varepsilon_{dd}| > 1/2$ . The anisotropic character of the dipole–dipole interaction becomes particularly relevant when the quasi-2D condition is relaxed. In particular, solitons in 3D dipolar BECs are fundamentally unstable against collapse, as reflected in the decrease in the frequency of the breathing mode of the soliton for larger values of  $\varepsilon_{dd}$  [168] (figure 22).

Although  $\varepsilon_{dd} < 0$  is attainable for magnetic dipoles in a rotating magnetic field, the combination with Feshbach resonances to reduce the contact interactions makes experiments, e.g. in chromium, very complicated. Recently a similar idea, but without the necessity of dipole tuning,

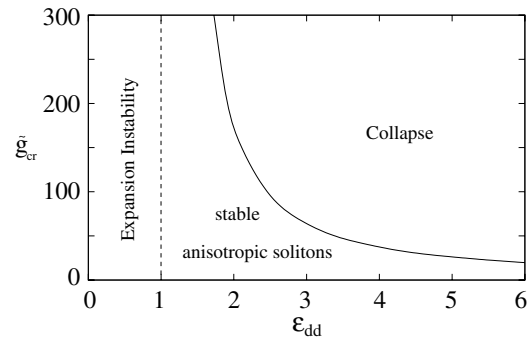


**Figure 23.** Stability diagram of an anisotropic soliton as a function of  $\varepsilon_{dd}$  and  $\tilde{g}_{cr} = g_{cr}/\sqrt{2\pi}l_z$ , where for  $g > g_{cr}$  the soliton is unstable against collapse even for  $\varepsilon_{dd} > 1$ .

has been proposed by Tikhonenkov *et al* [169]. In this new proposal the dipoles are considered as polarized on the 2D plane. A similar Gaussian ansatz on the  $xy$ -plane as above with unequal widths  $l_x$  and  $l_y$  shows the appearance of a minimum in the energy functional  $E(l_x, l_y)$  for  $\varepsilon_{dd} > 1$ , and thus the existence of stable anisotropic solitons. However, even if the latter condition is fulfilled there is a critical universal value  $\tilde{g}_{cr}$  (which decreases with  $\varepsilon_{dd}$ ) such that for  $\tilde{g} > \tilde{g}_{cr}$  the minimum of  $E(l_x, l_y)$  disappears [170] (see figure 23). As a consequence, contrary to the case of isotropic solitons (with  $\varepsilon_{dd} < 0$ ) there are a critical number of particles per soliton even if the soliton remains 2D. In addition, as for the case of isotropic solitons, anisotropic solitons are also unstable in 3D environments.

A major difference between bright solitons in non-dipolar and dipolar BECs concerns the soliton–soliton scattering properties. Whereas solitons in 1D non-dipolar BECs scatter elastically, the scattering of dipolar solitons is inelastic due to the lack of integrability [158]. The solitons may transfer center-of-mass energy into internal vibrational modes, resulting in intriguing scattering properties, including soliton fusion [168] (see figure 24), the appearance of strong inelastic resonances [171] and the possibility of observing 2D-soliton spiraling as that already observed in photorefractive materials [165].

For defocusing non-linearity ( $a > 0$ ) the local NLSE supports dark-soliton solutions, i.e. density notches (accompanied by phase slips) that propagate with no change of shape, again due to the compensation between dispersion and non-linearity [172]. Dark solitons have been created in non-dipolar quasi-1D BECs [151–153], but become fundamentally unstable in higher dimensions against vibrations of the nodal plane which lead to the so-called *snake instability*. This instability which was previously studied in the context of non-linear optics [173, 174] leads in the context of non-dipolar BEC to the soliton breakdown into vortex rings and sound excitations [175–178]. In contrast, a dark soliton in a dipolar BEC may become stable in a 3D environment [146] if the BEC is placed in a sufficiently deep 2D optical lattice (characterized by an effective mass on the lattice plane  $m^* > m$  [179] and a regularized local coupling constant  $\tilde{g}$ ). This effect may be understood by considering the phonon-like excitations of the dark soliton plane:  $\epsilon = \sqrt{\sigma/M}q$ , where  $M$  is the (negative) soliton mass per unit area and  $\sigma$  is the surface tension

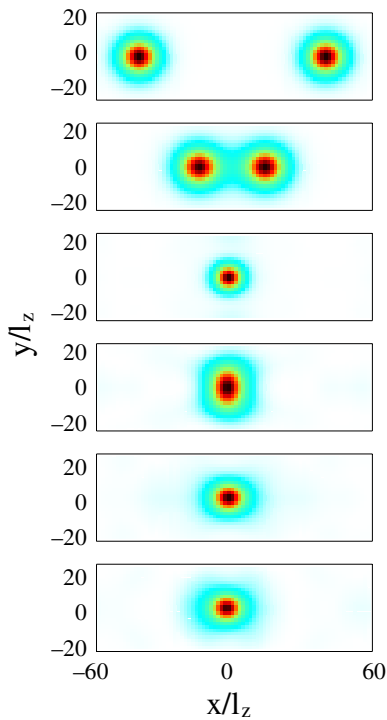


**Figure 24.** Density plot of the fusion of two dipolar 2D solitons for  $\tilde{g} = 20$ ,  $\varepsilon_{dd} = -2.1$  and initial relative momentum  $kl_z = 0.01$  along  $x$ . From top to bottom,  $\omega_z t / 2000 = 0, 1, 2, 3, 4$  and  $5$ .

of the nodal plane. For non-dipolar BECs one always has  $\sigma > 0$ , and hence the phonon spectrum is always unstable leading to the above-mentioned snake instability. However, for dipolar BECs the surface tension  $\sigma$  becomes negative when  $m/m^* < 3C_{dd}/(3\tilde{g} + 2C_{dd})$  [146], and hence the nodal plane is stabilized for a sufficiently deep optical lattice (large  $m^*/m$ ) and a sufficiently large dipole–dipole interaction. Very recently, solitons in quasi-1D dipolar BECs have been studied theoretically [180, 181].

## 7.2. Vortices

Quantized vortices constitute one of the most important consequences of superfluidity, playing a fundamental role in various physical systems, such as superconductors [182] and superfluid helium [183]. Vortices and even vortex lattices have been created in BECs in a series of milestone experiments [184–186]. Contrary to normal fluids, a vortex in a BEC cannot be created by any rotation, but there is a critical angular velocity  $\Omega_c$ . Only for angular velocities  $\Omega > \Omega_c$  it is energetically favorable to form a vortex [187] (the critical rotation for vortex nucleation is actually larger, since also dynamical instabilities at the condensate boundaries must be considered [188]). O’Dell and Eberlein [189] have recently studied the critical  $\Omega_c$  in a dipolar condensate in the Thomas–Fermi regime, by means of the solution discussed in section 5. For BECs in axially symmetric traps with the axis along the dipole orientation it has been shown that  $\Omega_c$  is decreased due to the dipole–dipole interaction in oblate traps and increased in prolate traps. This modification can be traced back to the

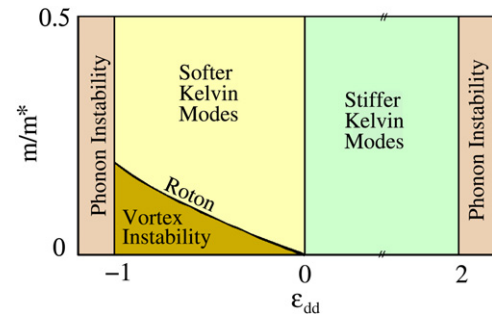


**Figure 25.** Stable/unstable regimes, as a function of the ratio  $m/m^*$  and  $\varepsilon_{dd}$ , for straight vortex lines when the dipoles are oriented along the vortex line.

modification of the Thomas–Fermi radius due to the dipole–dipole interaction, rather than changes in the vortex core. However, the dipole–dipole interaction may induce crater-like structures close to the vortex core for the case of  $a < 0$ , or even anisotropic vortex cores, as recently shown by Yi and Pu [190]. The effect of the dipolar interaction on the dynamical instability leading to the nucleation of vortices in the TF regime was addressed in [191, 192].

At higher rotating frequencies, more vortices enter the condensate and a vortex lattice develops [185, 186]. In non-dipolar BECs vortices form so-called Abrikosov lattices, i.e. triangular lattices with hexagonal symmetry. Interestingly, this is not necessarily the case in dipolar condensates [193, 194]. In particular, with increasing  $\varepsilon_{dd}$  or high filling factor, the vortex lattice may undergo transitions between different symmetries: triangular, square, stripe vortex crystal and bubble states [193]. In addition for vortex lattices in double well potentials the competition between tunneling and inter-layer dipole–dipole interaction should lead to a quantum phase transition from a coincident phase to a staggered one [194].

Vortex lines are in fact 3D structures with transverse helicoidal excitations known as Kelvin modes [195, 196]. Kelvin modes, which play an important role in the physics of superfluid helium [183], have also been experimentally observed in BECs [197]. The long-range character of the dipole–dipole interaction links different parts of the vortex line, and hence the 3D character of the vortex lines is much more relevant in dipolar BECs. Remarkably the dipole–dipole interaction may significantly modify the vortex-line stability. In the presence of an additional optical lattice (which leads to an effective mass  $m^*$  along the vortex line direction) the dispersion of Kelvin modes shows a roton-like minimum [198], which for sufficiently large dipole–dipole interaction and large  $m^*$  may reach zero energy, leading to a thermodynamical instability related to a second-order-like phase transition from a straight vortex into a twisted vortex line [199] (see figure 25).

## 7.3. Pattern formation

Pattern formation in driven systems is a general non-linear phenomenon occurring in many scenarios ranging from hydrodynamics and non-linear optics to liquid crystals and chemical reactions [200]. Faraday patterns have recently been observed in non-dipolar BECs by a modulation of the harmonic

confinement [201] which leads to a periodic modulation of the system non-linearity [202]. Faraday patterns offer an important insight into the elementary excitations in a BEC, and hence pattern formation may be remarkably different in dipolar BECs, especially in the presence of a roton–maxon excitation spectrum (section 5). Most remarkably, whereas for non-dipolar BECs the pattern size decreases monotonically with the driving frequency, patterns in dipolar BECs present a highly non-trivial dependence characterized by abrupt pattern-size transitions [121].

Faraday pattern formation in driven systems is the (transient) result of an externally driven dynamical instability. However, an interaction-induced dynamical instability may lead as well to pattern formation. In this sense, the phonon instability, which, as discussed in section 5, leads to collapse in 3D dipolar gases (also in 2D and 3D non-dipolar BECs), does not necessarily lead to collapse in 2D geometries. In contrast, the 2D phonon instability leads to the formation of a soliton gas, and to transient pattern formation, which, if avoiding collapse, may lead to the formation of a 2D stable soliton [146]. Dynamical roton instability leads typically to local collapses [116], although a sufficiently strong trapping may stabilize a biconcave BEC profile [104] (as mentioned in section 5.3). Another possibility lies in using a phase-separated two-component gas, one dipolar and the other not. Rosensweig patterns very similar to that of figure 1 are then predicted to be observed on the interface [15].

## 8. Dipolar effects in spinor condensates

Spinor BECs, composed of atoms in more than one Zeeman state, constitute an extraordinary tool for the analysis of multicomponent superfluids. Whereas magnetic trapping confines the BEC to weak-field seeking magnetic states, optical trapping enables confinement of all magnetic substates, hence freeing the spin degree of freedom [204]. Interestingly, interatomic interactions allow for a coherent transfer of population between different Zeeman states (spin-changing collisions), leading to a fascinating physics in both what concerns ground-state properties and spin dynamics [205–210].

The energy scale associated with spin-preserving collisions is given by the chemical potential, which for typical alkali gases (and even for chromium in the absence of Feshbach resonances) is much larger than the dipole–dipole interaction. In contrast, the energy associated with spin-changing collisions is typically much smaller, since it is provided by the difference between *s*-wave scattering lengths in different spin channels [205], which is very small. Hence the dipole–dipole interaction may become comparable to the energy of spin-changing collisions, and as a consequence even alkali spinor BECs (in particular <sup>87</sup>Rb) can be considered in this sense as dipolar gases as well. The dipole–dipole interaction may hence play a significant role in the ground-state properties and the dynamics of spinor condensates.

### 8.1. Ground state

Pu *et al* [211] have shown that ferromagnetic spinor BECs (as it is the case of <sup>87</sup>Rb in  $F = 1$ ) placed at different sites of a strong optical lattice behave as single magnets oriented in the effective magnetic field induced by the combination of an external magnetic field and the dipole–dipole interaction of other sites. Interestingly, the collectively enhanced magnetic moment of the condensates at each site enhances the magnetic dipole–dipole interaction between sites, which may become sufficiently strong even for alkali atoms [211]. As a consequence, such an array of effective magnets can undergo a ferromagnetic (1D lattice) or antiferromagnetic (2D lattice) phase transition under the magnetic dipolar interaction when external magnetic fields are sufficiently weak [211, 212]. In addition, for 1D lattices the intersite dipole–dipole interaction may distort the ground-state spin orientations and lead to the excitation of spin waves, which possess a particular dispersion relation which depends on the transverse width of the condensates [213].

The dipole–dipole interaction may play an important role in the properties of trapped spinor BECs, especially in the absence of significant external magnetic fields. In particular, whereas in the absence of an external magnetic field the spinor BEC is rotationally invariant in spin space, the dipole–dipole interaction breaks this symmetry, inducing new quantum phases which can be reached by tuning the effective strength of the dipole–dipole interaction via a modification of the trapping geometry [214]. For the case of spin-1 BECs, for very low magnetic fields (typically below 10  $\mu$ G) the phase diagram presents due to the dipole–dipole interaction three different ground state phases, characterized by different spin textures: a polar-core vortex phase, a flower phase and a chiral spin-vortex phase [215]. The latter has chirality in the formation of the spin vortex, and the topological spin structure spontaneously yields a substantial net orbital angular momentum. A classical-spin approach to the ground state properties of dipolar spinor BECs was used in [216].

### 8.2. Dynamics and Einstein–de Haas effect

The dipole–dipole interaction has been shown to play quite a small role in the ground-state properties of chromium BECs [217, 218]. However, the effects of the dipole–dipole interaction on the spinor dynamics may be much more intriguing. The short-range interactions in a spinor condensate may occur in different scattering channels, corresponding to different total spins of the colliding pair [205]

$$\hat{V}_{sr} = \frac{1}{2} \int d\mathbf{r} \sum_{S=0}^{2F} g_S \hat{\mathcal{P}}_S(\mathbf{r}), \quad (8.1)$$

where  $\hat{\mathcal{P}}_S$  is the projector on the total spin  $S$  (necessarily even due to symmetry reasons),  $g_S = 4\pi\hbar^2 a_S/m$  and  $a_S$  is the *s*-wave scattering length for the channel of total spin  $S$ . The short-range interactions necessarily preserve the spin projection  $S_z$  along the quantization axis.

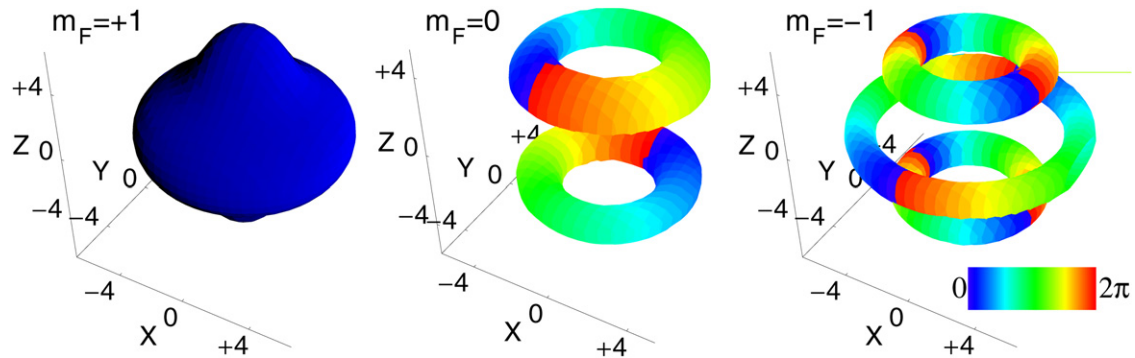


**Figure 26.** Isodensity surfaces of  $m_F = +1$ ,  $m_F = 0$  and  $m_F = -1$  spinor components corresponding to the densities:  $7.96 \times 10^{13} \text{ cm}^{-3}$ ,  $7.96 \times 10^{13} \text{ cm}^{-3}$  and  $7.96 \times 10^{12} \text{ cm}^{-3}$ , respectively. The color on the surface represents the phase of the component wavefunction (with the scale given on the right). Note the characteristic vortex ring patterns. The trap frequency  $\omega_{x,y,z} = 2\pi \times 100 \text{ Hz}$  and the magnetic field  $B = -0.029 \text{ mG}$ . The density plots are taken at 140 ms. Figure courtesy of M Gajda and M Brewczyk.

The dipole–dipole interaction for a spinor BEC is of the form

$$\hat{V}_{\text{dd}} = \frac{C_{\text{dd}}}{2} \int d\mathbf{r} \int d\mathbf{r}' \frac{1}{|\mathbf{r} - \mathbf{r}'|^3} \hat{\psi}_m^\dagger(\mathbf{r}) \hat{\psi}_{m'}^\dagger(\mathbf{r}') \times [\mathbf{S}_{mn} \cdot \mathbf{S}_{m'n'} - 3(\mathbf{S}_{mn} \cdot \mathbf{e})(\mathbf{S}_{m'n'} \cdot \mathbf{e})] \hat{\psi}_n(\mathbf{r}) \hat{\psi}_{n'}(\mathbf{r}'), \quad (8.2)$$

where  $\mathbf{S} = (S_x, S_y, S_z)$  are the spin- $F$  matrices and  $C_{\text{dd}} = \mu_0 \mu_B^2 g_F^2 / 4\pi$  (for  $^{52}\text{Cr}$   $F = 3$  and  $C_{\text{dd}} = 0.004 g_6$ ) with  $\mathbf{e} = (\mathbf{r} - \mathbf{r}') / |\mathbf{r} - \mathbf{r}'|$ .

Interestingly, contrary to the short-range interaction the dipole–dipole interaction does not necessarily conserve the spin projection along the quantization axis due to the anisotropic character of the interaction. In particular, if the atoms are initially prepared into a maximally stretched state, say  $m_F = -F$ , short-range interactions cannot induce any spinor dynamics due to the above-mentioned conservation of total magnetization  $S_z$ . Dipole–dipole interactions, in contrast, may induce a transfer into  $m_F + 1$ . If the system preserves cylindrical symmetry around the quantization axis, this violation of the spin projection is accompanied by a transfer of angular momentum to the center of mass, resembling the well-known Einstein–de Haas effect [218, 219]. Due to this transfer an initially spin-polarized dipolar condensate can generate dynamically vorticity (see figure 26).

Unfortunately, the Einstein–de Haas effect is destroyed in the presence of even rather weak magnetic fields. Typically, magnetic fields well below 1 mG are necessary to observe the effect. Due to the dominant role of Larmor precession, and invoking rotating-wave-approximation arguments, the physics must be constrained to manifolds of preserved magnetization, where the system presents a regularized dipole–dipole interaction [220]. However, the dipole–dipole interaction may have observable effects also under conserved magnetization, since the regularized dipole–dipole interaction may lead also in that case to spin textures [220].

A significant Einstein–de Haas effect may be recovered, however, under particular resonant conditions as studied by Gawryluk *et al* [221], who studied the particular case of Rb BECs in  $F = 1$ , initially prepared into  $m_F = 1$ . In that case, the population transfer away from the  $m_F = 1$  state

is typically very small, but it can be significantly enhanced by applying a resonant magnetic field, such that the Zeeman energy of an atom in the  $m_F = 1$  state is totally transferred into the kinetic energy of the rotating atom in  $m_F = 0$ ,  $\mu B = E_{\text{kin}}$ . Typically, the resonant  $B$  is small ( $\sim 100 \mu\text{G}$ ), but can be tuned directly, or by adjusting the trap geometry and thus the rotational energy of the atoms, reaching up to 1 mG. Gawryluk *et al* demonstrated that at the resonance, a significant transfer of the initial population of the  $m_F = 1$  state occurs on a time scale inversely proportional to the dipolar energy  $t_{\text{transfer}} \simeq \hbar / C_{\text{dd}} n$ . As mentioned above, such a transfer is accompanied by the formation of vorticity (see figure 26) [218, 219, 221].

An alternative possibility for the observation of the Einstein–de Haas effects at finite fields may also be provided by an artificial quadratic Zeeman effect induced by either microwave [222] or optical fields [223]. This effective quadratic Zeeman effect may allow for a resonance between e.g.  $m_F = -F$  and  $m_F = -F + 1$  and hence lead to a significant enhancement of the Einstein–de Haas transfer [223].

### 8.3. Experimental results

Recent 2D experiments at Berkeley [224] have demonstrated the dipolar character of spin-1  $^{87}\text{Rb}$  spinor BECs. In particular, these experiments show the spontaneous decay of helical spin textures (externally created by magnetic field gradients) toward a spatially modulated structure of spin domains (see figure 27). The formation of this modulated phase has been ascribed to magnetic dipolar interactions that energetically favor short-wavelength domains over the long-wavelength spin helix. Interestingly, the reduction of dipolar interactions (by means of radio-frequency pulses) results in a suppression of the modulation.

These experiments have attracted a great deal of theoretical interest, in particular in the dipole–dipole interaction-induced distortion of the excitation spectrum of a spinor BEC [225, 226]. Recently Cherng and Demler have analyzed (in the context of the above-mentioned 2D experiments [224]) the possibility of roton softening (similar to that discussed in section 5.6) in the spectrum of spin excitations. This roton instability may lead as a function of the quadratic Zeeman effect and the magnetic field orientation

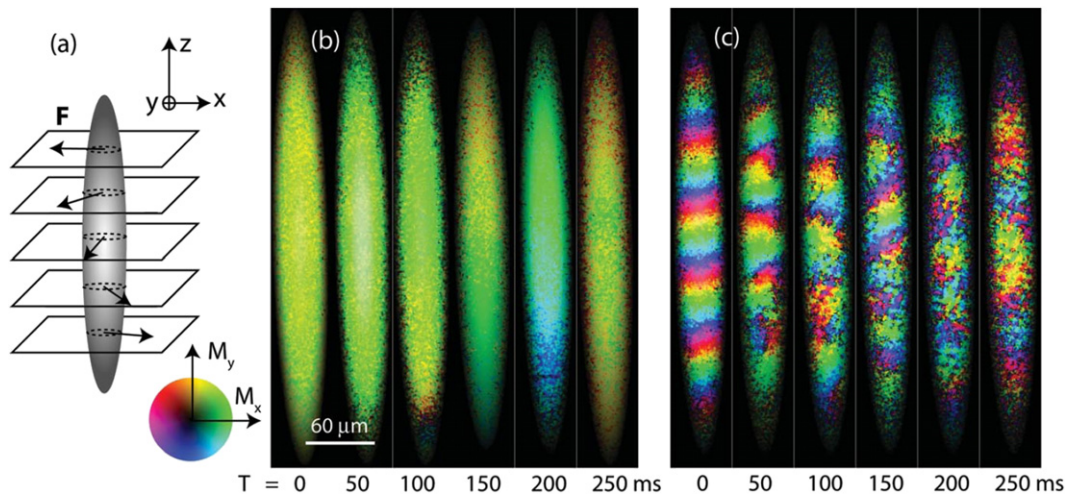


**Figure 27.** Spontaneous dissolution of helical textures in a quantum degenerate  $^{87}\text{Rb}$  spinor Bose gas. A transient magnetic field gradient is used to prepare transversely magnetized (b) uniform or (a), (c) helical magnetization textures. The transverse magnetization column density after a variable time  $T$  of free evolution is shown in the imaged  $x$ - $z$  plane, with orientation indicated by hue and amplitude by brightness (color wheel shown). (b) A uniform texture remains homogeneous for long evolution times, while (c) a helical texture with pitch  $\lambda = 60 \mu\text{m}$  dissolves over  $\sim 200$  ms, evolving into a sharply spatially modulated texture. Figure reprinted with permission from [224]. Copyright 2008 by the American Physical Society.

with respect to the normal of the 2D trap to different spin textures (checkerboard, striped phase) and may pave the way toward a supersolid phase. The latter is a long pursued phase in condensed matter physics which possesses both periodic crystalline order and superfluidity [227–229] (see also the next section). However, instability against finite-momentum excitations does not necessarily lead to the appearance of a stable modulation (as it is the case of the roton instability discussed in section 5.6) and more work on the physics in the unstable regime is clearly necessary. Recent experiments at Berkeley have reported on possible first traces of supersolidity in a spinor  $^{87}\text{Rb}$  BEC [230].

## 9. Dipolar gases in optical lattices

One of the most fruitful fields of research both from the experimental and the theoretical points of view in the last years has been the study of ultra-cold atomic samples in optical lattices, which are non-dissipative periodic potential energy surfaces for the atoms, created by the interference of laser fields. The study of cold atoms in periodic potentials is of primary interest because it allows one to reproduce problems traditionally encountered in condensed matter and solid-state physics in a new setting, where a high degree of control is possible and where the Hamiltonian which governs the system is in general very close to ideal. With the present developments there is even the possibility to investigate, with appropriately designed atomic systems, phenomena which do not exist in condensed matter.

We will first summarize the physics of weakly interacting atomic gases in optical lattices in section 9.1, and describe the first measurement of dipolar effects in alkali atoms in section 9.2. After introducing the physics of strongly correlated systems with contact interaction in section 9.3, we will devote sections 9.4 and 9.5, respectively, to the quantum

phases and the metastable states found in 2D lattices in the presence of long-range interactions. In section 9.6, we discuss the novel physics introduced by the presence of two or many 2D optical lattice layers. In section 9.7, we discuss proposals on how to tailor the interaction potential and create lattice spin models with polar molecules and finally, in section 9.8, we will mention the possibility of formation of self-assembled regular structures in cold dipolar gases.

### 9.1. Bose–Einstein condensates in optical lattices

In the presence of weak optical lattices, when the coherence of the system is preserved, the Gross–Pitaevskii equation provides a good description of the system. Due to the presence of the periodic potential and interactions, analogies to phenomena typical of solid-state physics and non-linear optics are, respectively, possible [14, 231–233].

As previously explained, in the most common cases, interactions in ultra-cold gases are dominated by  $s$ -wave scattering, which can be in very good approximation considered a point-like interaction. In the case of full coherence, the system is described by a macroscopic wavefunction and obeys the GPE (4.5). In the presence of optical lattices,  $V_{\text{ext}}$  is periodic and given by  $V_{\text{ext}}(\mathbf{r}) = \sum_n V_n^{\text{opt}} \sin^2(\pi x_n/d_n)$ , where the index  $n$  runs over the dimensions of the lattice and  $d_n$  is the lattice constant in the  $n$ th direction. For lattices created by counterpropagating laser beams of wavelength  $\lambda$ , the lattice spacing is  $d = \lambda/2$ . The depth of the lattice potential  $V_n^{\text{opt}}$  depends linearly on the intensity of the laser light.

It is well known that the spectrum of a single particle in a periodic potential is characterized by bands of allowed energies and energy gaps [234]. The counterparts of the energy eigenstates delocalized over the whole lattice (Bloch states) are the wavefunctions centered at the different lattice sites (Wannier functions). For deep enough periodic potentials,

when the Wannier functions are well localized at the lattice sites, the so-called tight binding regime is reached: the first band takes the form  $E(q) = -2J \sum_n \cos(q_n d_n)$ ,  $q_n$  being the quasi-momenta in the different lattice directions and  $J$  the tunneling parameter between neighboring wells. For low enough interactions and temperature, the physics of the system is well approximated by the one taking place in the first energy band. Under those assumptions, the discretized non-linear Schrödinger (DNLS) equation [235–239] provides a good description of the system.

The excitations on top of the GP solution can be found by generalizing the Bogoliubov method to include the periodic potential. They show a phononic branch with renormalized sound velocity [240–242]. For a moving condensate, one finds complex frequencies at the edge of the Brillouin zone [243], highlighting the presence of dynamical instabilities [244].

Among the numerous phenomena described theoretically and observed experimentally are collective oscillations [245], Bloch oscillations [246], dynamical instabilities [247], Josephson oscillations [248], non-linear self-trapping [249], gap solitons [154]. The collective oscillations can be described through an effective macroscopic dynamics accounting for the periodic potential and their frequency is rescaled in terms of the effective mass [179]. Instead, the physics underlying the other phenomena is dominated by a crucial interplay between the periodic potential and interactions.

In the alkalis usually used in experiments with optical lattices, s-wave scattering dominates over all other types of interactions. When the s-wave scattering length is reduced, e.g. by means of a Feshbach resonance, the presence of other types of interaction is relatively enhanced and can be probed. In the next section, we present the first measured effects of dipole–dipole interaction for a quantum gas in an optical lattice, performed with potassium atoms.

### 9.2. Bloch oscillation damping due to dipole–dipole interactions

Bloch oscillations have been one of the first solid-state phenomena to be investigated with cold atoms [250, 251], observed shortly after Bloch oscillations of electrons in semiconducting heterostructures [252–254]. They consist of oscillations in space in the presence of a constant acceleration, due to the change of sign of the effective mass along the first energy band. For electrons, the acceleration is provided by a constant electric field, while for cold atoms it is produced by a linear increase in time of the relative detuning of the two laser beams creating the optical lattice or, in a vertical setup, by gravity.

With Bose–Einstein condensates, Bloch oscillations can be measured with a higher precision thanks to the smaller width of the momentum distribution [246]. However, in the presence of interatomic interactions, the onset of dynamical instabilities in the outer region of the Brillouin zone causes a damping of the oscillations. Due to the relevance of Bloch oscillations as a tool of precision measurement of accelerations and small forces at small distance from surfaces [255–258], attempts at reducing interactions have been pursued first with polarized

fermions [259] and then with bosons with reduced s-wave scattering length [134, 260].

The experiment in [134] has highlighted for the first time effects of dipole–dipole interactions on alkali atoms and has shown how their interplay with the contact interaction can be exploited to reduce interaction-induced decoherence of Bloch oscillations in a 1D optical lattice. When the scattering length is tuned to zero by means of a Feshbach resonance, the magnetic dipole–dipole interaction becomes the limiting factor for the coherence time. The point of minimum decoherence is shifted to negative or positive values of the scattering length, depending on the orientation of the dipoles with respect to the axis of the lattice (see figure 28).

The values of the scattering lengths which maximize the lifetime in the different configurations have been predicted through the solution of 1D DNLS and GP equations including the dipolar potential. The 3D geometry has been accounted for, assuming the condensate to be in the transversal ground state. The dipole–dipole interaction contributes both to the regularization of the on-site interactions and also to the intersite interactions. Although the compensation of the on-site dipole–dipole interaction and the short-range interactions explains the sign of the displacement (toward  $a < 0$  or  $a > 0$ ) of the decoherence minimum, the dipole-induced intersite interactions are crucial for the quantitative understanding of the experimental results in [134]. In this sense the experiments in [134] also constitute the first observation of intersite effects in dipolar gases in optical lattices. Due to the intersite interactions, the dipole–dipole interaction can be only partially compensated by the short-range interactions, and as a consequence an incomplete reduction of the decoherence rate of the  $^{39}\text{K}$ -based interferometer is observed (with a minimum residual rate of 0.05 Hz).

In the experiments in [134], the interactions at the decoherence minimum were much weaker than the transversal confinement, justifying the approximation of assuming the BEC in the transversal ground state. This is, however, not the general case. For shallower transversal confinements the intersite dipole–dipole interaction may significantly modify and even destabilize the spectrum of elementary excitations of a BEC in an optical lattice [117, 120]. In particular, the intersite interactions may induce rotonization and even roton instability (see also section 5.6) under appropriate conditions, and may (for a sufficiently shallow transversal confinement) lead to a dynamical instability that could also damp Bloch oscillations [120]. Interestingly, the intersite dipole–dipole interaction induces a hybridization of transversal modes at different sites (and a corresponding band-like spectrum) even if the hopping is completely suppressed [117]. Remarkably, whereas a single lattice site could be stable, a stack of non-overlapping dipolar BECs may become roton unstable, showing once more that polar gases in optical lattices differ qualitatively from short-range interacting gases.

### 9.3. Strongly correlated lattice gases. Bose–Hubbard Hamiltonian

For deep optical lattices and small numbers of atoms per site, the coherent description of the system provided by the

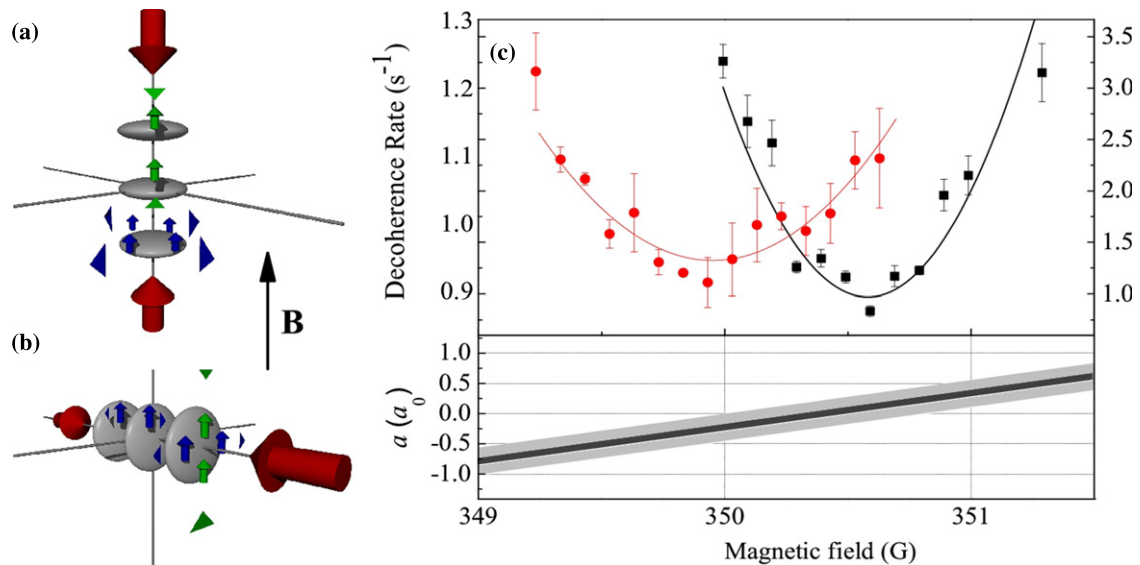


**Figure 28.** Decoherence of Bloch oscillations in  $^{39}\text{K}$  around the scattering length zero-crossing, due to the interplay of contact and dipolar interactions. The character of the dipolar interaction depends on the relative orientation of the lattice and the magnetic field: (a) prevalently repulsive interaction; (b) prevalently attractive interaction. (c) The width of the momentum distribution after a few 100 ms of Bloch oscillations shows a minimum when the contact interaction compensates the dipolar one: circles are for the case (a), while squares are for the case (b). The lines are parabolic fits to the data, which constrain the position of the zero-crossing in a comparison with theory (black region in the lower panel) better than Feshbach spectroscopy (gray region). Figure courtesy of Modugno.

GPE breaks down due to the growing effect of correlations. One of the greatest achievements of the past years was the experimental observation [16] of the superfluid to Mott insulator transition [15, 261]. In this session, we will introduce the main theory for ultra-cold atoms in optical lattices in the case of point-like interaction, providing the background for the case of long-range interactions, which will be treated in the following sections.

Under usual experimental conditions, the single-band approximation mentioned in section 9.1 is appropriate. In order to allow for the breaking of the coherence of the system, the field operator is replaced by its single-band many-mode expansion  $\hat{\psi}(\mathbf{r}) = \sum_i w_i(\mathbf{r})\hat{a}_i$ , with  $\hat{a}_i$  being the annihilation operator for one boson in the Wannier function  $w_i(\mathbf{r})$  localized at the bottom of the lattice site  $i$ .

Neglecting the overlap beyond nearest neighboring densities, defining

$$J = - \int w_i^*(\mathbf{r}) \left( -\frac{\hbar^2 \Delta}{2m} + V_{\text{ext}}(\mathbf{r}) \right) w_{i+1}(\mathbf{r}) d^3r, \quad (9.1)$$

$$U = g \int |w_i(\mathbf{r})|^4 d^3r, \quad (9.2)$$

and  $n_i = \hat{a}_i^\dagger \hat{a}_i$ , one can derive [15] the famous Bose–Hubbard Hamiltonian

$$H = -J \sum_{\langle ij \rangle} \hat{a}_i^\dagger \hat{a}_j + \sum_i \left[ \frac{U}{2} n_i(n_i - 1) - \mu n_i \right], \quad (9.3)$$

extensively studied in condensed matter physics. In optical lattices, the Hamiltonian parameters can be accurately controlled by changing the light intensity: ramping it up increases the interaction term  $U$  due to a stronger localization

of the wavefunctions at the bottom of the lattice wells, and at the same time exponentially decreases the tunneling  $J$ .

When tunneling is suppressed compared with interactions, this Hamiltonian presents a quantum phase transition between a superfluid phase, characterized by large number fluctuations at each lattice site, and a Mott insulating phase where each lattice well is occupied by precisely an integer number of atoms without any number fluctuations. The nature of this phase transition and the qualitative phase diagram can be inferred based on very simple arguments [261].

At zero tunneling  $J = 0$  and commensurate filling (exactly an integer number  $n$  of atoms per well), the interaction energy is minimized by populating each lattice well with exactly  $n$  atoms. Energy considerations indicate that the filling factor  $n$  is energetically favored in the range of chemical potential  $(n-1)U < \mu < nU$ . The state with precisely integer occupation at the lattice sites is called the Mott insulating state. Since a particle–hole excitation at  $J = 0$  costs an energy  $\Delta E = U$  equal to the interaction energy, the Mott state is the lowest energy state at commensurate filling. For a tunneling  $J$  different from zero the energy cost to create an excitation decreases thanks to the kinetic energy favoring particle hopping. However, for large interactions and small tunneling, the gain in kinetic energy ( $\sim J$ ) is not yet sufficient to overcome the cost in interaction energy ( $\sim U$ ), which leads to the existence of Mott insulating states also at finite tunneling. For large enough tunneling, instead, particle hopping becomes energetically favorable and the system becomes superfluid. The regions in the  $J$  versus  $\mu$  phase diagram where the Mott insulating state is the ground state are called *Mott lobes* (see figure 29). For non-commensurate filling, there are extra atoms free to hop from site to site at no energy cost, so that the phase of the system is always superfluid. The superfluid

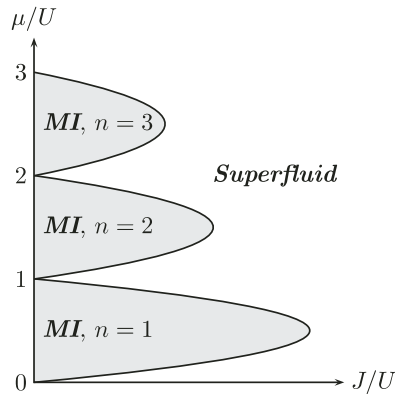


**Figure 29.** Schematic phase diagram for the ground state of the Bose-Hubbard Hamiltonian (9.3).

phase at non-commensurate densities survives down to  $J = 0$  for  $\mu/U = [\rho]$  where the symbol  $[\rho]$  indicates the integer part of the density. Due to the finite energy cost required to add or remove one particle, the Mott phase is gapped and incompressible, while in the superfluid regions the gap vanishes and the system is compressible.

In order to find the shape of the lobes at finite  $J$  sophisticated calculations are required. Apart from the mean-field approximation [261–263], which works only qualitatively in one dimension and works better and better in larger dimensions, there is no exact analytical method which allows one to calculate the boundary of the lobes. Improvements are achieved by high order perturbative strong coupling expansions [264, 265] and exact numerical results are obtained using quantum Monte Carlo techniques (see e.g. [266–268]).

In the experiments, the phase transition has been identified by looking at the interference of the expanded cloud and the measurement of the gapped excitations in the Mott phase [16]. The SF–MI shell structure which arises in the presence of an external confinement [15, 269, 270] has been observed using spatially selective microwave transition and spin-changing collisions [270] or using clock shifts [271], and the underlying ordering in the lattice in the Mott phase has been inferred from the measurement of the periodic quantum correlations in the density fluctuations in the cloud after expansion [272, 273]. The interference of the expanding cloud and spatial noise correlation measurements prove to be useful tools to identify also the exotic quantum phases expected to appear in the presence of dipole–dipole interaction.

#### 9.4. Quantum phases of dipolar lattice gases

Dipole–dipole interactions add to the Bose–Hubbard model a new essential ingredient, given by long-range and anisotropic interactions. For a lattice of polarized dipoles, as sketched in figure 30, the extended Bose–Hubbard Hamiltonian in the presence of long-range interaction is

$$H = -J \sum_{(ij)} \hat{a}_i^\dagger \hat{a}_j + \sum_i \left[ \frac{U}{2} n_i (n_i - 1) - \mu n_i \right] + \sum_{\ell} \sum_{(ij)\ell} \frac{U_{\ell}}{2} n_i n_j, \quad (9.4)$$

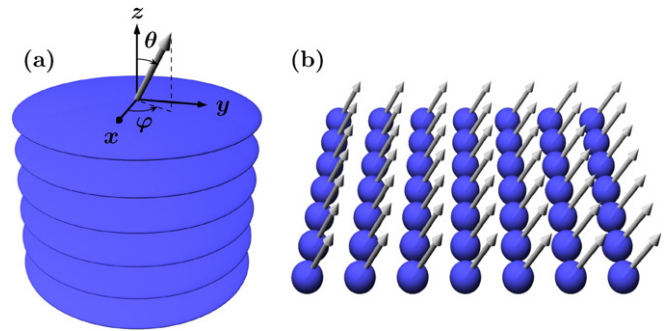


**Figure 30.** Schematic representation of a gas of polarized dipoles in a 1D optical lattice (a) and in a single 2D optical lattice layer (b).

where the vector  $\ell$  is the distance between the two optical lattice sites  $i$  and  $j$ .

The extended Bose–Hubbard Hamiltonian (9.4) has been extensively studied. It has been predicted that in 2D lattices the presence of finite range interactions (where the sum over  $\ell$  is generally cut off at the nearest or next-nearest neighbor) gives rise to novel quantum phases, like the charge-density wave (checkerboard), namely an insulating phase with modulated density, and the supersolid phase, presenting the coexistence of superfluidity and of a periodic spatial modulation of the density, different from that of the lattice [274–276] (see also discussion in section 5.6).

The presence of insulating phases at fractional filling factors can be inferred readily following the criteria explained in the previous section, which predict that (e.g.) a checkerboard ordering of the atoms (see figure 31(GS)) at  $J = 0$  is stable against particle–hole excitations in the range of chemical potential  $0 < \mu < 4U_{\text{NN}}$ ,  $U_{\text{NN}}$  being the first nearest-neighbor interaction (and neglecting for the sake of simplicity all following ones). Analogous to the standard Mott insulating phase, these insulating phases at fractional filling factor exist in some low tunneling region of the  $\mu$  versus  $J$  phase diagram.

In [277], it has been pointed out that 1D lattice systems of spinless bosons interacting with long-range interactions possess a further insulating phase, which they call Haldane Bose insulator (HI), presenting some analogies with the famous Haldane gapped phase in quantum spin-1 chains [278]. This is a gapped phase, which unlike the checkerboard phase does not break the translational symmetry of the lattice, but is characterized by an underlying hidden order, namely a non-trivial ordering of the fluctuations which appear in alternating order separated by strings of equally populated sites of arbitrary length. These studies were extended to a confined 1D dipolar gas in [279].

The existence of the supersolid phase in solid helium has not yet been unambiguously proven experimentally: while on the one hand the interpretation of the first experimental results measuring a non-classical rotational inertia [280–282] remains controversial, microscopic calculations [283] indicate that disorder-based mechanisms, such as the presence of superfluid dislocations, grain boundaries and ridges, should be responsible for the more recent observations of supersolidity [284, 285]. Even if bulk supersolid remains in many respects more challenging than lattice supersolid, the

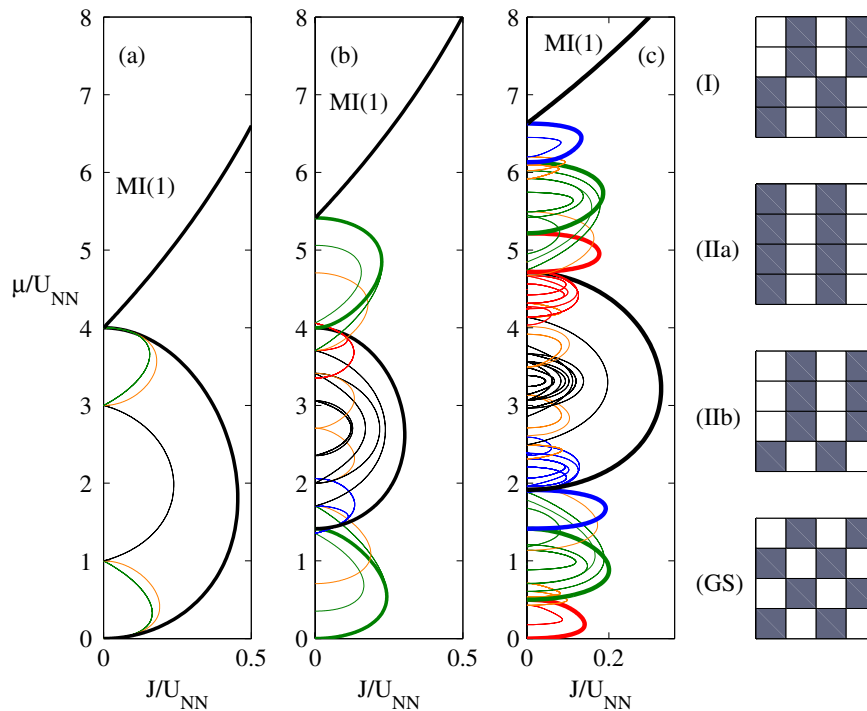


**Figure 31.** (a), (b), (c) Phase diagram with a range of the dipole–dipole interaction cut at the first, second and fourth nearest neighbor, respectively. The thick line is the ground state and the other lobes correspond to the metastable states, the same color corresponding to the same filling factor. In (a), (b), (c) the ground state filling factors are multiples of  $1/2$ ,  $1/4$  and  $1/8$ , respectively. In (a), (b), (c) the metastable state filling factors are  $m/4$ ,  $m/8$  and  $m/16$ , respectively ( $\forall m \neq 1$ ). Metastable configuration appearing at the first nearest neighbor (I) and second (IIa–IIb), and the corresponding ground state (GS); the metastable states remain stable for all larger ranges of the dipole–dipole interaction. The above phase diagrams are calculated for  $U/U_{\text{NN}} = 20$ . This value of the dipole–dipole interaction is much stronger than the one currently available in systems of chromium atoms, where  $U/U_{\text{NN}} \approx 400$  (for  $\varepsilon_{\text{dd}} \approx 0.16$  and spherical localization of the bottom of the potential well at  $s = 20E_{\text{R}}$ , where  $E_{\text{R}}$  is the recoil energy at  $\lambda = 500$  nm).

question of the stability of the supersolid phase in the presence of the lattice is not trivial and has been only recently settled by exact quantum Monte Carlo simulations. Checkerboard supersolid (at  $\rho \approx 1/2$ ) is expected for dominant nearest-neighbor interaction, while star (at  $\rho \approx 1/4$ ) and striped (at  $\rho \approx 1/2$ ) supersolids<sup>14</sup> are predicted for non-vanishing nearest-neighbor interaction [286, 287]. There have been several studies devoted to the stability of the supersolid phase versus phase separation [288, 289], which is identified by a negative compressibility. Agreement seems to be reached on the conclusion that the checkerboard supersolid is stabilized at  $\rho > 1/2$  by a finite on-site interaction and a strong enough nearest-neighbor interaction [290], while it phase separates for nearest-neighbor interactions at densities smaller than  $1/2$  (unless a strong enough nearest-neighbor hopping is introduced [291]). Instead, the striped supersolid, obtained for large next nearest-neighbor interaction, exists for all doping away from  $\rho = 1/2$  both in the hard-core and in the soft-core cases [288, 289, 291]. Finally, at large next nearest-neighbor interaction, the star supersolid can always be obtained by doping a star solid at  $\rho = 1/4$  with vacancies and by doping it with bosons in the case the  $\rho = 1/2$  ground state is a striped

<sup>14</sup> The star supersolid shows modulations of the density and order parameter such that in a  $2 \times 2$  elementary cell, one (the other) diagonal contains sites with different (equal) density and order parameter; the striped supersolid presents alternating horizontal or vertical stripes of higher and lower density and order parameter.

crystal [291, 292]. The most important conclusion on which most papers agree<sup>15</sup> is that no supersolid phase is found at commensurate density. Analogous results have been recently discussed for 1D geometries [294, 295], the most important difference being the absence of phase separation.

Providing an alternative setting in which to look for the supersolid phase, cold atoms with long-range interactions are particularly appealing [277, 286, 287, 290, 296, 297]. Dipolar atoms and polar molecules are good candidates to create such physical systems, bringing into play the extra feature of the anisotropy of the interaction. Dipolar gases have been first identified as possible candidates to provide a long-range interaction system in [286]. The on-site parameter  $U$  in (9.4) is given by two contributions: one arises from the  $s$ -wave scattering  $U_s = 4\pi\hbar^2 a/m \int n^2(\mathbf{r}) d^3r$  and the second one is due to the on-site dipole–dipole interaction  $U_{\text{dip}} = 1/(2\pi)^3 \int \widetilde{U}_{\text{dd}}(\mathbf{q}) \widetilde{n}^2(\mathbf{q}) d^3q$ ,  $\widetilde{U}_{\text{dd}}(\mathbf{q})$  and  $\widetilde{n}(\mathbf{q})$  being the Fourier transforms of the dipole potential and density, respectively [101]. Because of the localization of the wavefunctions at the bottom of the optical lattice wells, the long-range part of the dipole–dipole interaction  $U_\ell$  is in very good approximation given by the dipole–dipole interaction potential at distance  $\ell$ ,  $U_\ell = (C_{\text{dd}}/4\pi)[1 - 3\cos^2(\theta_\ell)]/\ell^3$ , multiplied by the densities  $n_i$  and  $n_j$  in the two sites, where  $\theta_\ell$  is the angle between  $\ell$  and the orientation of the dipoles. The ratio between the total

<sup>15</sup> All apart from [293].

on-site interaction  $U = U_s + U_{\text{dip}}$  and the nearest-neighbor dipolar interaction  $U_{\text{NN}}$  determines much of the physics of the system. It can be varied by tuning the on-site dipole–dipole interaction  $U_{\text{dip}}$  from negative to positive by changing the vertical confinement, or by changing the s-wave scattering length via a Feshbach resonance, as recently demonstrated with chromium atoms [73].

Due to the anisotropic character of dipole–dipole interaction, a much richer physics is to be expected with respect to the case of only repulsive long-range interactions. By changing the optical lattice strength, the transverse confinement and the orientation of the dipoles, the parameters of the Bose–Hubbard Hamiltonian can be tuned over a wide range, the interaction can be made positive or negative and the tunneling parameter anisotropic. Exploiting all those degrees of freedom, one can scan in a single system checkerboard or striped ground states, and eventually collapse [286]. Very recently, in two works, the best available QMC codes were used to study the quantum phases of 2D dipolar gases [298, 299]. The main results of [298] were as follows: (i) existence and stability of lobes in the phase diagram containing insulator states: checkerboard, star solid and  $\nu = 1/3$  solid, and surrounding them supersolid regions; (ii) devil’s staircase region of the phase diagram with phases corresponding to commensurate filling; (iii) appearance of complex ‘wedding’ cake structures for harmonically confined dipolar gases; (iv) appearance of multiple metastable states, confirming the predictions of [316] (see below).

In [300], the case of chromium, including the real spinor character of the atoms, has been considered. The dipole–dipole interaction has been treated as a perturbation on top of the dominant spin-dependent contact interaction. Using a mean-field treatment with a trial wavefunction beyond on-site product wavefunction, the quantum phases have been identified and in particular an antiferromagnetic–ferromagnetic first order transition occurring simultaneously with the MI–SF transition.

The existence and observability of the above-mentioned quantum phases require a relative strength of the long-range dipole–dipole interaction that is not too small compared with the zero-range one. This can be achieved by reducing the s-wave scattering length, as demonstrated in [73]. However, the absolute energy scale has to be compared with recombination losses over the time scale of the experiments and finite temperature effects. This might make stronger dipolar interactions desirable and polar molecules the optimal candidates for the realization of this kind of physics. Recently, as already mentioned in section 3.1, the difficulties of creating heteronuclear polar molecules in deeply bound vibrational states have been successfully overcome [24–26] and a high-space density gas of polar molecules in their ground vibrational state has been obtained [25, 301]. These achievements open a new era toward quantum degenerate molecular gases of strongly interacting dipoles.

The search for supersolid and other exotic phases in cold atomic system in optical lattices is not, however, restricted to the case of dipolar atoms, Rydberg atoms or polar molecules [45, 302, 303]. Other optical lattice systems

are relevant, like Bose–Bose mixtures [304–306], Bose–Fermi mixtures [306–308], Fermi–Fermi mixtures [309], confined attractive [309, 310] and repulsive fermions [311], and bosonic gases in frustrated (triangular) lattices [312–315], as well as extended Bose–Hubbard Hamiltonians designed from underlying contact-interaction systems using proper laser excitations involving higher bands [296].

### 9.5. Metastable states of dipolar lattice gases

Beyond the richness of ground states discussed in the previous section, in the presence of long-range interactions, metastable insulating states are also predicted [316]. Similar physics appears also in the case of Bose–Bose mixtures, where local minima of the energy landscape indicate the presence of quantum emulsion states, i.e. metastable states characterized by microscopic phase separation, finite compressibility in the absence of superfluidity, thus with macroscopic properties analogous to those of a Bose glass [317–319].

To determine the existence of the insulating states at fractional filling factor and the metastable states in a gas of dipoles in an optical lattice, one has to apply exactly the same criteria defining the Mott insulating states in the case of on-site interaction only. A crucial difference is that for non-uniform atomic distributions in the lattice, the energy of particle–hole excitations is site dependent. For nearest-neighbor interaction and zero tunneling, the checkerboard ordering of the atoms (see figure 31(GS)) is the ground state in the range of chemical potential  $0 < \mu < 4U_{\text{NN}}$ . In a similar way, an ‘elongated-checkerboard’ ordering of the atoms (as shown in figure 31(I)) at  $J = 0$  is stable against particle–hole excitations in the range of chemical potential  $U_{\text{NN}} < \mu < 3U_{\text{NN}}$ ,  $U_{\text{NN}}$  being the first nearest-neighbor interaction (and neglecting for the sake of simplicity all following ones).

The phase diagram of the system for a  $4 \times 4$  elementary cell and different cut-off of the interaction range is shown in figure 31. In the presence of long-range interactions, there are insulating lobes corresponding both to ground and metastable states, characterized by integer and fractional filling factors and a non-uniform distribution of the atoms in the lattice (see the caption of figure 31 for details).

The filling factors allowed and the metastable configurations clearly depend strongly on the cut-off range of interactions. Due to the strongly decreasing  $r^{-3}$  behavior of the dipole–dipole interaction, in most theoretical approaches the interaction range is cut off at few nearest neighbors. This influences the results at very small particle or hole densities (in the particle–hole duality case of strong on-site interaction, as shown in figure 31), but only slightly changes the insulating part of the phase diagram at densities close to half filling [320]. This conclusion is confirmed by the results obtained in [321, 298] for dipolar atoms in a 1D and 2D optical lattice, respectively. Taking into account the infinite-range dipole–dipole interaction, one finds a Mott lobe in a given range on  $\mu$  for each rational filling factor (‘devil’s staircase’), but the dominant lobes are those corresponding to filling factors with smaller denominators.

The phase diagram of figure 31 is confirmed by the imaginary and real time evolution of the system. Depending

on the initial conditions, the imaginary time evolution converges to a different metastable configuration. In the real time evolution, the stability of those metastable configurations is reflected into typical small oscillations around the corresponding local minima of the energy landscape.

The stability of the metastable states has been studied with a path integral formulation in imaginary time [320, 322], which can describe the tunneling below a potential barrier (instanton effect). This analysis suggests that the metastable configurations are very stable when many sites must invert their population to reach another metastable state. However, especially in larger lattices, two metastable configurations might differ just by the occupation of few lattice sites. This, and the corresponding small energy differences, should be carefully taken into account in a realistic analysis at a finite temperature aimed at describing the experiments.

Because of the presence of those very many metastable states, in an experiment it will be very hard to reach the ground state or a given metastable configuration. It was checked that the presence of defects is strongly reduced in the result of the imaginary time evolution, when a local potential energy following desired patterns is added to the optical lattice. One can use superlattices in order to prepare the atoms in configurations of preferential symmetry. This idea is presently pursued by several experimental groups. Note that the configurations obtained in such a way will also remain stable once the superlattice is removed, thanks to dipole–dipole interaction.

Spatially modulated structures can be detected via the measurement of the spatial noise correlations function of the pictures produced after expansion [272, 273, 297]. Such a measurement is in principle able to recognize the defects in the density distribution, which could be exactly reconstructed starting from the patterns in the spatial noise correlation function. However, the signal-to-noise ratio required for single defect recognition is beyond present experimental possibilities, where the average over a finite number of different experimental runs producing the same spatial distribution of atoms in the lattice is required to obtain a good signal.

In view of the possible application of such systems as quantum memories one should be able to transfer in a controlled way the system from one configuration to another [320]. The real time evolution of the system was studied by appropriately varying the Hamiltonian parameters (tunneling coefficients and local chemical potentials) and it was shown that it is impossible to map this problem onto a simple adiabatic transfer process. This is due to the fact that, in spite of the modification of the lattice parameters, the metastable states survive unchanged till the point where the stability condition is not fulfilled anymore. The transition to any other state is then abrupt. A way around this problem is to push the system into the superfluid region and then drive it back into a different insulating state. The transfer between two metastable states turns out to be a quantum controlled process, where the Hamiltonian parameters must be controlled with very high precision to obtain the desired result.

### 9.6. Bilayer and multilayer dipolar lattice gases. Interlayer effects

In the previous subsections, we have discussed the case of a single 2D optical lattice layer. In the present experiments, usually 2D geometries are created as a series of pancake traps by means of a very strong 1D optical lattice in the perpendicular direction, which provides strong confinement and completely suppresses tunneling in that direction. In the presence of long-range interaction, in order to isolate each layer, one should also reduce the interaction between the different layers making the distance between the different layers much larger than the lattice spacing in the 2D plane. This can be achieved, e.g., by creating a 1D lattice in the perpendicular direction with two laser beams intersecting at a small angle  $\theta$ , which increases the lattice spacing in the third direction to  $d_{1D} = (\lambda/2)/\sin(\theta/2)$ . Alternatively, by using two different wavelengths for the 1D and 2D lattices, one can make the 1D distance larger or even smaller than the 2D lattice spacing. This might be useful in cases where inter-layer interactions do not have to be suppressed, but on the contrary are exploited to generate novel effects.

The case of two parallel 1D optical lattices without tunneling among the two wires has been considered in [323, 324]. In that work, the polarization of the dipoles is chosen such that only on-site intra-layer interaction and nearest-neighbor attractive interaction between the layers exist. Such an attractive inter-layer interaction leads to the formation of a pair superfluid (PSF) [325–328], i.e. a superfluid phase of pairs, composed of two atoms at the same axial position but in different wires. In the PSF phase, only simultaneous hopping of atoms in the two wires is involved. Due to the direct Mott to PSF transition the lowest excitations of the Mott state are not, as usually, given by particle–hole excitations, but rather by the creation and destruction of pairs. This change in the nature of the Mott excitations leads to a significant deformation of the Mott-insulator lobes, and may even induce a re-entrant shape of the lobe at small hopping.

The same scenario is expected for two 2D optical lattice layers, based on the mapping of this problem to the one of bosonic mixtures in 2D lattices [325–328]. However, the physics of dipolar atoms in layered 2D optical lattices is even richer, because of the long-range intra- and inter-layer anisotropic interactions. The case of dipoles pointing perpendicular to the 2D lattice plane, generating repulsive nearest-neighbor intra-layer and attractive nearest-neighbor inter-layer interactions, has been recently investigated [329]. A mean-field treatment of the effective pair Hamiltonian provides clear evidence of the existence of a pair-supersolid phase (PSS), which arises from two-particle and two-hole excitations on top of the checkerboard-like insulating phase at half-integer filling factor (see figure 32(b)).

When tunneling between the two layers is not completely suppressed (in the specific case, two uniform 2D layers without lattice), beyond the superfluid and pair-superfluid phases, a phase transition toward a maximally entangled state, where all particles populate either one layer or the other, has been shown [330].

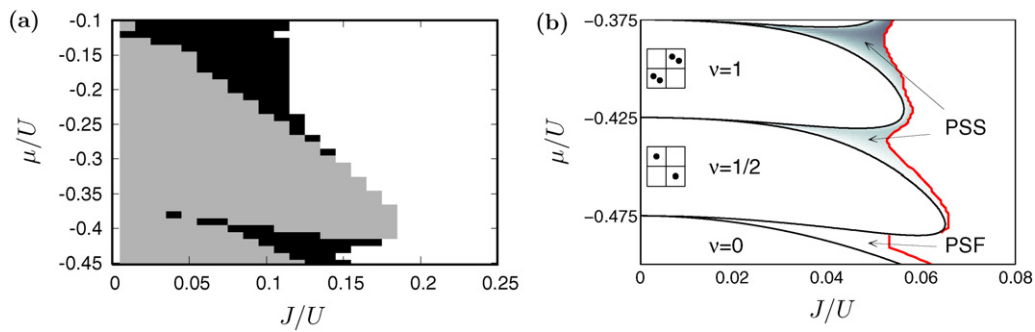


**Figure 32.** (a) Phase diagram for a system of two parallel 1D lattices in the presence of on-site intra-wire interaction  $U$  and nearest-neighbor inter-wire interaction  $W$ , for  $W/U = -0.75$ ; white represents 2SF, gray MI and black PSF (figure taken from [324]). (b) Effective MF phase diagram for a system of two 2D optical lattice layers in the presence of on-site intra-layer interaction  $U$ , nearest-neighbor intra-layer interaction  $U_{NN}$  and nearest-neighbor inter-wire interaction  $W$ , for  $W/U = -0.95$  and  $U_{NN}/U = 0.025$ ; the white regions inside the lobe are CB insulating with single or double site occupancy, the gray shaded region represents the PSS and the lower white region is PSF, as indicated by the arrows. The red (gray) line indicates the estimated limit of validity of the effective MF treatment [329].

In [331] the full 3D geometry for dipoles pointing along the perpendicular  $z$ -direction has been considered. For inter-layer attraction and positive on-site interaction, layered phases where the density distribution is the same on all lattice layers exist. For negative on-site interaction, instead, modulation of the density with period 3 along  $z$  has been found, reminiscent of the structure of high- $T_c$  cuprate superconductors. In this work there is no evidence of the pair-superfluid phase, because of the mean-field approach used.

### 9.7. Tailoring interactions with polar molecules

Thanks to their promisingly large dipole moments (typically of the order of a few Debye), polar molecules have been the subject of extensive theoretical investigation centered in the possibility of tailoring the shape of their interaction [332].

Polar molecules prepared in a mixture of rotational states interact through long-range dipole–dipole interaction even in the absence of an external electric field. The possible Mott phases present different ordering, depending on the preparation of the initial superposition. When the Mott state is melted the superfluid state can interpolate between homogeneous and antiferromagnetic ordering or phase separate depending on the Hamiltonian parameters [303].

On the other hand, appropriate static and/or microwave fields can be applied to design effective potentials between two molecules in their electronic and vibrational state [45, 333]. The mechanisms to induce tailored interactions rely on the simple rigid rotor Hamiltonian (see appendix B), providing the low energy rotational states of the molecules. Such rotational states can be coupled by static or microwave fields to design long-range interaction potentials, in contrast to the typical van der Waals interaction in the absence of external fields. In 2D, a static electric field induces a typical repulsive dipolar potential scaling as  $1/r^3$ , which leads to crystallization. An additional microwave field allows further shaping of the potential, even allowing an attractive part. As previously discussed, in the presence of such induced interactions, the system can be driven through crystalline, superfluid and normal phases [45, 333].

Further investigation has shown that the static electric field and the microwave field dressing the molecular rotational

levels can be chosen in such a way as to obtain dominant three-body interactions [334]. Hamiltonians with many-body interactions have been studied in the context of non-Abelian topological phases (like Pfaffian wavefunction accounting for the quantum Hall effect or systems with a low energy degeneracy characterized by string nets), multiple species in frustrated lattice topologies, ring exchange models (like the one responsible for the nuclear magnetism in helium 3) or undoped high- $T_c$  compounds and cuprate ladders. In typical condensed matter systems many-body interactions are rarely dominant and polar molecules provide a setting where they can be controlled and designed independently from two-body interactions.

A Hubbard model including an unconventional three-body interaction term  $\sum_{i \neq j \neq k} W_{ijk} n_i n_j n_k$  can be readily obtained. The Hamiltonian parameters for two- and three-body interactions depend explicitly on the applied fields. The three-body interaction is intrinsically long range due to the underlying dipole–dipole interaction.

The 2D and 1D quantum phase diagrams for strong three-body interactions have been recently investigated. In 2D [335], a rich variety of solid, supersolid, superfluid or phase separated phases are encountered. The several solid phases at fractional filling factor evolve, upon doping, into corresponding supersolid phases with complex spatial structures. In particular, the checkerboard supersolid at filling factor  $1/2$ , which is unstable for hard-core bosons with nearest-neighbor two-body interaction, is found to be stable in a wide range of tunneling parameters. In 1D [336], quantum Monte Carlo simulations have shown that strong three-body interactions give rise to an incompressible phase at filling factor  $2/3$ , which presents both charge-density wave (CDW) and bond (BOW) orders. At the same time, they have ruled out the solid phases at filling factors  $1/2$  and  $1/3$  predicted by Luttinger theory [334]. The solid phases at filling factor  $1/2$  is found only in the presence of additional nearest and next-nearest two-body interactions. These can be either CDW or BOW depending on the intensity of the two-body corrections. Instead, at filling factor  $1/3$ , the system is always superfluid.

By tuning the optical potential parameters and by means of external electric and magnetic fields, one can induce and

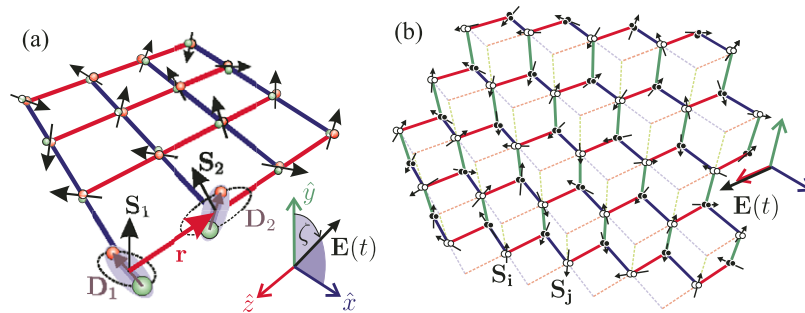


**Figure 33.** (a) Square lattice in 2D with nearest-neighbor orientation-dependent Ising interaction along  $\hat{x}$  and  $\hat{z}$ . (b) Two staggered triangular lattices with nearest-neighbor oriented along orthogonal triads. Figure courtesy of Zoller.

control the interaction between spin states of neutral atoms in an optical lattice and engineer quantum spin Hamiltonians [17, 337, 338]. Such proposals are aimed at the study of a variety of quantum phases, including the Haldane phase, critical phases, quantum dimers and models with complex topological order supporting exotic anyonic excitations. By including a spin degree of freedom in addition to the rotational degrees of freedom of polar molecules, spin models for half-integer and integer spins with larger coupling constants can be obtained [302, 339]. The main ingredient of these proposals is the dipole–dipole interaction: it couples strongly the rotational motion of the molecules, it can be designed by means of microwave fields (as explained above) and it can be made spin dependent, exploiting the spin-rotation splitting of the molecular rotational levels. The final goal is to reproduce models with emergent topological order, robust to arbitrary perturbations of the underlying Hamiltonian, and hence suitable for error-resistant qubit encoding and for quantum memories.

For spin  $1/2$ , it has been explicitly demonstrated how to construct two highly anisotropic spin models [302]. The first model (see figure 33(a)) is a 2D spin model with nearest-neighbor orientation-dependent Ising interactions. It has ideally a gapped two-fold degenerate ground subspace with zero local magnetization, which guarantees immunity to local noise [340]. The second model (see figure 33(b)) takes place on two staggered triangular lattices, equivalent to Kitaev’s honeycomb model [341]. In appropriate regimes, this model provides a ground state which encodes a topologically protected quantum memory.

### 9.8. Self-assembled structures

The long-range character of the dipole–dipole interaction allows the formation of self-assembled structures. Different situations have been the object of recent studies, ranging from the formation of chains of polar molecules in 1D optical lattices driven by the attractive part of the dipole potential, to the appearance of crystal ordering in 1D or 2D systems driven instead by the repulsive character of the interaction. In this section, we summarize the main results and possible applications.

The case studied in [342] considered a stack of 2D layers created by a strong 1D lattice. The dipoles are pointing

perpendicularly to the 2D layer, such that the interaction is repulsive in each layer and attractive for atoms located on top of each other in different layers. Collapse in the perpendicular direction is prevented by the complete suppression of tunneling by the strong 1D lattice. It has been found that the attraction in the perpendicular direction is responsible for the formation of chains of dipoles, where the longest chain is energetically favorable, while the shortest chain is favored by entropy. When temperature is decreased, condensation in the longest chain takes place. It has been pointed out that the physics is similar to the physics of rheological electro- and magneto-fluids.

In the 2D homogeneous system for dipoles pointing perpendicular to the plane, the repulsive interaction is responsible for the formation of hexagonal crystal ordering [45, 343–345], similar to the formation of Wigner crystals for electrons or ions interacting via the Coulomb repulsion [346, 347]. However, two important differences are found, namely that the transition to the crystal phase in dipolar systems happens at high density (instead of that at low density as for Coulomb systems), and the spectrum shows two phononic linear branches with different slopes (rather than the dispersion  $\omega \sim q^{1/2}$  typical of Coulomb crystals).

The formation of the crystal ordering has been identified as a first order phase transition [45, 345] which appears with a delta-peak at the inverse lattice spacing in the structure factor. The transition happens for  $r_s = 37 \pm 1$  [345], where  $r_s$  stands for the ratio between interaction energy and kinetic energy<sup>16</sup>. Contrary to Coulomb systems,  $r_s$  increases with density, which is why Bose–Einstein condensation is found at low densities and the dipole–dipole dominated crystalline phase at high densities. The quantum melting transition should be in reach for the typical parameters of polar molecules.

In [344] the excitation spectrum has been shown to develop a roton minimum as the density increases. However, the question about the possibility of having a supersolid in such systems is still open due to difficulties in getting reliable measures of the superfluid density [345]. In [120] a greater stability of supersolid phases has been conjectured for multi-layer systems, since the roton softening occurs at wavelengths much larger than the layer width, which should prevent global collapse.

<sup>16</sup> This result is consistent with the other results of  $r_s = 32 \pm 7$  [45] and  $r_s = 30$  [344].

In [348], it has been proposed to exploit the protection against short-range collisions provided by the crystalline ordering to use those self-assembled dipolar crystals as high-fidelity quantum memories. Furthermore, the self-assembled crystal could be used as a floating lattice structure for a second species of atoms or molecules [349]. The advantages of this proposal are that the lattice spacing can be tuned down to the hundred nanometer scale and that the second species is subject both to its own Bose–Hubbard coupling and to the coupling to lattice phonons.

In a system of two parallel 2D layers at distance  $l$  and dipoles pointing perpendicular to the layers, one finds intra-layer repulsion and inter-layer attraction (repulsion) for dipoles separated by a distance  $r < \sqrt{3}l$  ( $r > \sqrt{3}l$ ). It has been shown [350] that the hexagonal crystalline order is preserved in both layers, and as a function of the layer distance  $l$ , one goes from two independent crystals to a crystal of paired dipoles. Moreover, since the melting temperature is not monotonic in  $l$ , a solid–liquid–solid transition takes place for increasing  $l$  at a fixed temperature.

Furthermore, the formation of ordered patterns in 1D systems has been recently investigated in [36, 351–354]. In [352, 353], it has been pointed out that one-dimensional dipolar gases present strongly correlated phases beyond the strongly correlated Tonks–Girardeau regime. The crossover from the superfluid state to the ordered state takes place for increasing densities (like in 2D) and appears in the structure factor as additional peaks at the inverse lattice spacing. In the whole crossover, the gas preserves a Luttinger-liquid behavior, since no roton minimum nor long-range order is found.

In [36] the stability of such ordered structures with respect to the transverse confinement has been investigated, in analogy to what is known from Coulomb Wigner crystals [355]. By weakening the transverse confinement, or equivalently increasing the density or the strength of the dipolar interaction, a smooth crossover to a zigzag chain and to structures formed by multiple chains is predicted. Quantum fluctuations smoothen out these transitions, which are, respectively, first and second order phase transitions in a classical model, and also completely melt the crystal for low values of density or dipolar interaction.

## 10. Outlook

An epilogue, in the disguise of wrapping up the past, is really a way of warning us about the future.  
J. W. Irving, *The World According to Garp*.

### 10.1. From chromium to heteronuclear molecules to Rydberg atoms

The experimental realization of dipolar gases was first obtained with atomic chromium. Despite the large spin magnetism in chromium, the dipole moment is still small, classifying the dipolar interaction as a weak one, where the length scale of the interaction is much smaller than the interparticle spacing. In this regime we will probably see in the near future experiments on self-organized collective structures close to the instability

of the gas. In spinor gases first experimental steps have been done in this direction [224], as shown in section 8.

Rapid progress has been made in the creation of heteronuclear molecules (see section 3.1) in their vibrational ground state [25, 26]. These experiments still have to go some way to degeneracy; however, given the speed of the development we can expect this step to be taken in the near future. These gases—when the molecules are prepared in the rotational ground state—then cover the whole range of dipolar interaction strengths—from weak to strong interactions—as their electric dipole moment can be tuned via an external electric dc field. Even the three-body interaction can be controlled independently of the two-body interaction by the use of microwave fields [334]. These systems will therefore provide a rich toolbox for quantum simulation of spin systems.

Even dramatically larger dipolar interactions between Rydberg atoms have also become available in the regime of quantum degenerate gases since the first Rydberg excitation of Bose–Einstein condensates [52]. As the energy spectrum of Rydberg atoms involving a quantum defect is very similar to the level structure of a heteronuclear molecule, many of the proposed techniques to mix rotational states to tailor the dipolar interaction can be directly applied to Rydberg atoms. Despite their limited lifetime the huge size of the dipole moments—typically 1000 times larger than for heteronuclear molecules—opens up a whole new class of experiments on long-range interacting spin systems. Recently, the mapping of a long-range interacting spin system onto a frozen Rydberg gas was realized successfully and universal scaling of that strongly interacting system could be determined experimentally [356].

In terms of particle numbers this experiment was done in a regime where exact quantum calculations have no access. Therefore the quantum simulation of large and strongly interacting spin systems by mapping to other equivalent quantum systems—just as Richard Feynman proposed—is starting to become a reality. Dipolar gases will enrich this effort substantially.

### 10.2. Dipolar gases and trapped ions

One of the most promising and fascinating ideas that will allow one to investigate quantum systems bearing a very close similarity to ultra-cold atomic gases comes from somewhat unexpected directions. Namely, in recent years, there has been an enormous interest in ideas that could lead to the use of trapped ions for simulating quantum many-body systems.

Wunderlich had in 2001 [357, 358] the idea of using inhomogeneous magnetic fields and long wavelength radiation to solve the problem of individual ion addressing in ion traps—one of the most important obstacles to the implementation of quantum information processing with ultra-cold ions. As a byproduct Mintert and Wunderlich obtained the result that internal degrees of freedom of ions behave as coupled pseudo-spins, where the coupling is mediated by the phonons in the trap. This idea has been fully put forward by Porras and Cirac [359, 360], who have argued that trapped ions can be as attractive systems for quantum simulations as ultra-cold atoms or molecules in optical lattices. Effective quantum spin

systems that one can achieve with ions range from linear chains to 2D self-assembled, or optically prepared lattices, with very precise control of the parameters. The most interesting aspect in the present context is that the interactions mediated by phonons are of long-range character, and in fact typically decay with distance as  $1/r^3$ . The typical spin Hamiltonian one can simulate with ions has the form

$$H = \frac{1}{2} \sum_{i,j} J_{ij}^z S_i^z S_j^z - \frac{1}{2} \sum_{i,j} J_{ij}^x S_i^x S_j^x - \frac{1}{2} \sum_{i,j} J_{ij}^y S_i^y S_j^y - \sum_i (H_i^x S_i^x + H_i^y S_i^y + H_i^z S_i^z), \quad (10.1)$$

where the overall sign and magnitude of  $J_{ij}^{x,y,z}$  can be controlled, whereas the spatial dependence is  $J_{ij}^{x,y,z} \propto 1/|r_i - r_j|^3$ . When  $J^x = J^y$  these models correspond nearly exactly to hard-core Bose gases with dipole–dipole interactions, and in the presence of transverse and longitudinal ‘magnetic’ fields. The only difference is that the tunneling now has a non-local character, and its amplitude also decays as slowly as  $1/r^3$ , since the phonons allow for such long-range interactions.

The ingenious idea of Porras and Cirac has been followed in many directions. Phonons themselves may exhibit fascinating many-body quantum physics and undergo Mott insulator–superfluid transition [361]. One can realize mesoscopic spin-boson models with trapped ions [362], or quantum neural network models and fault resistant quantum computing [363, 364]. Recently, the idea of combining lattices (either optical ones consisting of microtraps [365] or lattices employing surface electrodes [366]) with ion traps has led to fascinating proposals for realization of antiferromagnetic spin models in a triangular lattice with adjustable couplings, where the different Néel orders can be realized [365]. As the parameters interpolate between these Néel orders, the system is expected to enter into quantum spin liquid states of various types. These predictions have been very nicely supported in [365], where exact diagonalization was compared with one of the first non-trivial applications of the so-called pair entangled projected states (PEPS) method.

All these proposals are not inventions of theoreticians: many of the leading experimental ion trapper groups are working on quantum simulations with ions, and the first spectacular experimental results have been obtained already [367].

### 10.3. ‘Dipolar art’

To conclude this review, we note that the excitement about the advances in dipolar gases is not only widespread among the experts in the cold atom and condensed matter community: to our amazement, it has also recently inspired the artist Brigitte Simon to work on ‘dipolar art’. This expert in artwork made of glass has for example designed many church stained glass windows. After discussing the physics behind the images of a collapsing dipolar BEC with some of us, she started to work on a glass window based on our measurements. Let us quote her: ‘I was fascinated when I discovered an article in the Frankfurter Allgemeine Zeitung in August 2008 [about the dipolar collapse, reproducing pictures from figure 19].

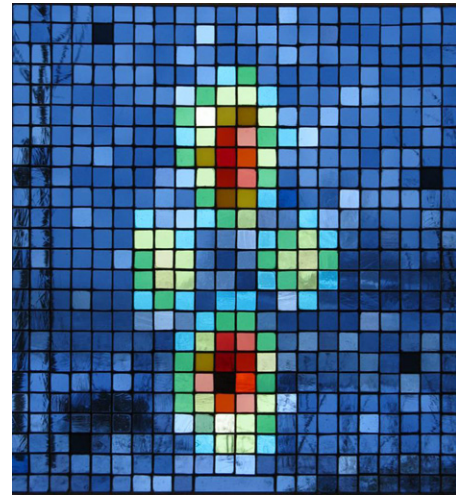


**Figure 34.** A stained glass window, composed of 524 one-inch squares, each selected from a wide variety of colors and precisely cut out of mouth-blown genuine antique glass from Bavaria, reproducing the shape of a collapsed dipolar BEC (compare with figure 19). The squares are framed with copper foil and soldered front and back. Figure courtesy of Simon.

Reading it over and over I tried to understand what a miracle had been created at Stuttgart University. Marveling at the photos I felt that there is Art in Science, and this is what I tried to capture’ (figure 34).

### Acknowledgments

The authors would like to thank many collaborators for illuminating discussions over several years, in particular J Arlt, G Astrakharchik, M C Bañuls, M A Baranov, N Barberán, I Bloch, K Bongs, J Boronat, S Braungardt, M Brewczyk, H P Büchler, J I Cirac, F Cucchietti, C Cohen-Tannoudji, J Dalibard, Ł Dobrek, O Dutta, W Ertmer, M Fattori, H Fehrmann, S Fishman, B Fröhlich, M Gajda, S Giovanazzi, K Góral, Ph Grangier, A Griesmaier, Ph Hauke, M Jonas-Lasinio, M Klawunn, C Klempt, T Koch, P Massignan, J Metz, G Modugno, M Modugno, G Morigi, R Nath, K Osterloh, P Pedri, M Pons, D Porras, G Pupillo, E Rasel, K Rzążewski, A Sanpera, K Sengstock, G V Shlyapnikov, B Simon, S Stringari, J Stuhler, Ch Trefzger, Ch Wunderlich, M Ueda, P Zoller and the late K Wódkiewicz.

TL and TP acknowledge support by the German Science Foundation (SFB/TRR 21 and SPP 1116), the Landesstiftung Baden Württemberg and the EU (Marie-Curie Grant MEIF-CT-2006-038959 to TL). CM acknowledges support by the EU (Marie-Curie Grant MEIF-CT-2006-023570). LS acknowledges support by the German Science Foundation (SFB407, SPP1116, SFB/TRR 21) and by ESF/DFG EUROQUASAR QuDeGPM. ML acknowledges Spanish MEC projects TOQATA (FIS2008-00784) and QOIT (Consolider Ingenio 2010), ESF/MEC project FERMIX (FIS2007-29996-E), EU Integrated Project SCALA, EU STREP project NAMEQUAM, ERC Advanced Grant QUAGATUA and the Humboldt Foundation Senior Research Prize.

## Appendix A. Fourier transform of the dipolar interaction

In this appendix, we sketch the main steps of the calculation of the Fourier transform (2.5) of the dipole–dipole interaction. Using spherical coordinates  $(r, \theta, \varphi)$ , with the polar axis along  $\mathbf{k}$  and the dipole moment in the  $y = 0$  plane (making the angle  $\alpha$  with  $\mathbf{k}$ ), one has

$$\begin{aligned} \widetilde{U}_{\text{dd}}(\mathbf{k}) &= \frac{C_{\text{dd}}}{4\pi} \iiint e^{-i\mathbf{k}\mathbf{r}\cos\theta} \\ &\times \frac{1 - 3(\sin\alpha \sin\theta \cos\varphi + \cos\alpha \cos\theta)^2}{r} \\ &\times \sin\theta \, dr \, d\theta \, d\varphi. \end{aligned} \quad (\text{A.1})$$

After integration over  $\varphi$  and the change of variable  $x = \cos\theta$ , we obtain

$$\begin{aligned} \widetilde{U}_{\text{dd}}(\mathbf{k}) &= \frac{C_{\text{dd}}}{4\pi} \int_b^\infty \frac{dr}{r} \int_{-1}^1 e^{-ikrx} \pi(3\cos^2\alpha - 1) \\ &\times (1 - 3x^2) \, dx, \end{aligned} \quad (\text{A.2})$$

where  $b$  is a cut-off at small distance introduced to avoid divergences at this stage. The integration on  $x$  is straightforward, and gives

$$\begin{aligned} \widetilde{U}_{\text{dd}}(\mathbf{k}) &= C_{\text{dd}}(1 - 3\cos^2\alpha) \\ &\times \int_{kb}^\infty \left( \frac{\sin u}{u^2} + \frac{3\cos u}{u^3} - \frac{3\sin u}{u^4} \right) du, \end{aligned} \quad (\text{A.3})$$

with  $u = kr$ . The last integral can be calculated by parts and has the value  $[kb \cos(kb) - \sin(kb)]/(kb)^3$ . We can now let the cut-off  $b$  go to zero; the last integral then approaches  $-1/3$  and thus we finally get expression (2.5) for the Fourier transform of the dipole–dipole interaction.

## Appendix B. Stark effect of the rigid rotor

In this appendix, we briefly recall basic results (see, e.g. [333]) concerning the behavior of a spinless diatomic molecule, modeled as a spherical rigid rotor, in an electric field  $\mathcal{E}$ , with an emphasis on the dependence of the average electric dipole moment (in the laboratory frame) on the applied field. We

assume that the molecule is in its electronic and vibrational ground state, and that the electronic ground state is a  $^1\Sigma$  state (as, e.g., in the case of bi-alkali molecules). For the sake of simplicity, we also neglect the hyperfine structure, although this is an issue relevant to experiments. The Hamiltonian for a rigid rotor reads as

$$\hat{H}_{\text{rot}} = B\hat{J}^2, \quad (\text{B.1})$$

where  $\hat{J}$  is the molecule angular momentum operator (in units of  $\hbar$ ) and  $B$  the *rotational constant*, linked to the equilibrium internuclear distance  $r$  and the reduced mass  $m_r$  by the relationship  $B = \hbar^2/(2m_r r^2)$ ; its typical order of magnitude is  $B/h \sim 10$  GHz. The eigenstates of (B.1) are the angular momentum eigenstates  $|J, m_J\rangle$  with energy  $BJ(J+1)$ , and are  $2J+1$  times degenerate. Figure B1(a) represents the first few eigenstates of (B.1), with energies  $0, 2B, 6B \dots$

This molecule is supposed to have a permanent dipole moment  $\hat{d}$  in the molecular frame. Then, in the presence of an external field  $\mathbf{E} = \mathcal{E}\mathbf{e}_z$ , the Stark Hamiltonian of the molecule reads as

$$\hat{H} = \hat{H}_{\text{rot}} - \hat{d} \cdot \mathbf{E} = \hat{H}_{\text{rot}} - d\mathcal{E}\cos\theta, \quad (\text{B.2})$$

where  $\theta$  is the angle between  $z$  and the internuclear axis. Figure B1(b) represents the first eigenstates of the Hamiltonian (B.2), diagonalized numerically, as a function of  $\mathcal{E}$ . The interaction with the electric field lifts the degeneracy between levels having different values of  $|m_J|$ . From this Stark map, the average dipole moment  $\langle d_z \rangle = d\langle \cos\theta \rangle$  for the ground state  $|\phi_0\rangle$  is obtained (via the Hellmann–Feynman theorem) as

$$\langle d_z \rangle = - \left\langle \phi_0 \left| \frac{\partial \hat{H}}{\partial \mathcal{E}} \right| \phi_0 \right\rangle = - \frac{\partial E_0}{\partial \mathcal{E}}, \quad (\text{B.3})$$

where  $E_0(\mathcal{E})$  is the ground state energy. The dipole moment is plotted in figure B1(c). One observes that  $\langle d_z \rangle$  increases linearly at small  $\mathcal{E}$  (more precisely, one has  $\langle d_z \rangle/d \sim d\mathcal{E}/(3B)$  for small fields), and tends asymptotically for  $d\mathcal{E} \gg B$  toward its saturated value  $d$ , although relatively slowly, as one can show that to leading order,  $\langle d_z \rangle/d \sim 1 - \sqrt{B/(2d\mathcal{E})}$  for  $d\mathcal{E} \gg B$  [368]. For typical values  $d \sim 1$  D and  $B/h \sim 10$  GHz, the electric field strength corresponding to  $d\mathcal{E} \sim B$  is on the order of  $10^4$  V cm $^{-1}$ , which, from the experimental point of view, is accessible in a relatively easy way.

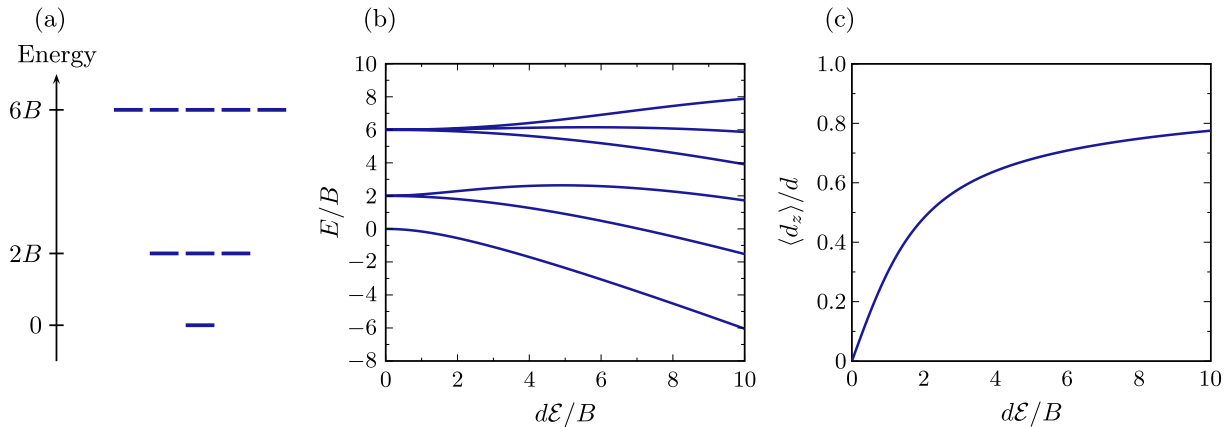


**Figure B1.** (a) Rotational spectrum of a diatomic molecule in zero field. (b) Dependence of the first energy levels on the applied electric field  $\mathcal{E}$ . (c) the ground state average dipole moment  $\langle d_z \rangle$  in the laboratory frame as a function of the applied field  $\mathcal{E}$ .

## References

- [1] Anderson M H, Ensher J R, Matthews M R, Wieman C E and Cornell E 1995 *Science* **269** 198
- [2] Bradley C C, Sackett C A, Tollett J J and Hulet R G 1995 *Phys. Rev. Lett.* **75** 1687
- [3] Davis K B, Mewes M O, Andrews M R, Vandrunen N J, Durfee D S, Kurn D M and Ketterle W 1995 *Phys. Rev. Lett.* **75** 3969
- [4] Mahan G D 1993 *Many-Particle Physics* (New York: Plenum)
- [5] Fetter A and Walecka J 1971 *Quantum Theory of Many-Particle Systems* (New York: McGraw-Hill)
- [6] Cornell E A and Wieman C E 2002 *Rev. Mod. Phys.* **74** 875–93
- [7] Ketterle W 2002 *Rev. Mod. Phys.* **74** 1131–51
- [8] Pitaevskii L P and Stringari S 2003 *Bose–Einstein Condensation* (Oxford: Clarendon)
- [9] DeMarco B and Jin D S 1999 *Science* **285** 1703
- [10] Truscott A G, Strecker K E, McAlexander W I, Partridge G B and Hulet R G 2001 *Science* **291** 2570
- [11] Schreck F, Khaykovich L, Corwin K, Ferrari G, Bourdel T, Cubizolles J and Salomon C 2001 *Phys. Rev. Lett.* **87** 080403
- [12] Hadzibabic Z, Stan C, Dieckmann K, Gupta S, Zwierlein M, Görlitz A and Ketterle W 2002 *Phys. Rev. Lett.* **88** 160401
- [13] Giorgini S, Pitaevskii L P and Stringari S 2008 *Rev. Mod. Phys.* **80** 1215–74
- [14] Bloch I, Dalibard J and Zwerger W 2008 *Rev. Mod. Phys.* **80** 885
- [15] Jaksch D, Bruder C, Cirac J I, Gardiner C W and Zoller P 1998 *Phys. Rev. Lett.* **81** 3108
- [16] Greiner M, Mandel O, Esslinger T, Hänsch T W and Bloch I 2002 *Nature* **415** 39
- [17] Lewenstein M, Sanpera A, Ahufinger V, Damski B, Sen(De) A and Sen U 2007 *Adv. Phys.* **56** 243
- [18] Köhler T, Góral K and Julienne P S 2006 *Rev. Mod. Phys.* **78** 1311
- [19] Chin C, Grimm R, Julienne P and Tiesinga E 2009 *Rev. Mod. Phys.* arXiv:0812.1496
- [20] Inoué S, Andrews M R, Stenger J, Miesner H J, Stamper-Kurn D M and Ketterle W 1998 *Nature* **392** 151
- [21] Courteille P, Freeland R S, Heinzen D J, van Abeelen F A and Verhaar B J 1998 *Phys. Rev. Lett.* **81** 69
- [22] Pethick C J and Smith H 2002 *Bose–Einstein Condensation in Dilute Gases* (Cambridge: Cambridge University Press)
- [23] Doyle J, Friedrich B, Krems R V and Masnou-Seeuws F 2004 *Eur. Phys. J. D* **31** 149
- [24] Ospelkaus S, Pe’er A, Ni K K, Zirbel J J, Neyenhuis B, Kotochigova S, Julienne P S, Ye J and Jin D S 2008 *Nature Phys.* **4** 622
- [25] Ni K K, Ospelkaus S, de Miranda M H G, Peer A, Neyenhuis B, Zirbel J J, Kotochigova S, Julienne P S, Jin D S and Ye J 2008 *Science* **322** 231
- [26] Deiglmayr J, Grochola A, Repp M, Mörthbauer K, Glück C, Lange J, Dulieu O, Wester R and Weidemüller M 2008 *Phys. Rev. Lett.* **101** 133004
- [27] Griesmaier A, Werner J, Hensler S, Stuhler J and Pfau T 2005 *Phys. Rev. Lett.* **94** 160401
- [28] Lahaye T, Metz J, Koch T, Fröhlich B, Griesmaier A and Pfau T 2009 *Pushing The Frontiers Of Atomic Physics: Proc. 21st Int. Conf. on Atomic Physics* ed R Côté *et al* (Singapore: World Scientific)
- [29] Menotti C, Lewenstein M, Lahaye T and Pfau T 2008 *CP970, Dynamics and Thermodynamics of Systems with Long-range Interaction: Theory and Experiments* ed A Campa *et al* (New York: American Institute of Physics)
- [30] Groh B and Dietrich S 1994 *Phys. Rev. Lett.* **72** 2422
- [31] Groh B and Dietrich S 1997 *Phys. Rev. Lett.* **79** 749
- [32] Rosensweig R E 1985 *Ferrohydrodynamics* (New York: Cambridge University Press)
- [33] de Gennes P G and Prost J 1995 *The Physics of Liquid Crystals* (Oxford: Oxford University Press)
- [34] Knieling H, Richter R, Rehberg I, Matthies G and Lange A 2007 *Phys. Rev. E* **76** 066301
- [35] Baranov M A 2008 *Phys. Rep.* **464** 71
- [36] Astrakharchik G E and Lozovik Y E 2008 *Phys. Rev. A* **77** 013404
- [37] Mehring M 1983 *Principles of High Resolution NMR in Solids* (Berlin: Springer)
- [38] Slichter C P 1996 *Principles of Magnetic Resonance* (Berlin: Springer)
- [39] Landau L D and Lifshitz E M 1977 *Quantum Mechanics* 3rd edn (New York: Butterworth-Heinemann)
- [40] Hensler S, Werner J, Griesmaier A, Schmidt P, Gorlitz A, Pfau T, Giovanazzi S and Rzǎzewski K 2003 *Appl. Phys. B* **77** 765
- [41] Giovanazzi S, Gorlitz A and Pfau T 2002 *Phys. Rev. Lett.* **89** 130401
- [42] Greene C H, Dickinson A S and Sadeghpour H R 2000 *Phys. Rev. Lett.* **85** 2458–61
- [43] Bendkowsky V, Butscher B, Nipper J, Shaffer J P, Löw R and Pfau T 2009 *Nature* **458** 1005
- [44] Kotochigova S, Julienne P S and Tiesinga E 2003 *Phys. Rev. A* **68** 022501
- [45] Büchler H P, Demler E, Lukin M, Micheli A, Prokof’ev N, Pupillo G and Zoller P 2007 *Phys. Rev. Lett.* **98** 060404
- [46] van de Meerakker S Y T, Bethlem H L and Meijer G 2008 *Nature Phys.* **4** 595
- [47] Doyle J M, Friedrich B, Kim J and Patterson D 1995 *Phys. Rev. A* **52** R2515
- [48] Weinstein J D, deCarvalho R, Guillet T, Friedrich B and Doyle J M 1998 *Nature* **395** 148
- [49] Egorov D, Lahaye T, Schöllkopf W, Friedrich B and Doyle J M 2002 *Phys. Rev. A* **66** 043401
- [50] Carr L D, DeMille D, Krems R V and Ye J 2009 *New J. Phys.* **11** 055049
- [51] Li W *et al* 2004 *Phys. Rev. A* **70** 042713
- [52] Heidemann R, Raitzsch U, Bendkowsky V, Butscher B, Löw R and Pfau T 2008 *Phys. Rev. Lett.* **100** 033601
- [53] Vogt T, Viteau M, Zhao J, Chotia A, Comparat D and Pillet P 2006 *Phys. Rev. Lett.* **97** 083003
- [54] Marinescu M and You L 1998 *Phys. Rev. Lett.* **81** 4596
- [55] Yi S and You L 2000 *Phys. Rev. A* **61** 041604
- [56] Yi S and You L 2001 *Phys. Rev. A* **63** 053607
- [57] Löw R, Gati R, Stuhler J and Pfau T 2005 *Europhys. Lett.* **71** 214
- [58] Jackson J D 1999 *Classical Electrodynamics* 3rd edn (New York: Wiley)
- [59] O’Dell D, Giovanazzi S, Kurizki G and Akulin V M 2000 *Phys. Rev. Lett.* **84** 5687
- [60] O’Dell D H J, Giovanazzi S and Kurizki G 2003 *Phys. Rev. Lett.* **90** 110402
- [61] Giovanazzi S, O’Dell D and Kurizki G 2001 *J. Phys. B: At. Mol. Opt. Phys.* **34** 4757
- [62] Giovanazzi S, O’Dell D and Kurizki G 2002 *Phys. Rev. Lett.* **88** 130402
- [63] Santos L, Shlyapnikov G V and Lewenstein M 2003 *Phys. Rev. Lett.* **90** 250403
- [64] O’Dell D, Giovanazzi S and Kurizki G 2003 *J. Mod. Opt.* **50** 2655
- [65] Dobrek Ł 2004 *Ultracold dipolar gases PhD Thesis* Universität Hannover
- [66] Beaufiles Q, Chicireanu R, Zanon T, Laburthe-Tolra B, Maréchal E, Vernac L, Keller J C and Gorceix O 2008 *Phys. Rev. A* **77** 061601

- [67] Schmidt P, Hensler S, Werner J, Griesmaier A, Gorlitz A, Pfau T and Simoni A 2003 *Phys. Rev. Lett.* **91** 193201
- [68] Griesmaier A, Stuhler J, Koch T, Fattori M, Pfau T and Giovanazzi S 2006 *Phys. Rev. Lett.* **97** 250402
- [69] Stuhler J, Griesmaier A, Koch T, Fattori M, Pfau T, Giovanazzi S, Pedri P and Santos L 2005 *Phys. Rev. Lett.* **95** 150406
- [70] Bell A S, Stuhler J, Locher S, Hensler S, Mlynek J and Pfau T 1999 *Europhys. Lett.* **45** 156
- [71] Schmidt P O, Hensler S, Werner J, Binhammer T, Gorlitz A and Pfau T 2003 *J. Opt. B: Quantum Semiclass. Opt.* **5** S170
- [72] Werner J, Griesmaier A, Hensler S, Stuhler J, Pfau T, Simoni A and Tiesinga E 2005 *Phys. Rev. Lett.* **94** 183201
- [73] Lahaye T, Koch T, Froehlich B, Fattori M, Metz J, Griesmaier A, Giovanazzi S and Pfau T 2007 *Nature* **448** 672
- [74] Hensler S, Greiner A, Stuhler J and Pfau T 2005 *Europhys. Lett.* **71** 918
- [75] Fattori M, Koch T, Goetz S, Griesmaier A, Hensler S, Stuhler J and Pfau T 2006 *Nature Phys.* **2** 765
- [76] Lounasmaa O V 1974 *Experimental Principles and Methods Below 1 K* (New York: Academic)
- [77] Cirac J I and Lewenstein M 1995 *Phys. Rev. A* **52** 4737–40
- [78] Glaum K, Pelster A, Kleinert H and Pfau T 2007 *Phys. Rev. Lett.* **98** 080407
- [79] Glaum K and Pelster A 2007 *Phys. Rev. A* **76** 023604
- [80] Huang K and Yang C N 1957 *Phys. Rev.* **105** 767
- [81] Pascual P and Gallindo A 1991 *Quantum Mechanics* (Heidelberg: Springer)
- [82] Derevianko A 2003 *Phys. Rev. A* **67** 033607
- [83] Mazets I E and Kurizki G 2007 *Phys. Rev. Lett.* **98** 140401
- [84] Yi S and You L 2004 *Phys. Rev. Lett.* **92** 193201
- [85] Derevianko A 2005 *Phys. Rev. A* **72** 039901
- [86] Derevianko A 2005 *Phys. Rev. A* **72** 044701
- [87] Bortolotti D C, Ronen S, Bohn J L and Blume D 2006 *Phys. Rev. Lett.* **97** 160402
- [88] Ronen S, Bortolotti D C, Blume D and Bohn J L 2006 *Phys. Rev. A* **74** 033611
- [89] Astrakharchik G E, Boronat J and Casulleras J 2007 *Phys. Rev. A* **75** 063630
- [90] Wang D W 2008 *New J. Phys.* **10** 053005
- [91] Pérez-García V M, Michinel H, Cirac J I, Lewenstein M and Zoller P 1996 *Phys. Rev. Lett.* **77** 5320
- [92] Pérez-García V M, Michinel H, Cirac J I, Lewenstein M and Zoller P 1997 *Phys. Rev. A* **56** 1424
- [93] Santos L, Shlyapnikov G V, Zoller P and Lewenstein M 2000 *Phys. Rev. Lett.* **85** 1791
- [94] Góral K, Rzążewski K and Pfau T 2000 *Phys. Rev. A* **61** 051601
- [95] O'Dell D H J, Giovanazzi S and Eberlein C 2004 *Phys. Rev. Lett.* **92** 250401
- [96] Eberlein C, Giovanazzi S and O'Dell D 2005 *Phys. Rev. A* **71** 033618
- [97] Giovanazzi S, Pedri P, Santos L, Griesmaier A, Fattori M, Koch T, Stuhler J and Pfau T 2006 *Phys. Rev. A* **74** 013621
- [98] Pollack S E, Dries D, Junker M, Chen Y P, Corcovilos T A and Hulet R G 2009 *Phys. Rev. Lett.* **102** 090402
- [99] Ruprecht P A, Holland M J, Burnett K and Edwards M 1995 *Phys. Rev. A* **51** 4704
- [100] Gammal A, Frederico T and Tomio L 2001 *Phys. Rev. A* **64** 055602
- [101] Góral K and Santos L 2002 *Phys. Rev. A* **66** 023613
- [102] Koch T, Lahaye T, Metz J, Froehlich B, Griesmaier A and Pfau T 2008 *Nature Phys.* **4** 218
- [103] Bohn J L, Wilson R M and Ronen S 2009 *Laser Phys.* **19** 547
- [104] Ronen S, Bortolotti D C E and Bohn J L 2007 *Phys. Rev. Lett.* **98** 030406
- [105] Dutta O, Jaaskelainen M and Meystre P 2006 *Phys. Rev. A* **73** 043610
- [106] Parker N G and O'Dell D H J 2008 *Phys. Rev. A* **78** 041601(R)
- [107] Bergeman T 1997 *Phys. Rev. A* **55** 3658
- [108] Singh K G and Rokhsar D S 1996 *Phys. Rev. Lett.* **77** 1667
- [109] Donley E A, Claussen N R, Cornish S L, Roberts J L, Cornell E A and Wieman C E 2001 *Nature* **412** 295
- [110] Yi S and You L 2002 *Phys. Rev. A* **66** 013607
- [111] Yi S and You L 2003 *Phys. Rev. A* **67** 045601
- [112] Ronen S, Bortolotti D C E and Bohn J L 2006 *Phys. Rev. A* **74** 013623
- [113] Jin D S, Ensher J R, Matthews M R, Wieman C E and Cornell E A 1996 *Phys. Rev. Lett.* **77** 420
- [114] Dutta O and Lewenstein M 2009 arXiv:0906.2115
- [115] Fischer U R 2006 *Phys. Rev. A* **73** 031602
- [116] Komineas S and Cooper N R 2007 *Phys. Rev. A* **75** 023623
- [117] Klawunn M and Santos L 2009 *Phys. Rev. A* **80** 013611
- [118] Giovanazzi S and O'Dell D H J 2004 *Eur. Phys. J. D* **31** 439
- [119] Pitaevskii L P and Lifshitz E M 1980 *Statistical Physics, part 2* (New York: Butterworth-Heinemann)
- [120] Wang D W and Demler E 2008 arXiv:0812.1838v1
- [121] Nath R and Santos L 2009 arXiv:0902.3969
- [122] Pomeau Y and Rica S 1994 *Phys. Rev. Lett.* **72** 2426
- [123] Jossierand C, Pomeau Y and Rica S 2007 *Phys. Rev. Lett.* **98** 195301
- [124] Dutta O and Meystre P 2007 *Phys. Rev. A* **74** 053604
- [125] Shlyapnikov G V and Pedri P 2006 *Conf. on Many-Body Phenomena in Dipolar Systems (Dresden, Germany)*
- [126] Dutta O, Kanamoto R and Meystre P 2007 *Phys. Rev. Lett.* **99** 110404
- [127] Dutta O, Kanamoto R and Meystre P 2008 *Phys. Rev.* **78** 043608
- [128] Read N and Green D 2000 *Phys. Rev. B* **61** 10267
- [129] Tewari S, Das Sarma S, Nayak C, Zhang C W and Zoller P 2007 *Phys. Rev. Lett.* **98** 010506
- [130] Ronen S and Bohn J L 2007 *Phys. Rev. B* **76** 043607
- [131] Wilson R, Ronen S, Bohn J L and Pu H 2008 *Phys. Rev. Lett.* **100** 245302
- [132] Wilson R M, Ronen S and Bohn J L 2009 *Phys. Rev.* **79** 013621
- [133] Fattori M, Roati G, Deissler B, D'Errico C, Zaccanti M, Jona-Lasinio M, Santos L, Inguscio M and Modugno G 2008 *Phys. Rev. Lett.* **101** 190405
- [134] Fattori M, D'Errico C, Roati G, Zaccanti M, Jona-Lasinio M, Modugno M and Modugno M I G 2008 *Phys. Rev. Lett.* **100** 080405
- [135] Mazzanti F, Zillich R E, Astrakharchik G E and Boronat J 2009 *Phys. Rev. Lett.* **102** 110405
- [136] Kagan Y, Surkov E L and Shlyapnikov G V 1996 *Phys. Rev. A* **54** R1753
- [137] Castin Y and Dum R 1996 *Phys. Rev. Lett.* **77** 5315
- [138] Gerton J M, Strekalov D, Prodan I and Hulet R G 2000 *Nature* **408** 692
- [139] Roberts J L, Claussen N R, Cornish S L, Donley E A, Cornell E A and Wieman C E 2001 *Phys. Rev. Lett.* **86** 4211
- [140] Sackett C A, Gerton J M, Welling M and Hulet R G 1999 *Phys. Rev. Lett.* **82** 876
- [141] Strecker K E, Partridge G B, Truscott A G and Hulet R G 2002 *Nature* **417** 150
- [142] Cornish S L, Thompson S T and Wieman C E 2006 *Phys. Rev. Lett.* **96** 170401
- [143] Lushnikov P M 2002 *Phys. Rev. A* **66** 051601(R)
- [144] Lahaye T, Metz J, Fröhlich B, Koch T, Meister M, Griesmaier A, Pfau T, Saito H, Kawaguchi Y and Ueda M 2008 *Phys. Rev. Lett.* **101** 080401

- [145] Metz J, Lahaye T, Fröhlich B, Griesmaier A, Pfau T, Saito H, Kawaguchi Y and Ueda M 2009 *New J. Phys.* **11** 055032
- [146] Nath R, Pedri P and Santos L 2008 *Phys. Rev. Lett.* **101** 210402
- [147] Ticknor C, Parker N G, Melatos A, Cornish S L, O'Dell D H J and Martin A M 2008 *Phys. Rev. A* **78** 061607(R)
- [148] Parker N G, Ticknor C, Martin A M and O'Dell D H J 2009 *Phys. Rev. A* **79** 013617
- [149] Deng L, Hagley E W, Wen J, Trippenbach M, Band Y, Julienne P S, Simsarian J E, Helmerson K, Rolston S L and Phillips W D 1999 *Nature* **398** 218–20
- [150] Khaykovich L, Schreck F, Ferrari G, Bourdel T, Cubizolles J, Carr L D, Castin Y and Salomon C 2002 *Science* **296** 1290
- [151] Burger S, Bongs K, Dettmer S, Ertmer W, Sengstock K, Sanpera A, Shlyapnikov G V and Lewenstein M 1999 *Phys. Rev. Lett.* **83** 5198–201
- [152] Denschlag J et al 2000 *Science* **287** 97
- [153] Becker C, Stellmer S, Soltan-Panahi P, Dörscher S, Baumert M, Richter E M, Kronjäger J, Bongs K and Sengstock K 2008 *Nature Phys.* **4** 496–501
- [154] Eiermann B, Anker T, Albiez M, Taglieber M, Treutlein P, Marzlin K P and Oberthaler M K 2004 *Phys. Rev. Lett.* **92** 230401
- [155] Litvak A G, Mironov V A, Fraiman G M and Yunakovskii A D 1975 *Sov. J. Plasma Phys.* **1** 60
- [156] Conti C, Peccianti M and Assanto G 2003 *Phys. Rev. Lett.* **91** 073901
- [157] Rotschild C, Cohen O, Manela O, Segev M and Carmon T 2005 *Phys. Rev. Lett.* **95** 213904
- [158] Królikowski W, Bang O, Rasmussen J J and Wyller J 2001 *Phys. Rev. E* **64** 016612
- [159] Bang O, Królikowski W, Wyller J and Rasmussen J J 2002 *Phys. Rev. E* **66** 046619
- [160] Tikhonenkov I, Malomed B A and Vardi A 2008 *Phys. Rev. A* **78** 043614
- [161] Gligorić G, Maluckov A, Hadžievski L and Malomed B A 2008 *Phys. Rev. A* **78** 063615
- [162] Zakharov V E and Shabat A B 1971 *JETP* **61** 118
- [163] Stegeman G I and Segev M 1999 *Science* **286** 1518
- [164] Peccianti M, Conti C, Assanto G, Luca A D and Umetsu C 2004 *Nature* **432** 733–7
- [165] Shih M F, Segev M and Salamo G 1997 *Phys. Rev. Lett.* **78** 2551
- [166] Richter R and Barashenkov I V 2005 *Phys. Rev. Lett.* **94** 184503
- [167] Rosanov N N, Rozhdstvenskii Y V, Smirnov V A and Fedorov S V 2003 *JETP Lett.* **77** 84
- [168] Pedri P and Santos L 2005 *Phys. Rev. Lett.* **95** 200404
- [169] Tikhonenkov I, Malomed B A and Vardi A 2008 *Phys. Rev. Lett.* **100** 090406
- [170] Nath R, Pedri P and Santos L 2009 *Phys. Rev. Lett.* **102** 050401
- [171] Nath R, Pedri P and Santos L 2007 *Phys. Rev. A* **76** 013606
- [172] Zakharov V E and Shabat A B 1972 *JETP* **64** 1627
- [173] Tikhonenko V, Christou J, Luther-Davies B and Kivshar Y S 1996 *Opt. Lett.* **21** 1129
- [174] Mamaev A V, Saffman M and Zozulya A A 1996 *Phys. Rev. Lett.* **76** 2262
- [175] Muryshev A E, van Linden van den Heuvell H B and Shlyapnikov G V 1999 *Phys. Rev. A* **60** R2665
- [176] Feder D L, Pindzola M S, Collins L A, Schneider B I and Clark C W 2000 *Phys. Rev. A* **62** 053606
- [177] Anderson B P, Haljan P C, Regal C A, Feder D L, Collins L A, Clark C W and Cornell E A 2001 *Phys. Rev. Lett.* **86** 2926
- [178] Muryshev A, Shlyapnikov G V, Ertmer W, Sengstock K and Lewenstein M 2002 *Phys. Rev. Lett.* **89** 110401
- [179] Krämer M, Pitaevskii L and Stringari S 2002 *Phys. Rev. Lett.* **88** 180404
- [180] Cuevas J, Malomed B A, Kevrekidis P G and Frantzeskakis D J 2009 *Phys. Rev. A* **79** 053608
- [181] Gligorić G, Maluckov A, Hadžievski L and Malomed B A 2009 *Phys. Rev. A* **79** 053609
- [182] de Gennes P G 1966 *Superconductivity of Metals and Alloys* (New York: Benjamin)
- [183] Donnelly R J 1991 *Quantized Vortices in Helium II* (Cambridge: Cambridge University Press)
- [184] Matthews M R, Anderson B P, Haljan P C, Hall D S, Wieman C E and Cornell E A 1999 *Phys. Rev. Lett.* **83** 2498–501
- [185] Madison K W, Chevy F, Wohlleben W and Dalibard J 2000 *Phys. Rev. Lett.* **84** 806–9
- [186] Abo-Shaeer J R, Raman C, Vogels J M and Ketterle W 2001 *Science* **292** 476–9
- [187] Fetter A L and Svidzinsky A A 2001 *J. Phys.: Condens. Matter* **13** R135–94
- [188] Sinha S and Castin Y 2001 *Phys. Rev. Lett.* **87** 190402
- [189] O'Dell D H J and Eberlein C 2007 *Phys. Rev. A* **75** 013604
- [190] Yi S and Pu H 2006 *Phys. Rev. A* **73** 061602
- [191] van Bijnen R M W, O'Dell D H J, Parker N G and Martin A M 2007 *Phys. Rev. Lett.* **98** 150401
- [192] van Bijnen R M W, Dow A J, O'Dell D H J, Parker N G and Martin A M 2009 arXiv:0905.1515
- [193] Cooper N, Rezayi E and Simon S 2005 *Phys. Rev. Lett.* **95** 200402
- [194] Zhang J and Zhai H 2005 *Phys. Rev. Lett.* **95** 200403
- [195] Thomson W 1880 *Phil. Mag.* **10** 155
- [196] Pitaevskii L P 1961 *JETP* **13** 451
- [197] Bretin V, Rosenbusch P, Chevy F, Shlyapnikov G V and Dalibard J 2003 *Phys. Rev. Lett.* **90** 100403
- [198] Klawunn M, Nath R, Pedri P and Santos L 2008 *Phys. Rev. Lett.* **100** 240403
- [199] Klawunn M and Santos L 2009 *New J. Phys.* **11** 055012
- [200] Cross M C and Hohenberg P C 1993 *Rev. Mod. Phys.* **65** 851
- [201] Engels P, Atherton C and Hofer M A 2007 *Phys. Rev. Lett.* **98** 095301
- [202] Staliunas K, Longhi S and de Valcárcel G J 2002 *Phys. Rev. Lett.* **89** 210406
- [203] Saito H, Kawaguchi Y and Ueda M 2009 *Phys. Rev. Lett.* **102** 230403
- [204] Stenger J, Inouye S, Stamper-Kurn D M, Miesner H J, Chikkatur A P and Ketterle W 1998 *Nature* **396** 345–8
- [205] Ho T L 1998 *Phys. Rev. Lett.* **81** 742–5
- [206] Ohmi T and Machida K 1998 *J. Phys. Soc. Japan* **67** 1822–5
- [207] Koashi M and Ueda M 2000 *Phys. Rev. Lett.* **84** 1066–9
- [208] Ciobanu C V, Yip S K and Ho T L 2000 *Phys. Rev. A* **61** 033607
- [209] Schmaljohann H, Erhard M, Kronjäger J, Kottke M, van Staa S, Cacciapuoti L, Arlt J J, Bongs K and Sengstock K 2004 *Phys. Rev. Lett.* **92** 040402
- [210] Chang M S, Hamley C D, Barrett M D, Sauer J A, Fortier K M, Zhang W, You L and Chapman M S 2004 *Phys. Rev. Lett.* **92** 140403
- [211] Pu H, Zhang W and Meystre P 2001 *Phys. Rev. Lett.* **87** 140405
- [212] Gross K, Search C P, Pu H, Zhang W and Meystre P 2002 *Phys. Rev. A* **66** 033603
- [213] Zhang W, Pu H, Search C and Meystre P 2002 *Phys. Rev. Lett.* **88** 060401
- [214] Yi S, You L and Pu H 2004 *Phys. Rev. Lett.* **93** 040403
- [215] Kawaguchi Y, Saito H and Ueda M 2006 *Phys. Rev. Lett.* **97** 130404
- [216] Takahashi M, Ghosh S, Mizushima T and Machida K 2007 *Phys. Rev. Lett.* **98** 260403
- [217] Diener R B and Ho T L 2006 *Phys. Rev. Lett.* **96** 190405
- [218] Santos L and Pfau T 2006 *Phys. Rev. Lett.* **96** 190404

- [219] Kawaguchi Y, Saito H and Ueda M 2006 *Phys. Rev. Lett.* **96** 080405
- [220] Kawaguchi Y, Saito H and Ueda M 2007 *Phys. Rev. Lett.* **98** 110406
- [221] Gawryluk K, Brewczyk M, Bongs K and Gajda M 2007 *Phys. Rev. Lett.* **99** 130401
- [222] Gerbier F, Widera A, Fölling S, Mandel O and Bloch I 2006 *Phys. Rev. A* **73** 041602
- [223] Santos L, Fattori M, Stuhler J and Pfau T 2007 *Phys. Rev. A* **75** 053606
- [224] Vengalattore M, Leslie S R, Guzman J and Stamper-Kurn D M 2008 *Phys. Rev. Lett.* **100** 170403
- [225] Lamacraft A 2008 *Phys. Rev. A* **77** 063622
- [226] Cherng R W and Demler E 2008 arXiv:0806.1991
- [227] Andreev A F and Lifshitz I M 1969 *Sov. Phys.—JETP* **29** 1107–12
- [228] Chester G V 1970 *Phys. Rev. A* **2** 256–8
- [229] Leggett A J 1970 *Phys. Rev. Lett.* **25** 1543–6
- [230] Vengalattore M, Guzman J, Leslie S, Serwane F and Stamper-Kurn D M 2009 arXiv:0901.3800
- [231] Hecker-Denschlag J, Simsarian J E, Haeffner H, McKenzie C, Browaeys A, Helmerson K, Cho D, Rolston S L and Phillips W D 2002 *J. Phys. B: At. Mol. Opt. Phys.* **35** 3095
- [232] Morsch O and Oberthaler M 2006 *Rev. Mod. Phys.* **78** 179
- [233] Kevrekidis P G, Frantzeskakis D J and Carretero-Gonzalez R (ed) 2007 *Emergent Nonlinear Phenomena in Bose-Einstein Condensates: Theory and Experiment (Springer Series on Atomic, Optical, and Plasma Physics)* (Berlin: Springer)
- [234] Ashcroft N W and Mermin N D 1976 *Solid State Physics* (Fort Worth, TX: Saunders College Publishing)
- [235] Hennig D and Tsironis G P 1999 *Phys. Rep.* **307** 333
- [236] Rasmussen K O, Cretegy T, Kevrekidis P G and Gronbech-Jensen N G 2000 *Phys. Rev. Lett.* **84** 3740
- [237] Trombettoni A and Smerzi A 2001 *Phys. Rev. Lett.* **86** 2353
- [238] Smerzi A and Trombettoni A 2003 *Phys. Rev. A* **68** 023613
- [239] Menotti C, Smerzi A and Trombettoni A 2003 *New J. Phys.* **5** 112
- [240] Taylor E and Zaremba E 2003 *Phys. Rev. A* **68** 053611
- [241] Krämer M, Menotti C, Pitaevskii L and Stringari S 2003 *Eur. Phys. J. D* **27** 247
- [242] Menotti C, Krämer M, Smerzi A, Pitaevskii L and Stringari S 2004 *Phys. Rev. A* **70** 023609
- [243] Wu B and Niu Q 2001 *Phys. Rev. A* **64** 061603
- [244] Machholm M, Pethick C J and Smith H 2003 *Phys. Rev. A* **67** 053613
- [245] Fort C, Cataliotti F S, Fallani L, Ferlaino F, Maddaloni P and Inguscio M 2003 *Phys. Rev. Lett.* **90** 140405
- [246] Morsch O, Müller J H, Cristiani M, Ciampini D and Arimondo E 2001 *Phys. Rev. Lett.* **87** 140402
- [247] Fallani L, Sarlo L D, Lye J E, Modugno M, Saers R, Fort C and Inguscio M 2004 *Phys. Rev. Lett.* **93** 140406
- [248] Cataliotti F S, Burger S, Fort C, Maddaloni P, Minardi F and Smerzi A T and Inguscio M 2001 *Science* **293** 843
- [249] Anker T, Albiez M, Gati R, Hunsmann S, Eiermann B, Trombettoni A, and Oberthaler M K 2005 *Phys. Rev. Lett.* **94** 020403
- [250] Dahan M B, Peik E, Reichel J, Castin Y and Salomon C 1996 *Phys. Rev. Lett.* **76** 4508
- [251] Wilkinson S R, Bharucha C F, Madison K W, Niu Q and Raizen M G 1996 *Phys. Rev. Lett.* **76** 4512
- [252] Feldmann J, Leo K, Shah J, Miller D A B, Cunningham J E, Meier T, von Plessen and Schulze G, Thomas P and Schmitt-Rink S 1992 *Phys. Rev. B* **46** 7252
- [253] Waschke C, Roskos H G, Schwedler R, Leo K, Kurz H and Köhler K 1993 *Phys. Rev. Lett.* **70** 3319
- [254] Lyssenko V, Valusis G, Löser F, Hasche T, Leo K and Köhler K 1997 *Phys. Rev. Lett.* **79** 301
- [255] Dimopoulos S and Geraci A A 2003 *Phys. Rev. D* **68** 124021
- [256] Carusotto I, Pitaevskii L, Stringari S, Modugno G and Inguscio M 2005 *Phys. Rev. Lett.* **95** 093202
- [257] Ferrari G, Poli N, Sorrentino F and Tino G M 2006 *Phys. Rev. Lett.* **97** 060402
- [258] Obrecht J M, Wild R J, Antezza M, Pitaevskii L P, Stringari S and Cornell E A 2007 *Phys. Rev. Lett.* **98** 063201
- [259] Roati G, de Mirandes E, Ferlaino F, Ott H, Modugno G and Inguscio M 2004 *Phys. Rev. Lett.* **92** 230402
- [260] Gustavsson M, Haller E, Mark M J, Danzl J G, Rojas-Kopeinig G and Nägerl H C 2008 *Phys. Rev. Lett.* **100** 080404
- [261] Fisher M P A, Weichman P B, Grinstein G and Fisher D S 1989 *Phys. Rev. B* **40** 546
- [262] Sheshadri K, Krishnamurthy H R, Pandit R and Ramakrishnan T V 1993 *Europhys. Lett.* **22** 257
- [263] Sachdev S 1999 *Quantum Phase Transitions* (Cambridge: Cambridge University Press)
- [264] Freericks J K and Monien H 1994 *Europhys. Lett.* **26** 545
- [265] Freericks J K and Monien H 1996 *Phys. Rev. B* **53** 2691
- [266] Scalettar R T, Batrouni G G and Zimanyi G T 1991 *Phys. Rev. Lett.* **66** 3144
- [267] Krauth W, Trivedi N and Ceperley D 1991 *Phys. Rev. Lett.* **67** 2307
- [268] Prokofev N V, Svistunov B V and Tupisyn I S 1998 *Phys. Lett. A* **238** 253
- [269] Batrouni G G, Rousseau V, Scalettar R T, Rigol M, Muramatsu A, Denteneer P J and Troyer M 2002 *Phys. Rev. Lett.* **89** 117203
- [270] Fölling S, Widera A, Müller T, Gerbier F and Bloch I 2006 *Phys. Rev. Lett.* **97** 060403
- [271] Campbell G K, Mun J, Boyd M, Medley P, Leanhardt A E, Marcassa L, Pritchard D E and Ketterle W 2006 *Science* **313** 649
- [272] Altman E, Demler E and Lukin M D 2004 *Phys. Rev.* **70** 013603
- [273] Fölling S, Gerbier F, Widera A, Mandel O, Gericke T and Bloch I 2005 *Nature* **434** 481
- [274] Bruder C, Fazio R and Schön G 1993 *Phys. Rev.* **47** 342
- [275] van Otterlo A and Wagenblast K H 1994 *Phys. Rev. Lett.* **72** 3598
- [276] Batrouni G G, Scalettar R T, Zimanyi G T and Kampf A P 1995 *Phys. Rev. Lett.* **74** 2527
- [277] Dallatorre E G, Berg E and Altman E 2006 *Phys. Rev. Lett.* **97** 260401
- [278] Haldane F D M 1983 *Phys. Rev. Lett.* **50** 1153–6
- [279] Amico L, Mazzarella G, Pasini S and Cataliotti F S 2008 arXiv:0806.2378
- [280] Kim E and Chan M H W 2004 *Nature* **427** 225
- [281] Kim E and Chan M H W 2004 *Science* **305** 1941
- [282] Kim E and Chan M H W 2006 *Phys. Rev. Lett.* **97** 115302
- [283] Pollet L, Boninsegni M, Kuklov A B, Prokof'ev N V, Svistunov B V and Troyer M 2007 *Phys. Rev. Lett.* **98** 135301
- [284] Sasaki S, Caupin F and Balibar S 2006 *Science* **313** 1098
- [285] Ray M W and Hallock R B 2008 *Phys. Rev. Lett.* **100** 235301
- [286] Góral K, Santos L and Lewenstein M 2002 *Phys. Rev. Lett.* **88** 170406
- [287] Kovrizhin D L, Pai G V and Sinha S 2005 *Europhys. Lett.* **72** 162
- [288] Batrouni G G and Scalettar R T 2000 *Phys. Rev. Lett.* **84** 1599
- [289] Hébert F, Batrouni G G, Scalettar R T, Schmid G, Troyer M and Dorneich A 2001 *Phys. Rev. B* **65** 014513
- [290] Sengupta P, Pryadko L P, Alet F, Troyer M and Schmid G 2005 *Phys. Rev. Lett.* **94** 207202
- [291] Chen Y C, Melko R G, Wessel S and Kao Y J 2007 *Phys. Rev. B* **77** 014524
- [292] Dang L, Boninsegni M and Pollet L 2008 *Phys. Rev. B* **78** 132512
- [293] Ng K K and Chen Y C 2008 *Phys. Rev. B* **77** 052506

- [294] Kühner T D, White S R and Monien H 2000 *Phys. Rev. B* **61** 12474
- [295] Batrouni G G, Hébert F and Scalettar R T 2006 *Phys. Rev. Lett.* **97** 087209
- [296] Scarola V W and Sarma S D 2005 *Phys. Rev. Lett.* **95** 033003
- [297] Scarola V W, Demler E and Sarma S D 2006 *Phys. Rev. A* **73** 051601(R)
- [298] Capogrosso-Sansone B, Trefzger C, Lewenstein M, Zoller P and Pupillo G 2009 arXiv:0906.2009
- [299] Pollet L, Picon J D, Büchler H P and Troyer M 2009 arXiv:0906.2126
- [300] Bernier J S, Sengupta K and Kim Y B 2007 *Phys. Rev. B* **76** 014502
- [301] Ospelkaus S, Ni K K, deMiranda M, Neyenhuis B, Wang D, Kotochigova S, Julienne P S, Jin D S and Ye J 2008 arXiv:0811.4618
- [302] Micheli A, Brennen G K and Zoller P 2006 *Nature Phys.* **2** 341
- [303] Barnett R, Petrov D, Lukin M and Demler E 2006 *Phys. Rev. Lett.* **96** 190401
- [304] Boninsegni M and Prokof'ev N V 2008 *Phys. Rev. B* **77** 092502
- [305] Mathey L, Danshita I and Clark C W 2009 *Phys. Rev. A* **79** 011602
- [306] Mathey L 2007 *Phys. Rev. B* **75** 144510
- [307] Büchler H P and Blatter G 2003 *Phys. Rev. Lett.* **91** 130404
- [308] Titvinidze I, Snoek M and Hofstetter W 2008 *Phys. Rev. Lett.* **100** 100401
- [309] Pour F K, Rigol M, Wessel S and Muramatsu A 2007 *Phys. Rev. B* **75** 161104(R)
- [310] Koga A, Higashiyama T, Inaba K, Suga S and Kawakami N 2008 *J. Phys. Soc. Japan* **77** 073602
- [311] Wang B and Duan L M 2008 *New J. Phys.* **10** 073007
- [312] Wessel S and Troyer M 2005 *Phys. Rev. Lett.* **95** 127205
- [313] Heidarian D and Damle K 2005 *Phys. Rev. Lett.* **95** 127206
- [314] Melko R G, Paramakanti A, Burkov A A, Vishwanath A, Sheng D N and Balents L 2005 *Phys. Rev. Lett.* **95** 127207
- [315] Boninsegni M and Prokof'ev N 2005 *Phys. Rev. Lett.* **95** 237204
- [316] Menotti C, Trefzger C and Lewenstein M 2007 *Phys. Rev. Lett.* **98** 235301
- [317] Roscilde T and Cirac J 2007 *Phys. Rev. Lett.* **98** 190402
- [318] Maška M, Lemański R, Freericks J and Williams C 2008 *Phys. Rev. Lett.* **101** 060404
- [319] Buonsante P, Giampaolo S M, Illuminati F, Penna V and Vezzani A 2009 *Eur. Phys. J. B* **68** 427
- [320] Trefzger C, Menotti C and Lewenstein M 2008 *Phys. Rev. A* **78** 043604
- [321] Burnell F J, Parish M M, Cooper N R and Sondhi S 2009 arXiv:0901.4366
- [322] Wen X G 2004 *Quantum Field Theory of Many-Body Systems* (Oxford: Oxford University Press)
- [323] Argüelles A and Santos L 2007 *Phys. Rev. A* **75** 053613
- [324] Argüelles A and Santos L 2008 *Phys. Rev. A* **77** 059904(E)
- [325] Kuklov A and Svistunov B 2003 *Phys. Rev. Lett.* **90** 100401
- [326] Altman E, Hofstetter W, Demler E and Lukin M 2003 *New J. Phys.* **5** 113
- [327] Kuklov A, Prokof'ev N and Svistunov B 2004 *Phys. Rev. Lett.* **92** 050402
- [328] Şöyler S G, Capogrosso-Sansone B, Prokof'ev N V and Svistunov B V 2009 *New J. Phys.* **11** 073036
- [329] Trefzger C, Menotti C and Lewenstein M 2009 *Phys. Rev. Lett.* **103** 035304
- [330] Wang D W 2007 *Phys. Rev. Lett.* **98** 060403
- [331] Yi S, Li T and Sun C P 2007 *Phys. Rev. Lett.* **98** 260405
- [332] Pupillo G, Micheli A, Büchler H P and Zoller P 2008 *Cold Molecules: Creation and Applications* ed R V Krems et al (London: Taylor and Francis)
- [333] Micheli A, Pupillo G, Büchler H P and Zoller P 2007 *Phys. Rev. A* **76** 043604
- [334] Büchler H P, Micheli A and Zoller P 2007 *Nature Phys.* **3** 726
- [335] Schmidt K P, Dorier J and Läuchli A M 2008 *Phys. Rev. Lett.* **101** 150405
- [336] Capogrosso-Sansone B, Wessel S, Büchler H P, Zoller P and Pupillo G 2009 *Phys. Rev. B* **79** 020503
- [337] Duan L M, Demler E and Lukin M D 2003 *Phys. Rev. Lett.* **91** 090402
- [338] García-Ripoll J J, Martín-Delgado M A and Cirac J I 2004 *Phys. Rev. Lett.* **93** 250405
- [339] Brennen G K, Micheli A and Zoller P 2007 *New J. Phys.* **9** 138
- [340] Douçot B, Feigel'man M V, Ioffe L B and Ioselevich A S 2005 *Phys. Rev. B* **71** 024505
- [341] Kitaev A 2006 *Ann. Phys.* **321** 2
- [342] Wang D W, Lukin M D and Demler E 2006 *Phys. Rev. Lett.* **97** 180413
- [343] Lozovik Y E, Volkov S Y and Willander M 2004 *JETP Lett.* **79** 473
- [344] Astrakharchik G E, Boronat J, Kurbakov I L and Lozovik Y E 2007 *Phys. Rev. Lett.* **98** 060405
- [345] Mora C, Parcollet O and Waintal X 2007 *Phys. Rev. B* **76** 064511
- [346] Wigner E 1934 *Phys. Rev.* **46** 1002
- [347] Bonsall L and Maradudin A A 1977 *Phys. Rev. B* **15** 1959
- [348] Rabl P and Zoller P 2007 *Phys. Rev. A* **76** 042308
- [349] Pupillo G, Griessner A, Micheli A, Ortner M, Wang D W and Zoller P 2008 *Phys. Rev. Lett.* **100** 050402
- [350] Lu X, Wu C Q, Micheli A and Pupillo G 2008 *Phys. Rev. B* **78** 024108
- [351] Arkhipov A S, Astrakharchik G E, Belikov A V and Lozovik Y E 2005 *JETP Lett.* **82** 39
- [352] Citro R, Orignac E, De Palo S and Chiofalo M L 2007 *Phys. Rev. A* **75** 051602
- [353] Palo S D, Orignac E, Citro R and Chiofalo M L 2008 *Phys. Rev. B* **77** 212101
- [354] Pedri P, De Palo S, Orignac E, Citro R and Chiofalo M L 2008 *Phys. Rev. A* **77** 015601
- [355] Fishman S, Chiara G D, Calarco T and Morigi G 2008 *Phys. Rev. B* **77** 064111
- [356] Löw R, Weimer H, Raitzsch U, Heidemann R, Bendkowsky V, Butscher B, Büchler H P and Pfau T 2009 arXiv:0902.4523
- [357] Mintert F and Wunderlich C 2001 *Phys. Rev. Lett.* **87** 257904
- [358] Wunderlich C and Balzer C 2003 *Adv. At. Mol. Opt. Phys.* **49** 295
- [359] Porras D and Cirac J I 2004 *Phys. Rev. Lett.* **92** 207901
- [360] Deng X L, Porras D and Cirac J I 2005 *Phys. Rev. A* **72** 063407
- [361] Porras D and Cirac J I 2004 *Phys. Rev. Lett.* **93** 263602
- [362] Porras D, Marquardt F, von Delft J and Cirac J 2008 *Phys. Rev. A* **78** 010101(R)
- [363] Pons M, Ahufinger V, Wunderlich C, Sanpera A, Braungardt S, Sen(De) A, Sen U and Lewenstein M 2007 *Phys. Rev. Lett.* **98** 023003
- [364] Braungardt S, Sen(De) A, Sen U and Lewenstein M 2007 *Phys. Rev. A* **76** 042307
- [365] Schmied R, Roscilde T, Murg V, Porras D and Cirac J I 2008 *New J. Phys.* **10** 045017
- [366] Schmied R, Wesenberg J H and Leibfried D 2009 *Phys. Rev. Lett.* **102** 233002
- [367] Friedenauer A, Schmitz H, Glückert J, Porras D and Schätz T 2008 *Nature Phys.* **4** 757–61
- [368] Loison J C, Durand A, Bazalgette G, White R, Audouard E and Vigué J 1995 *J. Phys. Chem.* **99** 13591